UNIVERSIDAD NACIONAL AUTÓNOMA DE MÉXICO
POSGRADO EN CIENCIAS FÍSICAS

QUANTUM PHASE TRANSITIONS IN THE SEMIMICROSCOPIC ALGEBRAIC CLUSTER MODEL

TESIS
QUE PARA OPTAR POR EL GRADO DE:
DOCTOR EN CIENCIAS (FÍSICA)

PRESENTA:
M. EN. C. DAVID STEFAN LOHR ROBLES

TUTORES PRINCIPALES:
DR. PETER OTTO HESS BECHSTEDT
INSTITUTO DE CIENCIAS NUCLEARES, UNAM

DR. ENRIQUE LÓPEZ MORENO
FACULTAD DE CIENCIAS, UNAM

COMITÉ TUTOR:
DR. JORGE GUSTAVO HIRSCH GANIEVICH
INSTITUTO DE CIENCIAS NUCLEARES, UNAM
DR. EFRAÍN RAFAEL CHÁVEZ LOMELÍ
INSTITUTO DE FÍSICA, UNAM

CIUDAD UNIVERSITARIA, CD. MX., JUNIO 2022

Agradecimientos

Principalmente agradezco al Dr. Peter Hess y al Dr. Enrique López Moreno por haber dirigido el presente trabajo de tesis. Agradezco su tiempo, sus enseñanzas y sus comentarios respecto al trabajo.

Agradezco al Dr. Jorge Hirsch y al Dr. Efraín Chávez por haber sido miembros del Comité Tutor, y por sus comenatrios sobre el tema de investigación e interés en el trabajo.

Agradezco a los sinodales: Dr. Roelof Bijker, Dr. Enrique Martínez Quiroz, Dr. Elí Aguilera Reyes y Dra. Myriam Mondragón, por sus importantes comentarios y sugerencias sobre la tesis, que ayudaron a mejorarla. También agradezco al Dr. Luis Acosta y al Dr. Victor Velázquez por haber sido sinodales durante el examen de candidatura al grado de doctor, y por sus preguntas y comentarios que ayudaron a mejorar el presente trabajo.

Agradezco al M. en C. Antonio Jáuregui por su apoyo y enseñanzas durante mis estudios de Licenciatura y Maestría. También agradezco al Dr. Alfonso Mondragón y a la Dra. Enriqueta Hernández por su apoyo y enseñanzas durante mis estudios de Maestría.

Agradezco al Instituto de Ciencias Nucleares, UNAM, por el lugar proporcionado durante los estudios de doctorado.

Agradezco a mi familia por su apoyo.

Agradezco al Consejo Nacional de Ciencia y Tecnología (CONACyT) por el apoyo económico a través de la beca (No. 728381) proporcionada durante los estudios de doctorado.

Abstract

In this thesis the phenomenon of quantum phase transitions is studied within the framework of the semimicroscopic algebraic cluster model. The dynamics of the cluster system is described by a Hamiltonian operator composed of Casimir operators of two dynamical symmetries: SU(3) and SO(4). The number of parameters in the Hamiltonian depends on the number of interactions considered, and when continuously increasing the intensity of some of these parameters quantum phase transitions occur. The study of phase transition is done using the catastrophe theory formalism applied to the semi-classical potential, which is obtained as the expectation value of the Hamiltonian in the coherent state basis of the model. The semi-classical potential depends on control parameters, which are linear combinations of the interaction parameters, and on the parameter variables of the coherent states. Separatrices are constructed which divide the parameter space in regions where the qualitative behaviour of the potential is the same. The structural changes of the potential when going from one region to another are identified as phase transitions. First, second and third order phase transitions are found in the model. Two examples are considered: The system of two spherical systems $^{16}\mathrm{O} + \alpha \rightarrow {}^{20}\mathrm{Ne}$, and the system of two deformed systems $^{12}\mathrm{C} + {}^{12}\mathrm{C} \rightarrow {}^{24}\mathrm{Mg}$. Signatures of quantum phase transitions in these systems are identified as avoided energy levels of the state 0_2^+ with the ground state 0_1^+. In this thesis a novel method based on catastrophe theory to obtain the Maxwell set is developed.

Additionally the same methods are applied to an effective model of QCD and a first order phase transition is found and further physical information is extracted.

Resumen

En esta tesis presentamos un estudio de las transiciones de fase cuánticas en el modelo semimicroscópico de cúmulos nucleares. La dinámica del sistema de cúmulos es descrita por un operador Hamiltoniano, que es una combinación lineal de operadores de Casimir de dos simetrías dinámicas: SU(3) y SO(4). El número de parámetros en el Hamiltoniano depende del número de interacciones consideradas y cuando se varía la magnitud de algunos de estos parámetros hasta alcanzar un valor crítico ocurre una transición de fase. El estudio de las transiciones de fase es hecho usando el formalismo de la teoría de catástrofes aplicado al potencial semiclásico, el cual se obtiene como el valor esperado del Hamiltoniano en la base de estados coherentes del modelo. El potencial semiclásico depende de los parámetros de control, que son funciones de los parámetros de interacción del Hamiltoniano, y de los parámetros de los estados coherentes. El espacio de parámetros es dividido en regiones donde el comportamiento cualitativo del potencial es el mismo mediante separatrices. Los cambios estructurales del potencial que ocurren al variar los parámetros de una región a otra son identificados como transiciones de fase; y en este modelo encontramos transiciones de fase de primer, segundo y tercer orden. Dos ejemplos de sistemas de cúmulos son estudiados: el sistema de dos cúmulos esféricos $^{16}\mathrm{O}+\alpha \rightarrow {}^{20}\mathrm{Ne}$ y el sistema de dos cúmulos deformados $^{12}\mathrm{C}+{}^{12}\mathrm{C} \rightarrow {}^{24}\mathrm{Mg}$. Las señales de transiciones de fase cuánticas en estos sistemas se identifican como niveles evitados de energía del estado 0_2^+ con el estado base 0_1^+. En esta tesis se desarrolla un nuevo método basado en la teoría de catástrofes para obtener la separatriz llamada conjunto de Maxwell.

Adicionalmente, los mismos métodos son aplicados a un modelo efectivo de QCD para demostrar la utilidad de los métodos desarrollados. Una transición de fase de primer orden es descrita y es posible extraer más información del sistema físico.

Contents

Chapter 1

Introduction

The study of phase transitions is of significant importance in different areas of physics. The properties of a physical system are defined by value of the parameters that describe them. The variation of the parameters can imply structural changes in those properties when they reach a critical value. In this way, methods that focus on this relationship between the change of parameters and its effect on the physical properties of a system are very useful. When dealing with quantum mechanical finite systems that depend on control parameters, smooth changes reminiscent of classical phase transitions can arise in the physical observables. In the limit to the case of a system with infinite degrees of freedom these changes become more drastic and singularities begin to appear; a semi-classical approach is therefore needed. For this reason this type of phenomena is referred to as quantum phase transitions (QPTs) [1].

In algebraic models in nuclear physics the study of QPTs has developed special interest in recent times. The effects of the QPTs have been associated to structural changes in nuclei [2,3], as well as with the shape and stability of nuclei [4–6]. The interacting boson model (IBM) [7–9] has been a very popular model for the study of QPTs [4, 10–19], where the different phases are associated with different dynamical symmetries [20–26]. In Ref. [27] an extensive review on the study of QPTs in the IBM and its comparison to experimental data of certain isotopic chains is presented. The Lipkin-Meshkov-Glick (LMG) model [28] in nuclear physics and the Dicke model [29,30] in optics have also been the testing bed for many recent studies on QPTs and their properties [31–40].

The use of catastrophe theory [41–43] as a systematic and effective way to study QPTs in nuclear models has been previously applied in Refs. [4,19,27,34,44–46]. The structure of the potentials analysed in those articles was relatively simple and it was possible to use the catastrophe theory program. If the potential is complicated enough the application of catastrophe theory to the problem is not as direct, and one has to resort to approximations or numerical calculations, particularly when obtaining the Maxwell set separatrix [41]. In the present work we developed a method based on the essence of catastrophe theory to construct the Maxwell set. This shall prove itself useful when dealing with more involved and complicated potentials, and maintaining an analytical approach, although in some cases numerical analysis is inevitable.

This thesis is based on the results of two publications [47,48] and will be structured as follows: In Chapter 2 we introduce the semimicroscopic algebraic cluster model (SACM),

an algebraic cluster model which observes the Pauli exclusion principle (PEP) and explain its advantages over other algebraic nuclear models. The semi-classical potential of the interaction is obtained. The catastrophe theory methodology is explained in detail and a simple example, the *cusp catastrophe* potential, is used to illustrate it. The definition of a QPT is established and the same example potential is used to observe the effects of the QPT in the energy levels of the Hamiltonian. Then using the methods described the separatrix of parameter space are constructed for the SACM, where the semi-classical potential has the same qualitative behaviour. We search for signatures of QPTs in the energy levels of the 0^+ states and in other physical observables for two cluster examples: The system of two spherical clusters $^{16}\mathrm{O} + \alpha \rightarrow {}^{20}\mathrm{Ne}$, and the system of two deformed clusters $^{12}\mathrm{C} + {}^{12}\mathrm{C} \rightarrow {}^{24}\mathrm{Mg}$. In Chapter 3 the methods developed in the previous chapter are directly applied to an effective model of quantum chromodynamics (QCD), in order to show their usefulness. In Chapter 4 conclusions are drawn and an outline of possible future work in this line of study is discussed.

Chapter 2

The SACM and its quantum phase transitions

In nuclear physics different methods exist to study the structure of nuclei and their properties. Cluster models are among them, which are further divided in two groups: algebraic and microscopic cluster models. The microscopic models consist in fully describing the interaction between the nucleons and the Pauli exclusion principle is taken into account. Detailed reviews of the latest results in microscopic cluster models can be found in Refs. [49, 50]. The advantages of algebraic models is the comparatively ease of computational time efficiency and in the obtaining of analytical expressions for the physical quantities, where significant symmetries and use of groups theory is employed to further facilitate the task. The algebraic cluster models are also divided in models which observe the Pauli exclusion principle (PEP) and those models which do not satisfy it. A review of the recent advances in algebraic cluster models of the latter type can be found in Ref. [51].

In the present work we will focus in an algebraic cluster model which satisfies the PEP, namely the semimicroscopic algebraic cluster model (SACM) [52, 53]. In recent times there has been some research done within the SACM to understand the importance of the PEP [54–56]. Additional complexity is found in a model satisfying the PEP compared to one that does not. Primarily in the construction of the physical space of the model and in the structure of the semi-classical potential obtained as the expectation value of the Hamiltonian operator describing the interaction in the basis of coherent states. However, we believe that these additional complexities encountered are worthwhile resolving, as models which satisfy the PEP offer a more accurate description of the physical structure of the nuclei. One of the purposes of this work is to develop a methodology, based on catastrophe theory, which may be easily applied to an involved function and extract information of possible quantum phase transition in nuclei and of the respective physical properties associated. We start by describing the main characteristics of the SACM.

2.1 Introduction to the SACM

In the SACM the internal structure of the clusters is described by the SU(3) shell model [57–59], while the relative motion of the cluster is described by the vibron model [60, 61].

This model, then, takes into account microscopic aspects of the description of the nuclei and relates them to the phenomenological approach. The interaction between the clusters is described by a Hamiltonian given in terms of the group Casimir operators and the space of the model is microscopic, taking into account the Pauli exclusion principle. It is in this way that the model is *semi*-microscopic.

The relative motion of the clusters is described by the creation $\boldsymbol{\pi}^\dagger$ and annihilation $\boldsymbol{\pi}$ operators of the π bosons with angular momentum $\ell = 1$, and their products form the generators of the $\mathrm{U}_R(3)$ group [52], where the R subscript refers to the relative part. A cut-off is introduced so that the total number of bosons $N = n_\pi + n_\sigma$ remains constant and the number of π bosons ranges from n_0 to N. This is done by introducing the σ bosons with angular momentum $\ell = 0$ and their creation $\boldsymbol{\sigma}^\dagger$ and annihilation $\boldsymbol{\sigma}$ operators. The product of pairs of creation and annihilation operators conserving the number of bosons: $\boldsymbol{\pi}^\dagger_m \boldsymbol{\pi}^{m'}, \boldsymbol{\pi}^\dagger_m \boldsymbol{\sigma}, \boldsymbol{\sigma}^\dagger \boldsymbol{\pi}^m, \boldsymbol{\sigma}^\dagger \boldsymbol{\sigma}$, are the generators of the group $\mathrm{U}_R(4)$.

Physical operators are constructed as tensor products of the generators of the group $\mathrm{U}_R(4)$. The number operator, and the m components of the angular momentum operator and the quadrupole operator are given by

$$\begin{aligned} \boldsymbol{n}_\pi &= \sqrt{3}[\boldsymbol{\pi}^\dagger \otimes \boldsymbol{\pi}]^{[0]}_0 \\ \boldsymbol{L}_{R,m} &= \sqrt{2}[\boldsymbol{\pi}^\dagger \otimes \boldsymbol{\pi}]^{[1]}_m \\ \boldsymbol{Q}_{R,m} &= \frac{\sqrt{3}}{2}[\boldsymbol{\pi}^\dagger \otimes \boldsymbol{\pi}]^{[2]}_m. \end{aligned} \tag{2.1}$$

The tensor product $[\boldsymbol{\pi}^\dagger \otimes \boldsymbol{\pi}]^{[S]}_m$ is given as the angular momentum coupling of the rank-1 tensors $\boldsymbol{\pi}^\dagger$ and $\boldsymbol{\pi}$ to total spin S, explicitly it is:

$$[\boldsymbol{\pi}^\dagger \otimes \boldsymbol{\pi}]^{[S]}_m = \sum_{m_1,m_2} (1m_1 1m_2|Sm)\pi^\dagger_{m_1}\pi^{m_2}, \tag{2.2}$$

where $(1m_1 1m_2|Sm)$ is the Clebsch-Gordan coefficient.

The basis states of the Hamiltonian are determined by noting that the relative motion has a $\mathrm{U}_R(4)$ group structure. The complete basis will be constructed as the direct product of the relative motion part and the internal cluster structure part, which is described by the SU(3) group [52, 53]. There are two group chains of $\mathrm{U}_R(4)$ which contain the group $\mathrm{SO}_R(3)$ of angular momentum. The first one is

$$\mathrm{U}_R(4) \supset \mathrm{SU}_R(3) \supset \mathrm{SO}_R(3) \supset \mathrm{SO}_R(2), \tag{2.3}$$

with quantum numbers

$$n_\pi = N, N-1, \ldots, 1, 0 \tag{2.4}$$

$$L_R = n_\pi, n_\pi - 2, \ldots, 1 \text{ or } 0 \tag{2.5}$$

$$m_R = L_R, L_R - 1, \ldots, -L_R + 1, -L_R. \tag{2.6}$$

where N is the total number of bosons, n_π is the number of π bosons and L is the angular momentum.

The second group chain is

$$\mathrm{U}_R(4) \supset \mathrm{SO}_R(4) \supset \mathrm{SO}_R(3) \supset \mathrm{SO}_R(2), \tag{2.7}$$

with quantum numbers

$$\omega = N, N-2, \ldots, 1 \text{ or } 0 \tag{2.8}$$
$$L_R = \omega, \omega-1, \ldots, 1, 0 \tag{2.9}$$
$$m_R = L_R, L_R-1, \ldots, -L_R+1, -L_R, \tag{2.10}$$

and one can speak of two dynamical symmetries limits: $\mathrm{SU}_R(3)$ and $\mathrm{SO}_R(4)$ [62], which will define the structure of the Hamiltonian of the system. The basis is then labelled by the quantum numbers provided by the first group chain, i.e. the basis used when calculating the eigenvalues of the Hamiltonian is that of the SU(3) group chain.

The space of the SACM is obtained calculating the product

$$(\lambda_1, \mu_1) \otimes (\lambda_2, \mu_2) \otimes (n_\pi, 0) = \sum_{\lambda,\mu} m_{\lambda\mu}(\lambda, \mu) \tag{2.11}$$

where (λ_k, μ_k) is the SU(3) irreducible representation (irrep) of the individual clusters, $(n_\pi, 0)$ is the relative motion irrep, and $m_{\lambda,\mu}$ denotes the multiplicity of the particular irrep. The resulting sum contains irreps not present in the SU(3) shell model space of the total nucleus [57, 58, 63–65]. As a necessary condition to observe the Pauli exclusion principle, these non overlapping irreps are removed from the final SACM space.

An important aspect to mention concerning the number of π bosons n_π is that of the Wildermuth condition [66]: This imposes a minimal number of π bosons $n_\pi \geq n_0$. As an example let us consider the cluster system $^{16}\mathrm{O} + \alpha \rightarrow {}^{20}\mathrm{Ne}$ as depicted in Fig. 2.1. The number of oscillation quanta in the shell model for ^{16}O is 12, and for α is zero, while the number of oscillation quanta in the shell model for ^{20}Ne is 20. Therefore, 8 oscillation quanta needs to be added to account for the difference, and for this example we have $n_0 = 8$. This can also be seen in the way the model space is constructed in (2.11). As ^{16}O and α are spherical clusters we have $(\lambda_1, \mu_1) = (\lambda_2, \mu_2) = (0, 0)$, the irrep of the relative motion is $(8, 0)$ accounting for Wildermuth condition, and the resulting product is $(8, 0)$ which is the ground state irrep of the ^{20}Ne nucleus.

The Hamiltonian considered is a function of Casimir operators of the SU(3) and SO(4) groups, up to second order. The explicit expression of the particular Hamiltonian used here is

$$\begin{aligned}\boldsymbol{H} = {} & \hbar\omega \boldsymbol{n}_\pi + (\bar{a} - \bar{b}\Delta\boldsymbol{n}_\pi)\boldsymbol{C}_2(\boldsymbol{n}_\pi, 0) + (a - b\Delta\boldsymbol{n}_\pi)\boldsymbol{C}_2(\lambda, \mu) + \xi \boldsymbol{L}^2 \\ & + \frac{c}{4}\left[(\boldsymbol{\pi}^\dagger \cdot \boldsymbol{\pi}^\dagger) - (\boldsymbol{\sigma}^\dagger)^2\right]\left[(\boldsymbol{\pi} \cdot \boldsymbol{\pi}) - (\boldsymbol{\sigma})^2\right] + t_1 \boldsymbol{K}^2.\end{aligned} \tag{2.12}$$

A more general Hamiltonian could be considered by adding more terms, e.g the third order Casimir operator of SU(3), but this added terms would only further complicate matters and for our purposes the present expression will suffice. The Hamiltonian (2.12) depends on seven parameters $\{\bar{a}, a, \bar{b}, b, c, \xi, t_1\}$ and $\hbar\omega = 45A^{-1/3} - 25A^{-2/3}$ MeV [67], where A is the number of nucleons of the total nucleus. In this chapter all parameters are in MeV units.

The second order Casimir operator of SU(3) is given by [68]:

$$\boldsymbol{C}_2(\lambda, \mu) = 4\boldsymbol{Q}^2 + \frac{3}{4}\boldsymbol{L}^2. \tag{2.13}$$

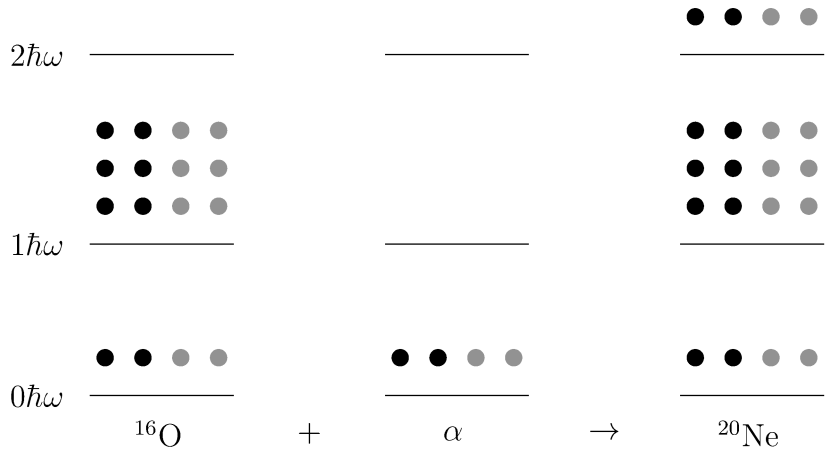

Figure 2.1: For the cluster system $^{16}\mathrm{O} + \alpha \rightarrow {}^{20}\mathrm{Ne}$ the protons and neutrons for each nuclei are depicted as black and gray dots, respectively, in their corresponding shell. The total oscillation quanta in the lhs is 12, while the oscillation quanta in the rhs is 20. A difference of $n_0 = 8$ oscillation quanta needs to be added according to the Wildermuth condition.

The total quadrupole operator $\boldsymbol{Q} = \boldsymbol{Q}_C + \boldsymbol{Q}_R$ is given as the sum of the cluster quadrupole operator $\boldsymbol{Q}_C = \boldsymbol{Q}_{C_1} + \boldsymbol{Q}_{C_2}$, which is further constructed as the sum of the quadrupole operator of the individual clusters, and the relative motion quadrupole operator $\boldsymbol{Q}_R$ given in (2.1). Exactly the same is said about the total angular momentum operator $\boldsymbol{L} = \boldsymbol{L}_C + \boldsymbol{L}_R$, where the relative motion angular momentum operator $\boldsymbol{L}_R$ is given in (2.1). The cluster quadrupole and angular momentum operators only act on the cluster part of the basis. The relative motion second order Casimir operator is given by

$$\boldsymbol{C}_2(\boldsymbol{n}_\pi, 0) = 4\boldsymbol{Q}_R^2 + \frac{3}{4}\boldsymbol{L}_R^2 = \boldsymbol{n}_\pi(\boldsymbol{n}_\pi + 3). \tag{2.14}$$

The operator multiplying parameter c is the second order Casimir operator of SO(4), which is not identified with a physical operator. Then, when the parameter c is equal to zero the Hamiltonian (2.12) is in the SU(3) dynamical symmetry limit, and a non-zero value of c indicates the case where the Hamiltonian has a term related to the SO(4) dynamical symmetry, which can be interpreted as a deformation limit. The Hamiltonian (2.12) can be further expanded by adding other Casimir operators such as the third order SU(3) Casimir operator, which introduces more parameters. The purpose of this would be to improve the fitting of energy levels to experimental data. However, the simple form of the Hamiltonian (2.12) serves as a useful starting point to the semi-classical study of quantum phase transitions. Adding more interaction terms to the Hamiltonian will only complicate the resulting semi-classical potential after the geometrical mapping, but this addition is not necessary for obtaining significant results of the phenomena of interest. The operator $\boldsymbol{K}^2$ is introduced to account for the degeneracy of excited states when dealing with deformed clusters, and its eigenvalue is the quantum number which labels the rotational bands.

2.2 Coherent states

The semi-classical potential is obtained as the expectation value of the Hamiltonian (2.12) in a trial wave function. The coherent states are the states where the uncertainty relation is minimum and usually provides good approximations to the ground states [69]. The trial function is constructed as the direct product of the coherent states, which accounts for the relative motion, and the state describing the cluster coupling. In the SACM the coherent states are defined as [70]:

$$\begin{aligned} |\alpha\rangle &= \mathcal{N}_{N,n_0}(\boldsymbol{\alpha}^*\cdot\boldsymbol{\pi}^\dagger)^{n_0}[\boldsymbol{\sigma}^\dagger + (\boldsymbol{\alpha}^*\cdot\boldsymbol{\pi}^\dagger)]^N|0\rangle \\ &= \frac{N!}{(N+n_0)!}\mathcal{N}_{N,n_0}\frac{d^{n_0}}{d\gamma^{n_0}}[\boldsymbol{\sigma}^\dagger + \gamma(\boldsymbol{\alpha}^*\cdot\boldsymbol{\pi}^\dagger)]^{N+n_0}|0\rangle\Big|_{\gamma=1} \end{aligned} \tag{2.15}$$

with

$$\mathcal{N}^{-2}_{N,n_0} = \frac{(N!)^2}{(N+n_0)!}\frac{d^{n_0}}{d\gamma_1^{n_0}}\frac{d^{n_0}}{d\gamma_2^{n_0}}[1+\gamma_1\gamma_2(\boldsymbol{\alpha}^*\cdot\boldsymbol{\alpha})]^{N+n_0}\Big|_{\gamma_1=\gamma_2=1} \tag{2.16}$$

the normalisation constant. The last line in (2.15) is written as such to facilitate algebraic manipulation when calculating expectation values. In Appendix A explicit calculation of the expectation values of the operators in the Hamiltonian is performed. The coherent states depend on complex and arbitrary variables α_m, with $m = -1, 0, 1$. The choice made in the characteristic of these variables has important consequences in the resulting semi-classical potential.

In this work we will consider two cases for the parametrisation of the α_m coherent state variables and explore their consequences. The first case is when the α_m variables transform as tensors, i.e. in the same way as the ${\boldsymbol{\pi}^\dagger}_m$ and $\boldsymbol{\pi}^m$ operators, and the following is satisfied:

$$\alpha^*_m = (-1)^{1-m}\alpha_{-m}, \tag{2.17}$$

and the lowering of the indices induces a phase.

In the second case they are arbitrarily complex variables. However, we will use the same property used in [47, 71, 72] where they satisfy the relation:

$$\alpha^*_m = \alpha_{-m}, \tag{2.18}$$

which corresponds to a parametrisation in spherical coordinates.

An important difference between both cases concern the expectation value of the relative part of angular momentum components $\boldsymbol{L}_{R,m}$ in the basis of coherent states. In the first case the expectation value vanishes. In the second case the expectation value for the x and y components are non-zero. The latter case is then useful when the inclusion of a $\boldsymbol{L}_x$ or $\boldsymbol{L}_y$ contribution in the Hamiltonian is necessary, such as in the case of the *cranking method* [68]. First steps toward the application of this method in the SACM have already been made in [71–73].

The semi-classical potential is defined as the expectation value of the Hamiltonian in

the complete basis of coherent states:

$$
\begin{aligned}
V(\boldsymbol{\alpha};c_i) &= \langle\alpha|\boldsymbol{H}|\alpha\rangle \\
&= (a+bn_0)\langle \boldsymbol{C}_2(\lambda_C,\mu_C)\rangle + \xi\langle \boldsymbol{L}^2\rangle + \frac{c}{4}(N+n_0)(N+n_0-1) + t_1\langle \boldsymbol{K}^2\rangle \\
&+ \Big\{\Big[\hbar\omega + 4(\bar{a}+a+(\bar{b}+b)(n_0-1)) - b\langle \boldsymbol{C}_2(\lambda_C,\mu_C)\rangle + 2\xi \\
&-\frac{c}{2}(N+n_0-1)\Big](\boldsymbol{\alpha}^*\cdot\boldsymbol{\alpha}) + (a+b(n_0-1))(\Gamma_1+\Gamma_2)[\boldsymbol{\alpha}^*\times\tilde{\boldsymbol{\alpha}}]^{[2]}_0\Big\}\frac{F_{11}(\boldsymbol{\alpha})}{F_{00}(\boldsymbol{\alpha})} \\
&+ \Big\{\Big[\bar{a}+a+(\bar{b}+b)(n_0-6)+\frac{c}{4}\Big](\boldsymbol{\alpha}^*\cdot\boldsymbol{\alpha})^2 - b(\Gamma_1+\Gamma_2)[\boldsymbol{\alpha}^*\times\tilde{\boldsymbol{\alpha}}]^{[2]}_0 \\
&-\xi 2\sqrt{3}[[\boldsymbol{\alpha}^*\times\tilde{\boldsymbol{\alpha}}]^{[1]}\times[\boldsymbol{\alpha}^*\times\tilde{\boldsymbol{\alpha}}]^{[1]}]^{[0]}_0 + \frac{3c}{4}[\boldsymbol{\alpha}^*\times\boldsymbol{\alpha}^*]^{[0]}_0[\tilde{\boldsymbol{\alpha}}\times\tilde{\boldsymbol{\alpha}}]^{[0]}_0\Big\}\frac{F_{22}(\boldsymbol{\alpha})}{F_{00}(\boldsymbol{\alpha})} \\
&- \frac{c\sqrt{3}}{4}\Big\{[\boldsymbol{\alpha}^*\times\boldsymbol{\alpha}^*]^{[0]}_0 + [\tilde{\boldsymbol{\alpha}}\times\tilde{\boldsymbol{\alpha}}]^{[0]}_0\Big\}\frac{F_{20}(\boldsymbol{\alpha})}{F_{00}(\boldsymbol{\alpha})} - b(\boldsymbol{\alpha}^*\cdot\boldsymbol{\alpha})^3\frac{F_{33}(\boldsymbol{\alpha})}{F_{00}(\boldsymbol{\alpha})}
\end{aligned}
\tag{2.19}
$$

where $\boldsymbol{\alpha}$ are the coherent state variables, and $c_i = \{\bar{a}, a, \bar{b}, b, c, \xi, t_1\}$ refers to the interaction parameters. We defined the notation: $\tilde{\alpha}_m = (-1)^{1-m}\alpha_{-m}$, for the case where $\boldsymbol{\alpha}$ is an arbitrary complex variable. The ket $|\alpha\rangle$ is shorthand notation for the complete basis wave function, which is the product of the coherent states, concerning the relative motion, and the internal cluster states: $|\alpha\rangle \equiv |\alpha\rangle|C_1\times C_2\rangle$.

In (2.19) (λ_C,μ_C) is an intermediate irrep of the cluster system given by the product of the individual clusters: $(\lambda_1,\mu_1)\otimes(\lambda_2,\mu_2)$. The deformation of the clusters is taken into account through Γ_k, which is the expectation value of the $m=0$ component of the quadrupole operator of cluster k [74]:

$$
\Gamma_k = \langle(\lambda_k,\mu_k)|Q^a_{C_k,0}|(\lambda_k,\mu_k)\rangle = \sqrt{\frac{5}{\pi}}\left(n_k + \frac{3}{2}(A_k-1)\right)\beta_k, \tag{2.20}
$$

where n_k is the total number of quanta of cluster k and β_k is the quadrupole deformation. The operator $Q^a_{C_k,0}$ is the $m=0$ component of the algebraic quadrupole operator and is related to the quadrupole operator $Q_{C_k,0}$ by the relation: $Q^a_{C_k,0} = 2\sqrt{2}Q_{C_k,0}$ [70]. The functions $F_{pq}(\alpha)$ are defined in [62] and are given by:

$$
\begin{aligned}
F_{pq}(\alpha^2) &= \frac{(N!)^2}{(N+n_0-\max(p,q))!} \\
&\times \sum_{k=\max(n_0-p,n_0-q)}^{N+n_0-\max(p,q)} \begin{pmatrix} N+n_0-\max(p,q) \\ k \end{pmatrix} \frac{(k+p)!}{(k+p-n_0)!}\frac{(k+q)!}{(k+q-n_0)!}\alpha^{2k}.
\end{aligned}
\tag{2.21}
$$

2.2.1 First case: Tensor parametrisation of coherent states

In Refs. [62, 74] the case of the $\boldsymbol{\alpha}$ variables transforming as tensors has already been treated in the SACM. In particular in [74] quantum phase transitions where studied when a parameter x is varied going from a Hamiltonian with SU(3) symmetry at $x=1$ to Hamiltonian with SO(4) symmetry at $x=0$. At a critical point x_c a quantum phase

transition is found as an abrupt change in the expectation value of π bosons at the ground state. The change in some of the excited state energy levels as a function of parameter x is also studied. Our approach will differ from [74] in two ways: First QPTs are studied within the SU(3) limit of the Hamiltonian (2.12) where the parameter c is zero, and then the SO(4) symmetry is taken into account by turning on the parameter c, where QPTs are also found.

The simplest way to satisfy the transformation rule (2.17) is with the following choice:

$$\begin{aligned} \alpha_0 &= i\alpha \\ \alpha_{\pm 1} &= 0, \end{aligned} \tag{2.22}$$

which was also used in [62]. In this parametrisation there is only a dependence on one variable α, which can be related to the distance between clusters [70]. Direct application of this particular choice in the semi-classical potential (2.19) is straightforward and leads to a one dimensional function dependent on three control parameters:

$$V(\alpha; c_i) = V_0 - (b+\bar{b})\left(A\alpha^2 \frac{F_{11}(\alpha)}{F_{00}(\alpha)} + B\alpha^4 \frac{F_{22}(\alpha)}{F_{00}(\alpha)} + \alpha^6 \frac{F_{33}(\alpha)}{F_{00}(\alpha)} + C\alpha^2 \frac{F_{20}(\alpha)}{F_{00}(\alpha)} \right), \tag{2.23}$$

with the constant value V_0 given by

$$V_0 = (a+n_0 b)\langle \boldsymbol{C}_2(\lambda_C, \mu_C)\rangle + \xi\langle \boldsymbol{L}_C^2\rangle + \frac{c}{4}(N+n_0)(N+n_0-1) + t_1\langle \boldsymbol{K}^2\rangle, \tag{2.24}$$

The 3 control parameters $c_i = \{A, B, C\}$ are linear combinations of the Hamiltonian parameters:

$$\begin{aligned} A &= -\frac{1}{b+\bar{b}}\Big[\hbar\omega - b\langle \boldsymbol{C}_2(\lambda_C,\mu_C)\rangle + 4\Big(a+\bar{a}+(b+\bar{b})(n_0-1)\Big) \\ &\quad + \Big(a+b(n_0-1)\Big)(\Gamma_1+\Gamma_2) + 2\xi - \frac{c}{2}(N+n_0-1)\Big] \\ B &= -\frac{1}{b+\bar{b}}\Big[a+\bar{a}+(b+\bar{b})(n_0-6) - b(\Gamma_1+\Gamma_2) + \frac{c}{2}\Big] \\ C &= \frac{1}{b+\bar{b}}\frac{c}{2}. \end{aligned} \tag{2.25}$$

2.2.2 Second case: Arbitrary parametrisation of coherent states

In the appendix of [62] the structure for this type of parametrisation was laid out. In Refs. [71, 72] this parametrisation of coherent sates was used to study QPTs in excited rotational states in the SACM with the *cranking method*, but the observation of QPTs in physical observables has not yet been discussed.

A way to satisfy the transformation rule (2.18) is with spherical coordinates:

$$\begin{aligned} \alpha_0 &= \alpha\cos\theta \\ \alpha_{\pm 1} &= \frac{\alpha}{\sqrt{2}} e^{\pm i\phi}\sin\theta, \end{aligned} \tag{2.26}$$

where the variables (α, θ, ϕ) have the domains: $\alpha \in [0, \infty)$, $\theta \in [0, \pi]$ and $\phi \in [0, 2\pi)$. Again, the α variable can be related to the distance between clusters and the angle variables to their orientation [70]. Using (2.26) and applying the couplings in the semi-classical potential (2.19) leads to a two dimensional potential dependent on four parameters:

$$V(\alpha, \theta; c_i) = V_0 + \Big(A + E\cos 2\theta\Big)\alpha^2 \frac{F_{11}(\alpha^2)}{F_{00}(\alpha^2)} + \Big(B + F\cos 2\theta + C\sin^2 2\theta\Big)\,\alpha^4 \frac{F_{22}(\alpha^2)}{F_{00}(\alpha^2)} - (b + \bar{b})\alpha^6 \frac{F_{33}(\alpha^2)}{F_{00}(\alpha^2)} + D\cos 2\theta \alpha^2 \frac{F_{20}(\alpha^2)}{F_{00}(\alpha^2)}, \tag{2.27}$$

and we can notice that the potential is independent of ϕ. The constant term V_0 is given by

$$V_0 = (a + n_0 b)\langle \boldsymbol{C}_2(\lambda_C, \mu_C)\rangle + \xi\langle \boldsymbol{L}_C^2\rangle + \frac{c}{4}(N + n_0)(N + n_0 - 1) + t_1\langle \boldsymbol{K}^2\rangle. \tag{2.28}$$

The control parameters $c_i = \{A, B, C, D, E, F\}$ of the potential are linear combination of the Hamiltonian parameters, and are given by

$$A = \hbar\omega - b\langle \boldsymbol{C}_2(\lambda_C, \mu_C)\rangle + 4\Big((a + \bar{a}) + (b + \bar{b})(n_0 - 1)\Big) - \frac{c}{2}(N + n_0 - 1) - \Big(a + b(n_0 - 1)\Big)(\Gamma_1 + \Gamma_2) + 2\xi \tag{2.29}$$

$$B = a + \bar{a} + (b + \bar{b})(n_0 - 6) + \frac{c}{2} + b(\Gamma_1 + \Gamma_2) \tag{2.30}$$

$$C = \xi - \frac{c}{4} \tag{2.31}$$

$$D = \frac{c}{2} \tag{2.32}$$

$$E = -3\Big(a + b(n_0 - 1)\Big)(\Gamma_1 + \Gamma_2) \tag{2.33}$$

$$F = 3b(\Gamma_1 + \Gamma_2). \tag{2.34}$$

In Appendix B we discuss the critical points of certain types of two variable functions dependent on parameters as it will be of use when applying catastrophe theory to the semi-classical potential (2.27) in the following sections.

2.3 Catastrophe theory

The catastrophe theory formalism provides a framework for the study of QPTs [41]. The essence of catastrophe theory lies in the determination of the characteristic of a function's critical points in terms of their parameters, i.e. one is able to tell how many maxima, minima and saddle points a function has depending of the values on the parameters taken. A critical point serves as an indication of stability. Then a change of the parameters can imply a change of the critical points of the function. There exists a great number of research and applications of catastrophe theory in very different areas of physics [75–83].

For our purpose the final goal of the methods of catastrophe theory is to divide the parameter space in regions where the function has qualitative similar behaviour. Two important separatrices are necessary for this: The bifurcation set and the Maxwell set [41]:

- The bifurcation set is the subspace of parameter space delimiting the emergence of critical points of the function.
- The Maxwell set is the subspace of parameter space where two or more extrema of the function coincide.

The importance of these subspaces lies in that they delimit regions of changes for the stability of the potential. In the case of the bifurcation set it means the emergence of new stability points, e.g. minima. In the case of the Maxwell set it means a change between two stability points, e.g. the global minimum jumps to a different one by a variation of the parameters.

Now we shall describe the steps of the catastrophe theory program to obtain these separatrices.

1. The fundamental root of the function is a critical point which is independent of the values taken by the parameters. A Taylor series expansion about the fundamental root is performed, and the first non constant terms are subsequently eliminated by specific selections of the control parameters. These selections define the *essential parameters* of the function [4]. The last Taylor series expansion term which can't be eliminated without vanishing the whole function is called the *germ* of the function. By performing a change of variables it is possible to eliminate the tail of the Taylor series, so that the germ is all that remains in that subspace of the essential parameter space [41].

2. Once that essential parameters of the function are defined we construct the critical manifold of the function. Given a one dimensional function $V(x; c_i)$ dependent on n parameters, the critical manifold is defined as the hyper-surface of critical points x_c spanned by the n parameters $(c_1, \ldots, c_n)$ satisfying $\nabla V(x_c; c_i) = 0$. The bifurcation set is identified as the subspace in parameter space where the mapping of the critical manifold to parameter space is singular [41], i.e. when the Jacobian determinant of this transformation vanishes.

3. The Maxwell set is commonly obtained by solving the so-called Clausius-Claperyon equations [41]. These are a set of differential equations, which even for the simple examples of the elementary catastrophe can prove to be quite complex. Then this method is not ideal when dealing with a more involved potential function, such as the semi-classical potential we will be treating in this work. A method was described in [47] analogous to the method for the bifurcation set to circumvent these difficulties. The new method consists in constructing the roots manifold, which is the hyper-surface of roots x_r spanned by the n parameters $(c_1, \ldots, c_n)$ satisfying $V(x_r; c_i) + V_0 = 0$, where V_0 is an arbitrary real number. The Maxwell set is identified as the subspace in parameter space where for two roots x_1 and x_2 the mapping of the roots manifold to the parameter space is singular for the same set of parameters.

In Appendix C explicit expressions for the bifurcation and Maxwell set of an arbitrary one dimensional function, depending on four parameters, are obtained.

2.3.1 Example: Cusp catastrophe

In this subsection we will apply the methods described in the previous subsection and in Appendix C to the simple example of the elementary cusp catastrophe [41]. The cusp catastrophe is given by

$$f(x;a,b,c) = \frac{a}{4}x^4 + \frac{b}{2}x^2 + cx, \tag{2.35}$$

where $x \in (-\infty, \infty)$ and a, b and c are real parameters. Parameter a only serves as a scale, with $a > 0$, as it can be factorised of (2.35), and the cusp catastrophe only depends on two essential parameters. The first term of the Taylor series expansion vanishes when $c = 0$ and the second term vanishes when $b = 0$, and no further term can be eliminated. Then, the *germ* of the cusp catastrophe is x^4.

The critical points of $f(x;a,b,c)$ are the x_c values for which the first derivative of (2.35) with respect to x is zero:

$$\left.\frac{\mathrm{d}f(x;a,b,c)}{\mathrm{d}x}\right|_{x=x_c} = ax_c^3 + bx_c + c = 0. \tag{2.36}$$

The critical manifold is then the surface of the critical points x_c spanned by a continuous variation of parameters (a,b,c). In Fig. 2.2 we plotted the critical manifold, for $a = 1$, spanned by (b,c).

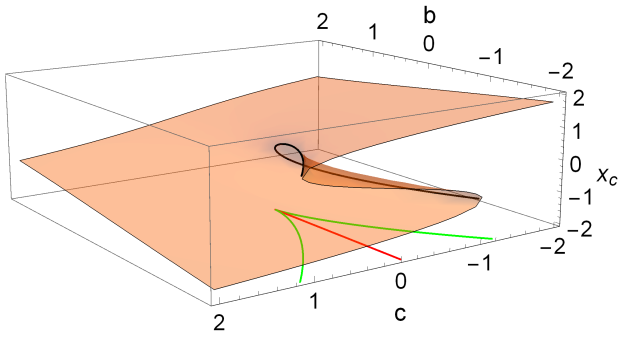

Figure 2.2: Critical manifold (b,c,x_c) for the cusp catastrophe with $a = 1$. The bifurcation set is shown as the green curve in the (b,c)-plane, which corresponds to the projection of the set of points where the tangent plane to the surface is vertical.

Our goal is now to apply the formulae in Appendix C and obtain the bifurcation and Maxwell sets for this simple case.

To obtain the bifurcation set we consider the mapping of the critical manifold to the parameter space: $(x_c;b,c) \mapsto (b,c)$, where we left a out as it only sets the scale and may be factored out. Solving (2.36) for c we can write it in terms of the critical point x_c and b:

$$c(x_c,b) = -ax_c^3 - bx_c. \tag{2.37}$$

Then the mapping is $(x_c, b) \mapsto (b, c)$, and the Jacobian determinant of the transformation is:

$$\det \begin{bmatrix} \frac{\partial b}{\partial x_c} & \frac{\partial b}{\partial b} \\ \frac{\partial c}{\partial x_c} & \frac{\partial c}{\partial b} \end{bmatrix} = \begin{vmatrix} 0 & 1 \\ \frac{\partial c}{\partial x_c} & \frac{\partial c}{\partial b} \end{vmatrix} = -\frac{\partial c}{\partial x_c}. \tag{2.38}$$

Using (2.37) we obtain the Jacobian determinant as:

$$-\frac{\partial c}{\partial x_c} = 3ax_c^2 + b. \tag{2.39}$$

The transformation is singular when the Jacobian determinant vanishes, i.e. when (2.39) equals zero or, solving for b, when

$$b(x_c) = -3ax_c^2. \tag{2.40}$$

In return, we can substitute this result in (2.37) to obtain c as a function of x_c

$$c(x_c) = 2ax_c^3. \tag{2.41}$$

We have now found the subspace in parameter space (b, c) parametrised by x_c known as the bifurcation set, and it is given by

$$\mathcal{C}_B = \{(b, c) = (-3ax_c^2, 2ax_c^3) \mid x_c \in \mathbb{R}\}. \tag{2.42}$$

In Fig. 2.2 the bifurcation set is shown as the projection in parameter space (b, c) where the tangent plane to the critical manifold is vertical. In Fig 2.3 parameter space (b, c) is drawn with a representative function depicted for each region. It is also possible to write the parametrise curve (2.42) as the more well known expression [41]:

$$\left(\frac{b}{3a}\right)^3 + \left(\frac{c}{2a}\right)^2 = 0, \tag{2.43}$$

which is obtained by eliminating x_c in (2.40) and (2.41).

The Maxwell set is the subspace in parameter space where two or more extrema of the function (2.35) have the same value, i.e. for x_1 and x_2 critical points we have

$$f(x_1; a, b, c) = f(x_2; a, b, c) = -f_0, \tag{2.44}$$

where f_0 is a real number. Condition (2.44) allow us to consider the roots of the function

$$f(x_r; a, b, c) + f_0 = 0. \tag{2.45}$$

The roots manifold is the surface of roots x_r of (2.45) spanned by a variation of parameters (a, b, c) for a fixed f_0.

The intersection of the critical manifold and the roots manifold, i.e. when a point x_1 is a critical point and $f(x_1; a, b, c)$ is equal to $-f_0$, occurs in the set of points when the tangent plane to the roots manifold is vertical. This is because a critical point emerges at the coalescence of two roots. Then, analogously, we may define the Maxwell set as the subspace in parameter space (b, c) where the mapping of the roots manifold to the

parameter space $(x_r; b, c) \mapsto (b, c)$ is singular for two different critical points x_1 and x_2. The first step is then to determine where the Jacobian determinant of this transformations is singular.

From (2.44) we can solve for c and get

$$c(x_r, a, b, f_0) = -\frac{a}{4}x_r^3 - \frac{b}{2}x_r - \frac{f_0}{x_r}. \tag{2.46}$$

Then the mapping is $(x_r, b) \mapsto (b, c)$, and the Jacobian determinant of the transformation is exactly the same as (2.38):

$$-\frac{\partial c}{\partial x_r} = \frac{3}{4}ax_r^2 + \frac{b}{2} - \frac{f_0}{x_r^2}. \tag{2.47}$$

The transformation is singular when (2.47) is equal to zero, this allows us to solve for b and we get:

$$b(x_r, a, f_0) = -\frac{3}{2}ax_r^2 + 2\frac{f_0}{x_r^2}. \tag{2.48}$$

In return, we can substitute this result in (2.46) to obtain c as a function of x_c and f_0

$$c(x_r, a, f_0) = \frac{a}{2}x_r^3 - 2\frac{f_0}{x_r}. \tag{2.49}$$

A way to prove that x_r is also a critical point is to directly substitute both (2.48) and (2.49) in (2.36), with $x_r = x_c$, and see that it is automatically satisfied.

In the Maxwell set mapping of the roots manifold must be singular for two different values x_1 and x_2 simultaneously for the same set of parameters, i.e. the following set of equations must be satisfied:

$$b(x_1, a, f_0) = b(x_2, a, f_0) \tag{2.50}$$
$$c(x_1, a, f_0) = c(x_2, a, f_0). \tag{2.51}$$

This sets of equations can be written as

$$-(x_1^2 - x_2^2)\left[\frac{3}{2}ax_1^2x_2^2 + 2f_0\right] = 0 \tag{2.52}$$
$$(x_1 - x_2)\left[\frac{1}{2}ax_1x_2\left(x_1^2 + x_1x_2 + x_2^2\right) + 2f_0\right] = 0. \tag{2.53}$$

From (2.53) we obtain that $x_1 = -x_2$, and directly substituting in (2.52) we get

$$x_1^2 \equiv x_r^2 = 2\sqrt{\frac{f_0}{a}}. \tag{2.54}$$

Substituting back (2.54) in (2.48) and (2.49) gives us:

$$b = -ax_r^2 \tag{2.55}$$
$$c = 0. \tag{2.56}$$

The subspace in parameter space (b, c) parametrised by x_r defined in (2.55) and (2.56) is the Maxwell set, and it is given by

$$\mathcal{C}_M = \{(b, c) = (-ax_r^2, 0) \mid x_r \in \mathbb{R}\}. \tag{2.57}$$

The Maxwell set in parameter space (b, c) is the negative half of the b-axis, shown as a dashed line in Fig. 2.3.

The results of the Maxwell set may be summarised as follows: The function $f(x; a, b, c)$ has two critical points when $b < 0$ and $c = 0$, localised at $x_\pm = \pm\sqrt{-b/a}$. They correspond to minima with a value of $f_0 = ab^2/4$.

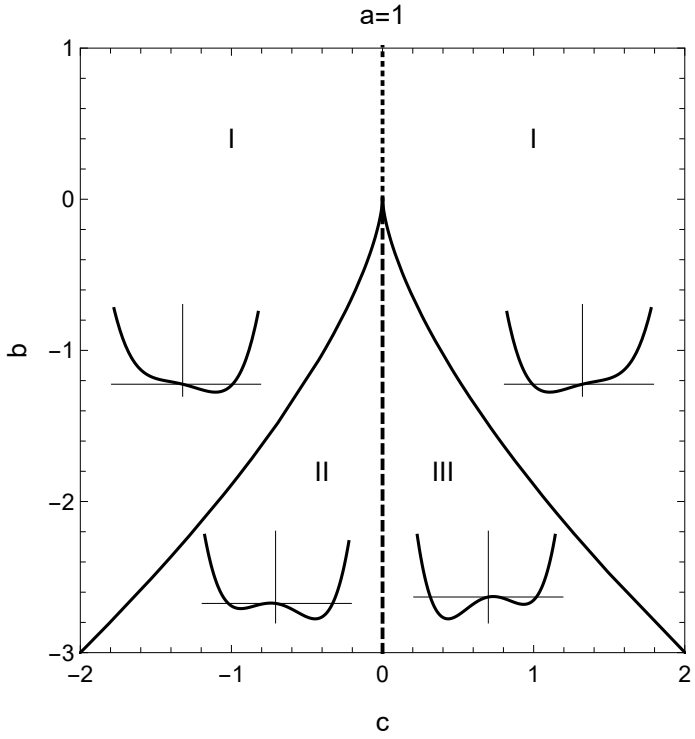

Figure 2.3: Parameter space (b, c) of the cusp catastrophe given in (2.35). Three different regions are identified and a representative function is shown in each of them. Crossing the dashed line from region II to region III results in a first order phase transition.

2.4 Quantum phase transitions

A phase transition is an important phenomenon in physics which is characterised by a drastic change in the physical properties of a system as a control parameter is varied. A common example is the phases of water, and how phase transitions occur when the temperature reaches a critical value, e.g. water evaporates when reaching $T_c = 100°\text{C}$.

Phenomena with similar qualities to that of phase transitions, but that takes place in a quantum level, with infinite degrees of freedom, are called a quantum phase transitions.

The traces of QPTs are usually more difficult to see in physical observables, as the changes produced as the control parameters are varied are more faint than the drastic changes in their classical counterparts. The study of QPTs in a wide variety of areas in physics is very rich ranging from non-Hermitian quantum mechanics to spin systems and collective models [84–93]. A very recent review on QPTs in algebraic and collective models can be found in [94]. In [95] a related phenomenon called excited state quantum phase transitions (ESQPT) was investigated in interacting many-body systems, and a recent review on this subject can be found in [96].

One is often able to construct separatrices in the space of control parameters which divide it in regions representatives of the different phases. Trajectories in parameter space can then be found when one varies the control parameters going from one region to another such that a phase transition occurs. Going from one phase to another means a change in the global minimum of the potential function describing the physical system.

One of the main properties of phase transitions is their order. A trajectory in parameter space can be parametrised by a single parameter s: $c(s)$. According to Ehrenfest's classification the order of a phase transition is defined by the discontinuity of the n-th derivative of the minimum of the potential with respect to the control parameters. Then, a phase transition is of n-th order if there exists a point s_0 where the first $n-1$ derivatives of the global minimum of the potential with respect to s is continuous and it is discontinuous for the n-th derivative:

$$\lim_{\epsilon\to 0}\left.\frac{\mathrm{d}^k V_{min}(c(s))}{\mathrm{d}s^k}\right|_{s_0-\epsilon} = \lim_{\epsilon\to 0}\left.\frac{\mathrm{d}^k V_{min}(c(s))}{\mathrm{d}s^k}\right|_{s_0+\epsilon}, \qquad k=1,2,\ldots,n-1 \tag{2.58}$$

$$\lim_{\epsilon\to 0}\left.\frac{\mathrm{d}^n V_{min}(c(s))}{\mathrm{d}s^n}\right|_{s_0-\epsilon} \neq \lim_{\epsilon\to 0}\left.\frac{\mathrm{d}^n V_{min}(c(s))}{\mathrm{d}s^n}\right|_{s_0+\epsilon}. \tag{2.59}$$

The order of the phase transition depends on the path taken in parameter space.

We shall continue with the cusp catastrophe example of the previous section to study the properties of its phase transitions.

2.4.1 Example: QPTs in the cusp catastrophe

Let us consider the Hamiltonian of the potential (2.35) of the cusp catastrophe in $\hbar = 2m = 1$ units:

$$H = p^2 + \frac{a}{4}x^4 + \frac{b}{2}x^2 + cx, \tag{2.60}$$

where p is the one dimensional momentum operator

$$p = -i\frac{\mathrm{d}}{\mathrm{d}x} \tag{2.61}$$

The main goal of this subsection is to try to match the phase transition analysis of the potential (2.35) with changes of the energy levels of the quantum Hamiltonian (2.60). This will prove useful when we deal with the QPTs in the semi-classical potential of the SACM in the following sections.

There are two QPTs in the cusp catastrophe, one of first order and one of second order. The first order phase transition happens when the c parameter changes from negative to

positive crossing the Maxwell set. Here the global minimum jumps from one located at $x < 0$ to a new one located at $x > 0$, as shown in Fig. 2.3.

In Fig. 2.4 we plot the path taken in parameter space for a first order QPT along with the associated energy levels of the Hamiltonian (2.60).

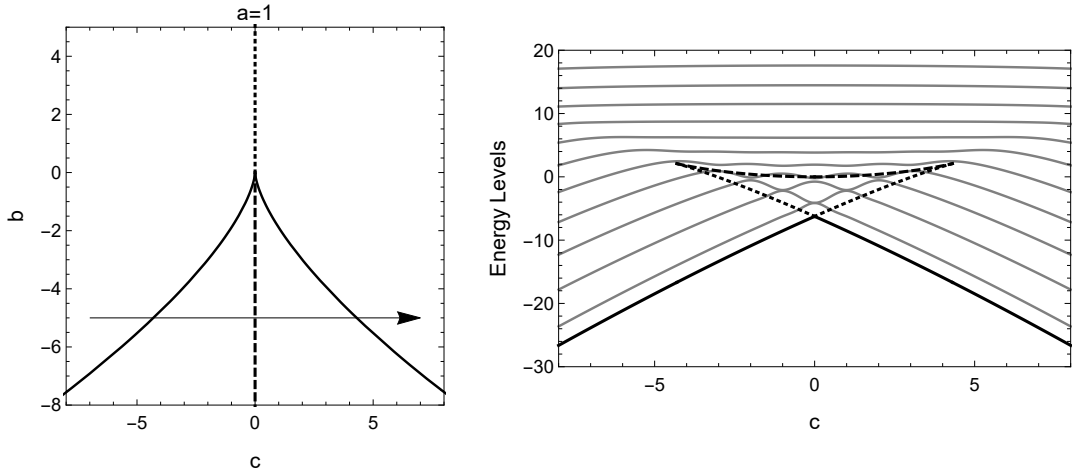

Figure 2.4: In the left plot we show the parameter space (b, c) of the cusp catastrophe for $a = 1$. The bifurcation set and the Maxwell set are depicted as a solid and dashed lines, respectively. The arrow is the trajectory taken, with fixed $b = -5$, where a first order phase transition occurs at $c = 0$, when crossing the Maxwell set. In the right plot we show the energy levels of the first bounded states as gray lines. The global minimum of the potential is depicted as a solid line, the local minimum is depicted as a dotted line and the local maximum is depicted as a dashed line. We can see that when the bifurcation set is crossed, and a second local minimum emerges, avoided energy levels crossings begin to occur for the excited states.

The second order phase transition happens at $c = 0$ when the parameter b changes from positive to negative passing through the origin $(b = 0, c = 0)$ where the potential is x^4, i.e. the *germ* of the potential. The phase transition occurs at $b = 0$. The critical points in this case can be easily found in (2.36) with $c = 0$:

$$x_1 = 0 \tag{2.62}$$

$$x_\pm = \pm\sqrt{-\frac{b}{a}}. \tag{2.63}$$

Here the global minimum at $x_1 = 0$ for $b > 0$ splits into two equally deep minima at $x_\pm = \pm\sqrt{b/a}$ for $b < 0$ and x_1 becomes a maximum. The potential evaluated at the global minimum x_1 for $b > 0$ is zero, and all derivatives with respect to b are also zero:

$$\left.\frac{\mathrm{d}^k V(x_1)}{\mathrm{d}b^k}\right|_{b=0^+} = 0, \qquad k = 1, 2, \ldots \tag{2.64}$$

The potential evaluated at the global minima $x_\pm$ for $b < 0$ is equal to:

$$V(x_\pm(b)) = -\frac{1}{4a}b^2. \tag{2.65}$$

The first two derivatives of (2.65) with respect to b evaluated at $b = 0$ are

$$\left.\frac{\mathrm{d}V(x_\pm)}{\mathrm{d}b}\right|_{b=0^-} = 0 \tag{2.66}$$

$$\left.\frac{\mathrm{d}^2V(x_\pm)}{\mathrm{d}b^2}\right|_{b=0^-} = -\frac{1}{2a}. \tag{2.67}$$

Comparing both results we encounter a discontinuity of the second derivative at $b = 0$:

$$\left.\frac{\mathrm{d}^2V(x_1)}{\mathrm{d}b^2}\right|_{b=0^+} \neq \left.\frac{\mathrm{d}^2V(x_\pm)}{\mathrm{d}b^2}\right|_{b=0^-} \tag{2.68}$$

and we say the phase transition is of second order.

In Fig. 2.5 we plot the path taken in parameter space for a second order QPT along with the associated energy levels of the Hamiltonian (2.60). After the point of the phase transition $b = 0$, as the parameter b decreases, pairs of eigenvalues become almost degenerate with negative energy. This is because the energy states begin to settle in the double wells, which are equally deep.

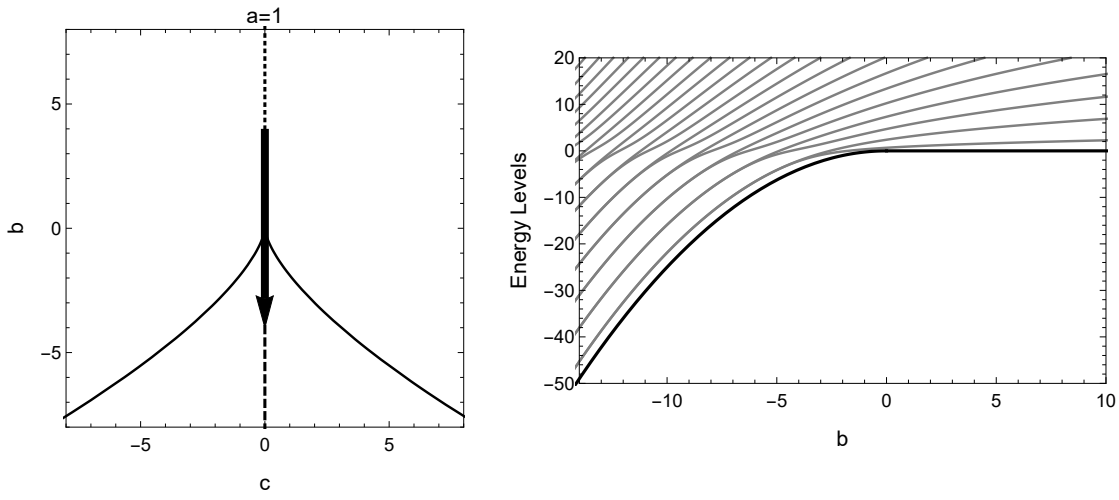

Figure 2.5: In the left plot we show the parameter space (b, c) of the cusp catastrophe for $a = 1$. The bifurcation set and the Maxwell set are depicted as a solid and dashed lines, respectively. The arrow is the trajectory taken, with fixed $c = 0$, where a second order phase transition occurs at $b = 0$, when crossing the origin $(b = 0, c = 0)$. In the right plot we show the energy levels of the first bounded states as gray lines. The potential global minimum is depicted as a solid line.

This analysis of QPT of the cusp catastrophe has been previously done in [86], where they focus on the QPT of the excited states, characterised by the avoided energy levels.

Parameter space regions		
Region	Number of extrema (minima)	Potential characteristics
I	1 (1)	For $c < 0$ ($c > 0$) a single minima is located at $x_c > 0$ ($x_c < 0$). For $c = 0$ the potential goes as x^2 in the limit $x \to 0$.
II	3 (2)	There are two coexisting minima at $x_- < 0$ and $x_+ > 0$, with $V(x_-) > V(x_+)$. In between there is a maximum.
III	3 (2)	There are two coexisting minima at $x_- < 0$ and $x_+ > 0$, with $V(x_-) < V(x_+)$. There is a maximum in between.
Maxwell set	3 (2)	At $b < 0$ and $c = 0$. There are two equally deep minima $V(x_\pm) = -b^2/(4a)$, located at $x_\pm = \pm\sqrt{-\frac{b}{a}}$. There is a maximum in between.
Bifurcation set	2 (1)	The potential has a minimum and a saddle point.

The purpose of this example was to show that the methods of catastrophe theory are useful in the study of QPTs, as has been previously done in many works [4,19,27,34,44–46], and to prepare ourselves for utilising these same methods for more complicated potentials. In the next section we will apply these same steps in the semi-classical potentials (2.23) and (2.27) of the SACM, and find a way to match the quantum behaviour of energy states and other observables to the semi-classical analysis.

2.5 Quantum phase transitions in the SACM

In order to test the semi-classical potentials of the SACM we need to consider particular examples to obtain value of n_0, $\hbar\omega$, and of the deformation parameter β_k of the k-th cluster. For this purpose in this work we shall consider two examples, one corresponds to a system of spherical clusters $^{16}\mathrm{O} + \alpha \to {}^{20}\mathrm{Ne}$, and the other to a system of two deformed clusters $^{12}\mathrm{C} + {}^{12}\mathrm{C} \to {}^{24}\mathrm{Mg}$.

First a semi-classical analysis of QPTs in the respective parameter space will be performed in the SU(3) limit of the Hamiltonian, and in a Hamiltonian with an added term of the SO(4) dynamical symmetry, and all information available will be extracted. Secondly, we will search for appropriate regions in parameter space and map back to the interaction parameter of the Hamiltonian in order to look for signatures of QPTs in physical observables, e.g. energy levels and probability transitions.

Summary of QPTs for the cusp catastrophe	
Transition	Behaviour of energy levels
Region I to region II	Avoided crossing energy levels begin to occur for excited states.
Region II to region II	*First order phase transition.* Avoided crossing energy level for the ground state.
$b > 0$ to $b < 0$ at $c = 0$	*Second order phase transition.* Almost degeneracy of energy pairs, starting with the ground state and first excited state.

2.5.1 Tensor parametrisation of coherent states

We start by recalling the one-dimensional semi-classical potential obtained in (2.23):

$$V(\alpha; c_i) = V_0 - (b + \bar{b}) \left(A\alpha^2 \frac{F_{11}(\alpha)}{F_{00}(\alpha)} + B\alpha^4 \frac{F_{22}(\alpha)}{F_{00}(\alpha)} + \alpha^6 \frac{F_{33}(\alpha)}{F_{00}(\alpha)} + C\alpha^2 \frac{F_{20}(\alpha)}{F_{00}(\alpha)} \right), \quad (2.69)$$

with the constant value V_0 given by

$$V_0 = (a + n_0 b)\langle \boldsymbol{C}_2(\lambda_C, \mu_C)\rangle + \xi \langle \boldsymbol{L}_C^2 \rangle + \frac{c}{4}(N + n_0)(N + n_0 - 1), \quad (2.70)$$

and the relation of parameters given by

$$\begin{aligned} A &= -\frac{1}{b + \bar{b}} \Big[\hbar\omega - b\langle \boldsymbol{C}_2(\lambda_C, \mu_C)\rangle + 4\Big(a + \bar{a} + (b + \bar{b})(n_0 - 1)\Big) \\ &\quad + \Big(a + b(n_0 - 1)\Big)(\Gamma_1 + \Gamma_2) + 2\xi - \frac{c}{2}(N + n_0 - 1) \Big] \\ B &= -\frac{1}{b + \bar{b}} \Big[a + \bar{a} + (b + \bar{b})(n_0 - 6) - b(\Gamma_1 + \Gamma_2) + \frac{c}{2} \Big] \\ C &= \frac{1}{b + \bar{b}} \frac{c}{2}. \end{aligned} \quad (2.71)$$

The origin $\alpha = 0$ is the fundamental root of the semi-classical potential (2.69). The functions $F_{pq}(\alpha)$ in (2.21) are polynomials in powers of α^2 with positive coefficients. Therefore, the potential does not have singularities for real α. For arbitrary n_0 and N the first terms of each of the rational functions that appear in the potential are:

$$\alpha^2 \frac{F_{11}(\alpha)}{F_{00}(\alpha)} = \frac{n_0 + N(n_0 + 1)^2\alpha^2 + N(N - 1)(n_0 + 2)^2(n_0 + 1)\frac{\alpha^4}{2!} + \dots}{1 + N(n_0 + 1)\alpha^2 + N(N - 1)(n_0 + 2)(n_0 + 1)\frac{\alpha^4}{2!} + \dots} \quad (2.72)$$

$$\alpha^4 \frac{F_{22}(\alpha)}{F_{00}(\alpha)} = \frac{n_0(n_0 - 1) + N(n_0 + 1)^2 n_0\alpha^2 + N(N - 1)(n_0 + 2)^2(n_0 + 1)^2\frac{\alpha^4}{2!} + \dots}{1 + N(n_0 + 1)\alpha^2 + N(N - 1)(n_0 + 2)(n_0 + 1)\frac{\alpha^4}{2!} + \dots} \quad (2.73)$$

$$\alpha^6 \frac{F_{33}(\alpha)}{F_{00}(\alpha)} = \frac{n_0(n_0 - 1)(n_0 - 2) + N(n_0 + 1)^2 n_0(n_0 + 1)\alpha^2 + \dots}{1 + N(n_0 + 1)\alpha^2 + N(N - 1)(n_0 + 2)(n_0 + 1)\frac{\alpha^4}{2!} + \dots} \quad (2.74)$$

$$\begin{aligned} \alpha^2 \frac{F_{20}(\alpha)}{F_{00}(\alpha)} &= N(N - 1)(n_0 + 2)(n_0 + 1)\alpha^2 \\ &\quad \times \frac{\frac{1}{2} + (N - 2)(n_0 + 3)\frac{\alpha^2}{3!} + \dots}{1 + N(n_0 + 1)\alpha^2 + N(N - 1)(n_0 + 2)(n_0 + 1)\frac{\alpha^4}{2!} + \dots}. \end{aligned} \quad (2.75)$$

Then, the first derivative of the potential with respect to α will have the global α factor, meaning that at $\alpha = 0$ the first derivative vanishes independently of all values of the parameters $\{A, B, C\}$.

Following the steps enumerated in a previous section, we begin by expanding (2.69) in a Taylor series about the fundamental root $\alpha = 0$:

$$V(\alpha; A, B, C) = V_0 - (b + \bar{b}) \left(T_0 + T_1\alpha^2 + T_2\alpha^4 + T_3\alpha^6 + \ldots\right), \tag{2.76}$$

where the first coefficients are given by:

$$T_0 = n_0 A + n_0(n_0 - 1)B + n_0(n_0 - 1)(n_0 - 2) \tag{2.77}$$

$$T_1 = N(n_0 + 1)\left[A + 2n_0 B + 3n_0(n_0 - 1) + \frac{1}{2}(N - 1)(n_0 + 2)C\right] \tag{2.78}$$

$$\begin{aligned} T_2 = \frac{1}{2}N(n_0 + 1)\Big[&(n_0(N + 1) + 2)A + (N(2n_0^2 - n_0 - 2) + (n_0 + 2)(2n_0 + 1))B \\ &+3n_0(N(n_0(n_0 - 2) - 2) + n_0(n_0 + 2)) + \frac{2}{3}(N - 1)(n_0 + 2)(n_0(N + 1) + 3)C\Big] \end{aligned} \tag{2.79}$$

The next coefficients become more convoluted and writing them explicitly is not worthwhile for our purpose as we only use the first three coefficients.

The coefficient T_1 is eliminated with the following relation of parameters:

$$\frac{1}{N}(n_0 + 1)\left[A + 2n_0 B + 3n_0(n_0 - 1) + \frac{1}{2}(N - 1)(n_0 + 2)C\right] = 0. \tag{2.80}$$

We can solve (2.80) for A and substitute the result in (2.79), then the coefficient T_2 is eliminated with the following relation of parameters:

$$\frac{1}{2}N(N - 1)(n_0 + 2)(n_0 + 1)\left[B + 3n_0 - \frac{1}{6}(n_0(N + 1) + 6)C\right] = 0. \tag{2.81}$$

We can solve (2.80) for B and substitute the result in T_3. Then, the coefficient of α^6 is eliminated with the following relation of parameters:

$$\frac{1}{6}N(N - 1)(N - 2)(n_0 + 3)(n_0 + 2)(n_0 + 1)\left[1 + \frac{1}{24}n_0(N + 1)C\right] = 0. \tag{2.82}$$

The next coefficient T_4 of α^8 is independent of parameters if (2.80), (2.81) and (2.82) are satisfied. This defines the *germ* of the potential as α^8.

Conditions (2.80), (2.81) and (2.82) define the essential parameters (r_1, r_2, r_3, r_4) as:

$$\begin{aligned} r_1 &= A + 2n_0 B + 3n_0(n_0 - 1) + \frac{1}{2}(N - 1)(n_0 + 2)C \\ r_2 &= B + 3n_0 - \frac{1}{6}\left(n_0(N + 1) + 6\right)C \\ r_3 &= -(b + \bar{b}) \\ r_4 &= \frac{1}{6}n_0(N + 1)C. \end{aligned} \tag{2.83}$$

The reason to define the essential parameter r_4 as such, and not exactly as (2.82), is so that there is a parameter carries the dependence on the c parameter in the semi-classical potential, i.e. of the SO(4) symmetry.

The next step is to rewrite the semi-classical potential (2.69) in terms of the essential parameters (2.83). To do this we start by subtracting V_0 and the constant term of the Taylor series expansion T_0 from the potential:

$$\begin{aligned}\bar{V}(\alpha;A,B,C) &= V(\alpha;A,B,C) - V_0 + (b+\bar{b})T_0 \\ &= -\frac{(b+\bar{b})}{F_{00}(\alpha)}\Big[A\Big(\alpha^2 F_{11}(\alpha) - n_0 F_{00}(\alpha)\Big) + B\Big(\alpha^4 F_{22}(\alpha) - n_0(n_0-1)F_{00}(\alpha)\Big) \\ &\quad +\alpha^6 F_{33}(\alpha) - n_0(n_0-1)(n_0-2)F_{00}(\alpha) + C\alpha^2 F_{20}(\alpha)\Big]. \end{aligned} \tag{2.84}$$

The new potential $\bar{V}$ now tends to zero as $\alpha \to 0$.

Using the explicit expression for the functions $F_{pq}(\alpha)$ and expanding term by term we may rewrite them to incorporate the essential parameters. This is done by rewriting the terms appearing in (2.84) as sums of new polynomials $Q_i(\alpha)$:

$$\begin{aligned} F_{00}(\alpha) &= N!n_0!\alpha^{2n_0}Q_0(\alpha) \\ \alpha^2 F_{11}(\alpha) - n_0 F_{00}(\alpha) &= N!n_0!\alpha^{2n_0}Q_1(\alpha) \\ \alpha^4 F_{22}(\alpha) - n_0(n_0-1)F_{00}(\alpha) &= N!n_0!\alpha^{2n_0}\left[2n_0Q_1(\alpha) + Q_2(\alpha)\right] \\ \alpha^6 F_{33}(\alpha) - n_0(n_0-1)(n_0-2)F_{00}(\alpha) &= N!n_0!\alpha^{2n_0}\left[3n_0(n_0-1)Q_1(\alpha)\right. \\ &\quad \left. +3n_0Q_2(\alpha) + Q_3(\alpha)\right] \\ \alpha^2 F_{20}(\alpha) &= N!n_0!\alpha^{2n_0}\left[\frac{1}{2}(N-1)(n_0+2)Q_1(\alpha)\right. \\ &\quad \left. -\frac{1}{6}(n_0(N+1)+6)Q_2(\alpha) + \frac{1}{6}n_0(N+1)Q_4(\alpha)\right], \end{aligned} \tag{2.85}$$

where the $Q_i(\alpha)$ polynomials are defined as:

$$\begin{aligned} Q_i(\alpha) &= \sum_{k=i}^{N} \frac{N!}{(N-k)!}\frac{(n_0+k)!}{n_0!}\frac{\alpha^{2k}}{k!(k-i)!} \\ Q_4(\alpha) &= \sum_{k=3}^{N} \frac{N!}{(N-k)!}\frac{(n_0+k)!}{n_0!}\frac{\alpha^{2k}}{(k+1)!(k-3)!}. \end{aligned} \tag{2.86}$$

In Appendix D we show in detail how the expressions in (2.85) were obtained.

With the results in (2.85) we go back to (2.84) and rewrite the potential as:

$$\bar{V}(\alpha;r_i) = \frac{r_3}{Q_0(\alpha)}\left[r_1Q_1(\alpha) + r_2Q_2(\alpha) + Q_3(\alpha) + r_4Q_4(\alpha)\right] \tag{2.87}$$

and the essential parameter are defined in (2.83).

For fixed values of N the potential tends to finite values as $\alpha \to \infty$. For practical reasons we are satisfied with small values of N for the semi-classical and quantum treatments. However, the exact energy levels are obtained in the limit $N \to \infty$. In this limit the potential will tend to either ∞ or $-\infty$ as $\alpha \to \infty$, and the potential will be said to

be either stable or unstable, respectively. In the former case the potential is said to have definite stable wells, while in the latter case these wells would disappear as $N \to \infty$. This property serves to construct a separatrix in parameter space characterising the stability of the potential. Potentials with parameter values in the stable region will be said to have physical meaning, while potentials in the unstable region are said to be unphysical. This separatrix is obtained by studying the potential (2.87) in the limit $\alpha \to \infty$:

$$\lim_{\alpha\to\infty} \bar{V}(\alpha; r_i) = r_3 N \left(r_1 + r_2(N-1) + (N-1)(N-2) + r_4 \frac{(N-1)(N-2)}{N+1} \right), \quad (2.88)$$

and determining for which sets of parameters do equation (2.88) vanishes. The stability separatrix is defined as:

$$r_1 + r_2(N-1) + (N-1)(N-2) + r_4 \frac{(N-1)(N-2)}{N+1} = 0. \quad (2.89)$$

The semi-classical potential depends on four parameters, but one of them r_3 serves as a scale, so that all analysis can be done in a three-dimensional parameter space (r_1, r_2, r_4). Parameter r_4 is proportional to parameter c of the SO(4) symmetry. Then, when $r_4 = 0$ we are in the SU(3) limit, and we are dealing with a two-dimensional parameter space (r_1, r_2). These are the two cases contained in the potential (2.87): One is related to a purely SU(3) symmetric Hamiltonian, and the other is a Hamiltonian with terms relating to SU(3) and SO(4) dynamical symmetries.

2.5.1.1 Separatrices in parameter space

Following the formulae in Appendix C the bifurcation and Maxwell sets of the semi-classical potential (2.87) will be obtained. For this purpose we rename the rational functions appearing in the potential in the following way

$$g_i(\alpha) \equiv \frac{Q_i(\alpha)}{Q_0(\alpha)}, \quad (2.90)$$

so that the potential has a similar form as the one written in Appendix C:

$$\bar{V}(\alpha; r_i) = r_1 g_1(\alpha) + r_2 g_2(\alpha) + g_3(\alpha) + r_4 g_4(\alpha). \quad (2.91)$$

Bifurcation set

The bifurcation set is the parametric surface in three-dimensional space described by

$$\mathcal{C}_B = \left\{ \Big(r_1(\alpha_c; r_4), r_2(\alpha_c; r_4), r_4 \Big) \mid \alpha_c, r_4 \in \mathbb{R} \right\} \quad (2.92)$$

with r_1 and r_2 parametric functions of the critical point x_c and of r_4:

$$\begin{aligned} r_1 &= \frac{1}{W(g_1', g_2')} \Big(W(g_2', g_3') + r_4 W(g_2', g_4') \Big) \\ r_2 &= -\frac{1}{W(g_1', g_2')} \Big(W(g_1', g_3') + r_4 W(g_1', g_4') \Big), \end{aligned} \quad (2.93)$$

where the prime indicates differentiation with respect to α and $W(f,g) = f(\alpha)g'(\alpha) - f'(\alpha)g(\alpha)$ is the Wronskian determinant.

Maxwell set

The Maxwell set is the parametric surface in three-dimensional space described by

$$\mathcal{C}_M = \{(r_1(\alpha_c; r_4), r_2(\alpha_c; r_4), r_4) \mid \alpha_c, r_4 \in \mathbb{R}\}\,, \tag{2.94}$$

with r_1 and r_2 parametric functions of the critical point x_c and of r_4:

$$\begin{aligned} r_1 &= \frac{1}{W(g_1,g_2)}\Big(W(g_2,g_3) + r_4 W(g_2,g_4)\Big) \\ r_2 &= -\frac{1}{W(g_1,g_2)}\Big(W(g_1,g_3) + r_4 W(g_1,g_4)\Big). \end{aligned} \tag{2.95}$$

This is only valid for the case $V_0 = 0$, i.e. where both minima are zero, which is the only case when $r_4 = 0$. When $r_4 \neq 0$, and we are interested in searching for two equally deep wells of the potential where $V_0 \neq 0$, we will follow the steps described in Appendix C.

Continuation of the Bifurcation set

A particularity of this potential is that both the bifurcation set and the Maxwell set are finite segments in parameter space, meaning they have a beginning and an end. Both sets are parametrised by the critical point α_c with a domain $\alpha_c \in [0, \infty)$. For simplicity we will treat the two-dimensional parameter space (r_1, r_2) with $r_4 = 0$, knowing that the separatrices in three-dimensional space can be obtained with the new r_4-axis perpendicular to the (r_1, r_2)-plane. The beginning and end of both sets are at $\alpha_c = 0$ and $\alpha_c \to \infty$, respectively. Those two points then are continued by other separatrices. The beginning for both sets is the origin $(r_1 = 0, r_2 = 0, r_4 = 0)$, which is continued by the r_2-axis, or in three-dimensions the (r_2, r_4)-plane. The end of the Maxwell set is continued by the stability separatrix defined in (2.89).

Our goal now is to find the continuation of the bifurcation set. Given that the beginning of the bifurcation set and Maxwell set is the same, their ending should also be connected, as they share some properties. Similarly to the stability separatrix, this separatrix is also a straight line, and their slope is obtained by connecting the ends of the bifurcation set and the Maxwell set.

This plane is given by

$$r_2 = m r_1 + b, \tag{2.96}$$

with the slope m given by

$$m = \lim_{\alpha_c \to \infty} \frac{r_2^B(\alpha_c, r_4) - r_2^M(\alpha_c, r_4)}{r_1^B(\alpha_c, r_4) - r_1^M(\alpha_c, r_4)}, \tag{2.97}$$

and the intersection with the r_2 axis is given by

$$b = \lim_{\alpha_c \to \infty} \frac{r_1^B(\alpha_c, r_4) r_2^M(\alpha_c, r_4) - r_1^M(\alpha_c, r_4) r_2^B(\alpha_c, r_4)}{r_1^B(\alpha_c, r_4) - r_1^M(\alpha_c, r_4)}, \tag{2.98}$$

where the slope is independent of the parameter r_4 and the intersection depends on the parameter r_4. Here we use r_i^B and r_i^M to refer to the parametric functions that define the bifurcation set in (2.93) and the Maxwell set in (2.95), respectively.

These five separatrices: bifurcation set, Maxwell set, stability separatrix, continuation of the bifurcation set, along with the r_2-axis divide the two-dimensional parameter space (r_1, r_2) in nine regions where the semi-classical potential has qualitatively similar behaviour. The parameter space and their regions are shown in Fig. 2.6, along with pictures of representative potentials. In the next table we describe the potentials characteristics for each of the regions.

Parameter space regions of Fig. 2.6		
Region	Number of minima	Potential characteristics
I	1	The potential has a minimum at $\alpha_0 = 0$ and it tends to a positive value as $\alpha \to \infty$.
II	2	The potential has two minima at $\alpha_0 = 0$ and at $\alpha_c > 0$, with $V(\alpha_0) < V(\alpha_c)$. The potential tends to a positive value as $\alpha \to \infty$.
III	2	The potential has two minima at $\alpha_0 = 0$ and at $\alpha_c > 0$, with $V(\alpha_0) > V(\alpha_c)$. The potential tends to a positive value as $\alpha \to \infty$.
IV	1	The potential has one minimum at $\alpha_c > 0$ and it tends to a positive value as $\alpha \to \infty$.
V	1	The potential has one minimum at $\alpha_0 = 0$, a maximum at $\alpha_c > 0$, and a second minimum at $\alpha \to \infty$. The potential tends to a positive value as $\alpha \to \infty$.
VI	1	The potential has one minimum at $\alpha_c > 0$ and it tends to a negative value as $\alpha \to \infty$.
VII	2	The potential has two minima at $\alpha_0 = 0$ and at $\alpha_c > 0$, with $V(\alpha_0) > V(\alpha_c)$. The potential tends to a negative value as $\alpha \to \infty$.
VIII	1	The potential has one minimum at $\alpha \to \infty$. The potential tends to a negative value as $\alpha \to \infty$.
IX	2	The potential has one minimum at $\alpha_0 = 0$, a maximum at $\alpha_c > 0$, and second minimum at $\alpha \to \infty$. The potential tends to a negative value as $\alpha \to \infty$.
Maxwell set	2	The potential has two minima at $\alpha_0 = 0$ and at $\alpha_c > 0$, with $V(\alpha_0) = V(\alpha_c)$. The potential tends to a positive value as $\alpha \to \infty$.
Bifurcation set	1	The potential has a minimum at $\alpha_0 = 0$ and a saddle point at $\alpha_c > 0$. The potential tends to a positive value as $\alpha \to \infty$.
r_2-axis	1	The potential at $\alpha_0 = 0$ goes as α^4 as $\alpha \to 0$ it corresponds to a minimum for $r_2 > 0$ and to a maximum for $r_2 < 0$. At $(r_1 = 0, r_2 = 0)$ the potential has a minimum at $\alpha_0 = 0$ which goes as α^6 as $\alpha \to 0$.

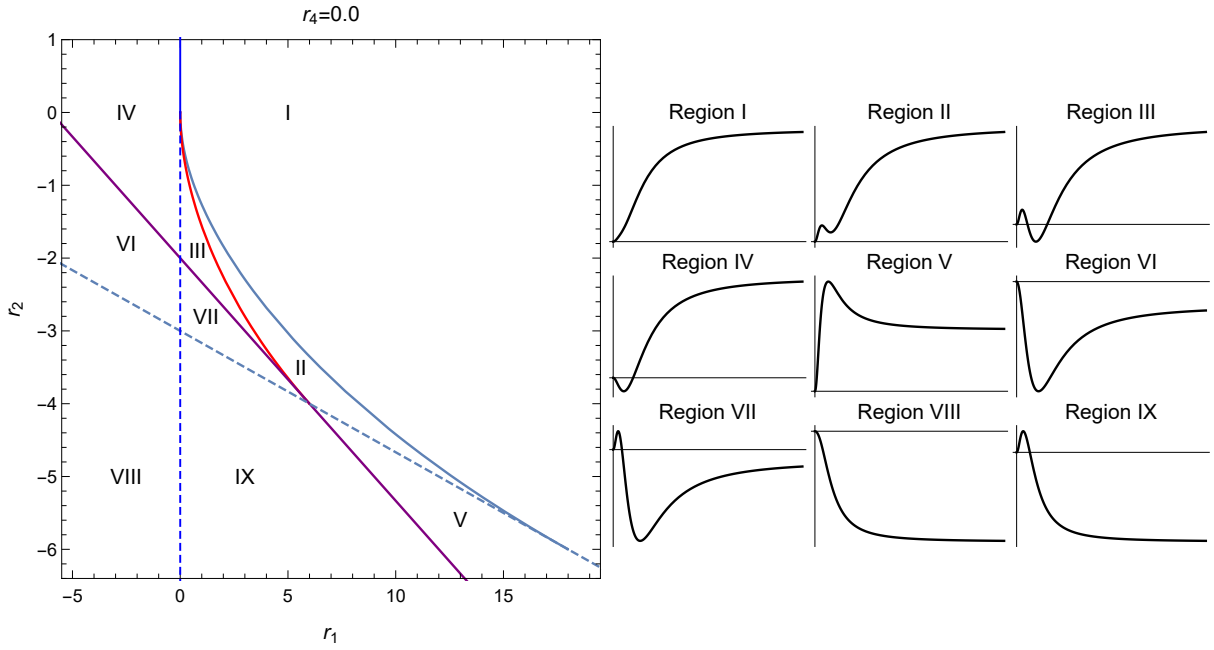

Figure 2.6: Parameter space (r_1, r_2) with $r_4 = 0$, corresponding to the SU(3) limit. The separatrices divide the parameter space in nine regions. In the right plots representative potentials for each region are depicted.

2.5.1.2 Example of two spherical clusters: $^{16}\mathrm{O} + \alpha \rightarrow {}^{20}\mathrm{Ne}$

A simple example to test the theoretical groundwork obtained by catastrophe theory applied to the SACM is that of a cluster system of two of spherical clusters. We choose the $^{16}\mathrm{O} + \alpha \rightarrow {}^{20}\mathrm{Ne}$ system. For this example we have: $n_0 = 8$, $\hbar\omega = 13.185$, deformations $\beta_{^{16}\mathrm{O}} = \beta_\alpha = 0$, and clusters irreps $(\lambda_1, \mu_1) = (\lambda_2, \mu_2) = (0, 0)$. In the numerical diagonalisation of the Hamiltonian we will consider 4 excitation quanta, i.e. $N = 4$. More accurate results when dealing with the fitting of the parameters to the experimental energy levels are obtained with larger values of N, but for the first energy levels the use of small values of N is sufficiently effective. Larger number of excitation quanta also means more computational time. In the semi-classical analysis the value of N has to be large, in order to allow the separatrices of the Maxwell and bifurcation sets to stabilise. However, the second order QPT separatrix is independent of the value of N, and the qualitative results obtained here are valid for any value of N.

According to the semi-classical analysis there are three QPTs in parameter space:

a) Going from region I to region IV crossing the (r_2, r_4)-plane (r_2-axis in the SU(3) limit) results in a *second order phase transition*, where the global minimum $V(\alpha_0) = 0$ at $\alpha_0 = 0$ disappears and continuously changes to a global minimum $V(\alpha_c) < 0$ at $\alpha_c > 0$.

b) Going from region II to region III crossing the Maxwell set results in a *first order phase transition*, where the previously local minimum $V(\alpha_c) > 0$ at $\alpha_c > 0$ becomes the global minimum $V(\alpha_c) < 0$ surpassing the minimum $V(\alpha_0) = 0$ at $\alpha_0 = 0$, i.e.

the global minimum $V(\alpha_0) = 0$ at $\alpha_0 = 0$ jumps to a global minimum $V(\alpha_c) < 0$ at $\alpha_c > 0$.

c) Going down the r_2-axis at a fixed $r_4 = 0$ crossing the origin $(r_1 = 0, r_2 = 0)$ results in a *third order phase transition*, where the global minimum $V(\alpha_0) = 0$ at $\alpha_0 = 0$ disappears and continuously changes to a global minimum $V(\alpha_c) < 0$ at $\alpha_c > 0$. The potential in the origin of parameter space $(r_1 = 0, r_2 = 0)$ goes as α^6 in the limit $\alpha \to 0$.

Different trajectories in parameter space can be drawn crossing the separatrices and going from one region to another. From the parameter relations in (2.83) and (2.71) we see that a change in the essential parameters r_i imply a change in the interaction parameters $\{\bar{a}, a, \bar{b}, b, c, \xi\}$. Of particular relevance in the study of phase transitions in the SU(3) limit is the parameter of the second order Casimir operator, which is related to the quadrupole operator, a and $\bar{a}$; while in the case of mixing SO(4) symmetry the parameter c is of importance. With this in mind a trajectory in parameter space is obtained by fixing the other parameters $\{\bar{b}, b, \xi, t_1\}$ appropriately and varying a, $\bar{a}$ and c depending on the case of interest.

Trajectory a)

In the table below we write down the set of parameters used to generate a trajectory in parameter space that goes from region I to region IV, crossing the r_2-axis:

Parameters for trajectory a) in example $^{16}\mathrm{O} + \alpha \to {}^{20}\mathrm{Ne}$						
$\bar{a}$	a	$\bar{b}$	b	c	ξ	t_1
$(-1.36, -0.94)$	0.0	-0.08	0.0	0.0	0.208	0.0

The global minimum of the semi-classical potential (2.69) can be obtained as a function of the absolute value of $\bar{a}$ as the parameters change along the trajectory described in a). At the point of crossing the r_2-axis a discontinuity of the second derivative with respect to $\bar{a}$ is present, characteristic of a second order phase transition. The ground state energy can be obtained by the diagonalisation of the Hamiltonian (2.12) as the parameters change along the same trajectory as a function of the absolute value of $\bar{a}$. In Fig. 2.7 we plotted both of these values and notice that the semi-classical value is higher according to the variational principle, in the bottom plot we overlap both plots and notice a very good agreement in their shapes.

In the left of Fig. 2.8 we show the trajectory in a) as an arrow crossing the r_2-axis in parameter space. In the bottom we plotted the energy of the first 0^+ states as a function of the absolute value of $\bar{a}$. Near the point of the phase transition at $\bar{a} = -1.11$, depicted as a vertical dashed line, a first avoided level crossing between the ground state 0_1^+ at energy zero and the excited state 0_2^+ occurs. As the magnitude of parameter $\bar{a}$ increases two more avoided energy level crossings occur, one between the 0_2^+ and 0_3^+ states and another again between the ground state 0_1^+ and the state 0_2^+.

Trajectory b)

In the table below we write down the set of parameters used to generate a trajectory in parameter space that goes from region II to region III, crossing the Maxwell set:

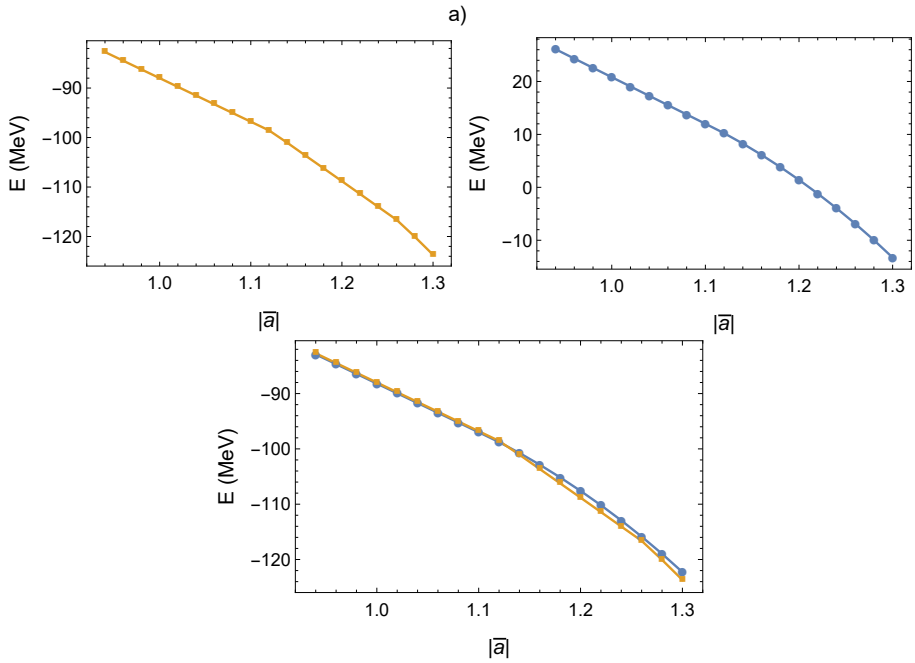

Figure 2.7: Case a): In the left plot of the top row is the quantum ground state (squares and yellow) obtained by the diagonalisation of the Hamiltonian. In the right plot of the top row is the semi-classical global minimum of the potential (circles and blue). Both of them are plotted as functions of the absolute value of $\bar{a}$. In the bottom plot a comparison between their profiles is shown.

Parameters for trajectory b) in example $^{16}\mathrm{O} + \alpha \to {}^{20}\mathrm{Ne}$						
$\bar{a}$	a	b	b	c	ξ	t_1
$(-0.884, -0.86)$	0.0	-0.036	0.0	0.0	0.208	0.0

In Fig. 2.9 we compare the global minimum of the semi-classical potential and the ground state energy value obtained by diagonalising the Hamiltonian along the parameters of trajectory b). In this case the semi-classical exhibits a discontinuity in the first derivative of the global minimum of the potential with respect to $\bar{a}$ at the point of crossing the Maxwell set. However, the ground state energy obtained by diagonalising the Hamiltonian exhibits no change. The direct comparison of their profile show a similar slope, but they do not share the main characteristic of the phase transition. Similarly, in the middle bottom plot of Fig. 2.8, we see how the energy of the states 0_2^+ and 0_3^+ just increases linearly as the magnitude of the parameter $\bar{a}$ increases, and no avoided energy levels crossings occur. In the middle top plot of Fig. 2.8 we show the trajectory taken in parameter space as an arrow crossing the Maxwell set.

Trajectory c)

In the table below we write down the set of parameters used to generate a trajectory in parameter space that goes along the r_2-axis, from positive r_2 to negative r_2, crossing the origin:

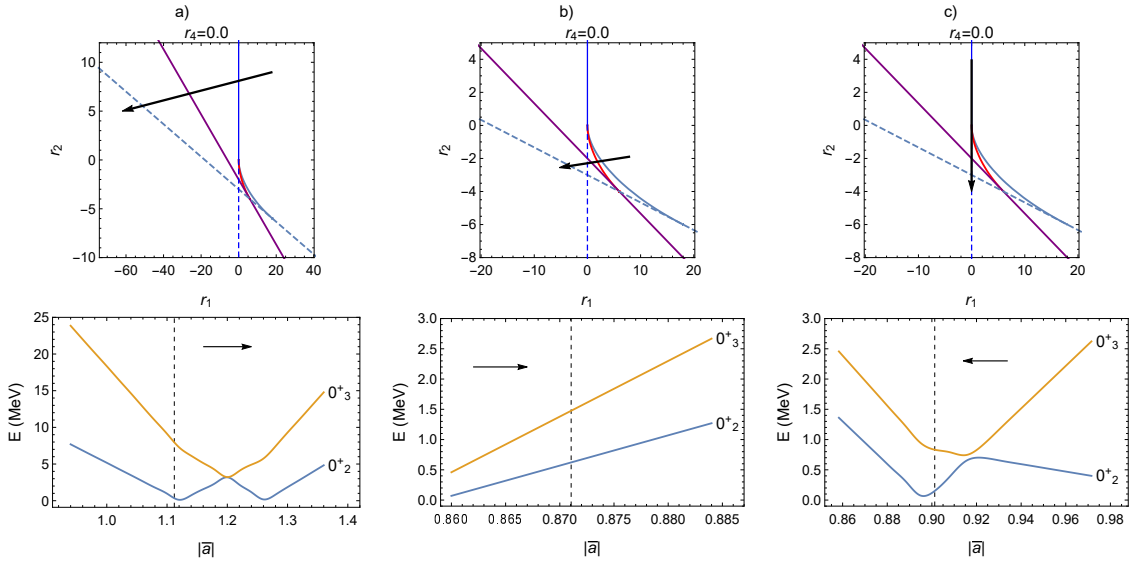

Figure 2.8: In the top row are the three different types of trajectories in (r_1, r_2) parameter space with $r_4 = 0.0$, for the example $^{16}\mathrm{O} + \alpha \rightarrow {}^{20}\mathrm{Ne}$. In the bottom row we plot the energy of the first three 0^+ states as a function of $|\bar{a}|$, and the arrow indicates the direction of the trajectory. The vertical dashed line represents the point of a phase transition. The values of the parameters used are: In a) $\bar{b} = -0.08$; in b) $\bar{b} = -0.036$; and in c) $r_1 = 0$. For all cases we used: $\xi = 0.208$ and $a = b = t_1 = 0$.

Parameters for trajectory a) in example $^{16}\mathrm{O} + \alpha \rightarrow {}^{20}\mathrm{Ne}$						
$\bar{a}$	a	b	b	c	ξ	t_1
$(-0.9715, -0.8583)$	0.0	$(-0.0539, -0.033)$	0.0	0.0	0.208	0.0

In Fig. 2.10 we compare the semi-classical and quantum ground state energies, and their change as a function of the absolute value of $\bar{a}$. In the semi-classical analysis, shown in the top right plot, the global minimum exhibits a discontinuity of its third derivative with respect to $\bar{a}$ at about $\bar{a} = -0.9$, which is when the trajectory in parameter space crosses the origin. In the quantum analysis, shown in the top left plot, the energy of ground state exhibits a noticeable change at the vicinity of the point of the phase transition. This change is also manifested in the energies of the 0^+ sates, shown in the bottom right plot of Fig. 2.8, where an avoided energy level crossing occurs between the ground state 0^+_1 and the state 0^+_2 at about $\bar{a} = -0.9$. In the top right plot in Fig. 2.8 the parameter space (r_1, r_2), with the path of the trajectory taken depicted as a black arrow, is shown. Something of notice is that in this case the magnitude of the absolute value of parameter $\bar{a}$ decreases as we move along the trajectory in parameter space.

It is interesting to notice that even though the semi-classical analysis describes a phase transition of different orders for the chosen trajectories here, signals of the phase transitions in the quantum calculation not always show up. This might be because the corresponding change in the interaction parameters is not significant enough to produce a noticeable effect.

In the following table we summarise the types of QPTs we obtained for semi-classical

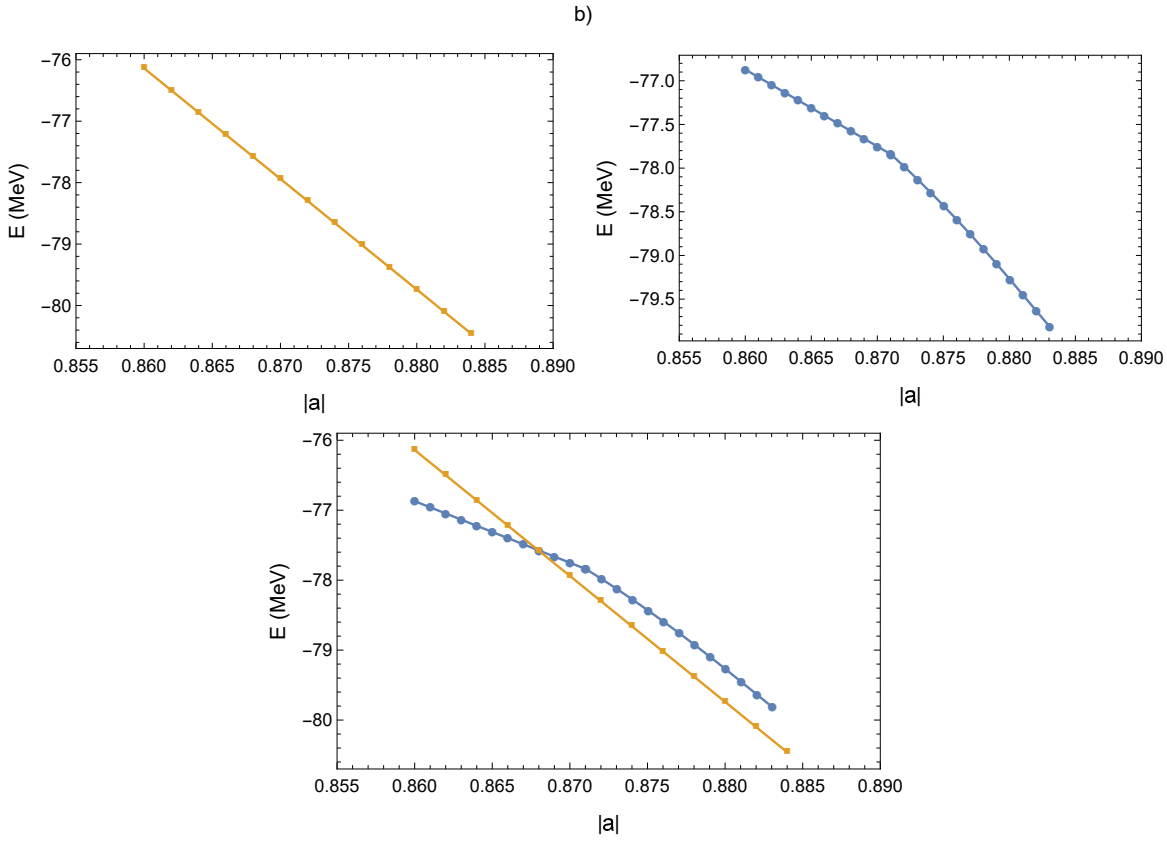

Figure 2.9: Case b): In the left plot of the top row is the quantum ground state (squares and yellow) obtained by the diagonalisation of the Hamiltonian. In the right plot of the top row is the semi-classical global minimum of the potential (circles and blue). Both of them are plotted as functions of the absolute value of $\bar{a}$. In the bottom plot a comparison between their profiles is shown.

potential (2.87) in the SACM, along with their characteristics and signatures in the energy levels obtained by diagonalizing the Hamiltonian for the example of the system of spherical clusters $^{16}\mathrm{O} + \alpha \to {}^{20}\mathrm{Ne}$:

Summary of QPTs for semi-classical potential (2.87): $^{16}\mathrm{O} + \alpha \to {}^{20}\mathrm{Ne}$		
Transition	Order of Transition	Behaviour of the energy levels
a) Region I to region VI	Second	Avoided crossing energy levels occur for the 0_1^+ ground state.
b) Region II to region III	First	Crossing the Maxwell set. No meaningful change occurs in the 0^+ energy levels.
c) $r_2 > 0$ to $r_2 < 0$ at $r_1 = r_4 = 0$	Third	Avoided crossing energy levels occur for the 0_1^+ ground state.

The Hamiltonian has a term representing the SO(4) *dynamical symmetry*

So far we have only studied the SU(3) limit, with $c = 0$, i.e. with $r_4 = 0$, in the

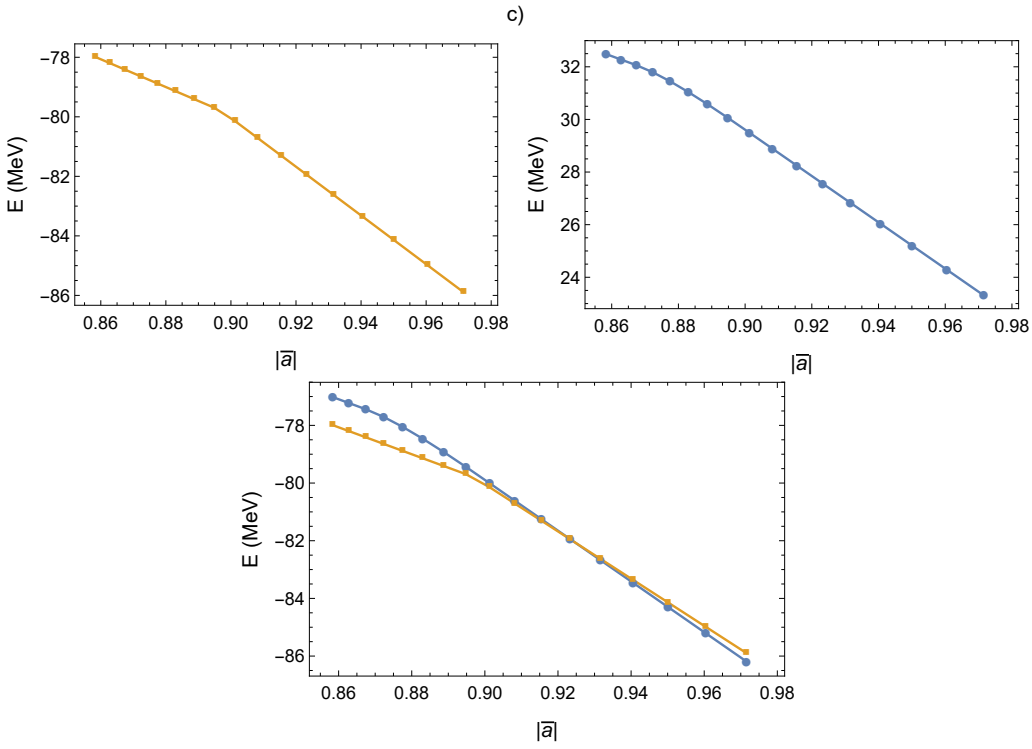

Figure 2.10: Case c): In the left plot of the top row is the quantum ground state (squares and yellow) obtained by the diagonalisation of the Hamiltonian. In the right plot of the top row is the semi-classical global minimum of the potential (circles and blue). Both of them are plotted as functions of the absolute value of $\bar{a}$. In the bottom plot a comparison between their profiles is shown.

two-dimensional parameter space (r_1, r_2). In what follows we shall move on to study the effects in phase transitions with the introduction of the new parameter.

The trajectories to consider now are in the three-dimensional space (r_1, r_2, r_4) and the separatrices they cross are now planes. However, we can always consider a fixed value of one of the parameters and visualize a two-dimensional slice to see where we are relative to the separatrices, i.e. whether we have crossed from one region to another.

To better illustrate the effect of the contribution of the term of the Hamiltonian related to the SO(4) symmetry, a trajectory may be constructed in a similar way as previously done. The interaction parameters $\{\bar{a}, a, \bar{b}, b, \xi, t_1\}$ are fixed (see table below) and parameter c is turned on and the SO(4) contribution is made stronger.

Parameters for trajectory a) in example $^{16}\mathrm{O} + \alpha \rightarrow {}^{20}\mathrm{Ne}$ with SO(4) symmetry						
$\bar{a}$	a	$\bar{b}$	b	c	ξ	t_1
-1.06	0.0	-0.08	0.0	$(0.0, 0.6)$	0.208	0.0

By increasing the magnitude of parameter c a trajectory is drawn in parameter space that starts in region I and ends in region IV crossing the (r_2, r_4)-plane, corresponding to a trajectory described in case a). In Fig. 2.11 we show two points in parameter space before and after crossing the separatrix, along with their corresponding semi-classical

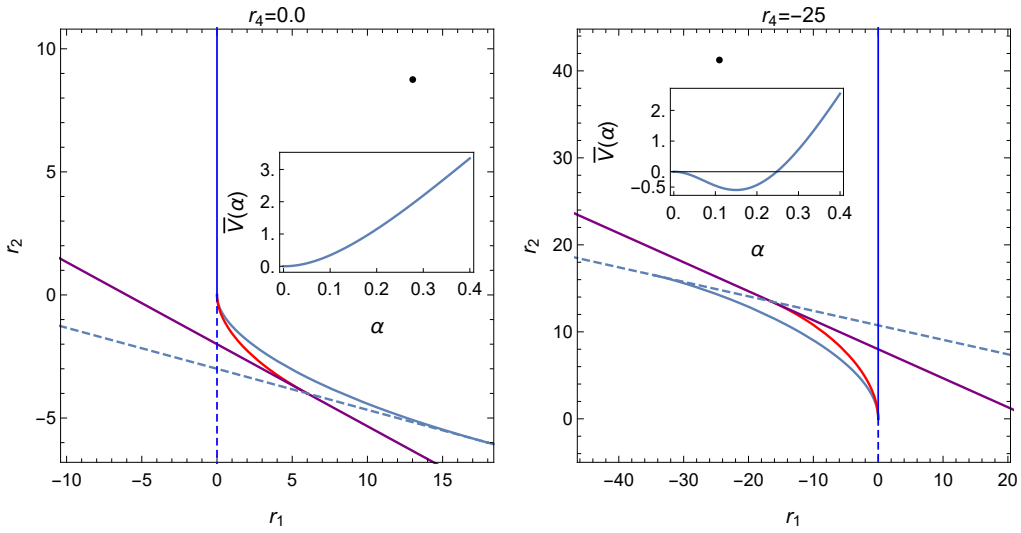

Figure 2.11: Parameter space (r_1, r_2) slices for different values of r_4: $r_4 = 0.0$ (left) and $r_4 = -25.0$ (right), corresponding to $c = 0$ and $c = 0.6$, respectively. The left plot corresponds to a point in region I, while the right plot to a point in region IV. At about $c = 0.2$, the (r_2, r_4)-plane separatrix is crossed. The inset shows the corresponding semi-classical potential. The values used for the interaction parameter are those in the table.

potentials, where we see the transitions from a spherical to a deformed minimum. When the term of SO(4) symmetry is included in the Hamiltonian we find that not all physical observables present signatures of the QPT. For example, contrary to the SU(3) limit, there are no avoided energy level crossings in the 0^+ states at the point of the phase transition. However, turning our attention to the transition probability $B(E2)$ of the 2_1^+ state to the ground state 0_1^+, we can see a slight change in the vicinity of the phase transition. In Fig. 2.12 we show the plots of some physical observables as a function of c. In the left plot are the first three 0^+ states, where no avoided energy level crossings are found. In the middle plot is the transition probability $B(E2)$ of the 2_1^+ state to the ground state 0_1^+, where a change in the vicinity of the crossing at $c = 0.2$ occurs. In the right plot is the expectation number of the number of π bosons in the ground state $\langle \boldsymbol{n}_\pi(0_1^+) \rangle$, calculated with the coherent states (yellow) and numerically with the diagonalisation of the Hamiltonian (blue). The semi-classical analysis with coherent states presents a sharp change, whereas in the numerical quantum analysis the change is more attenuated, occurring in a more continuous fashion. This distinction is characteristic of finite systems where the changes in the physical observables is not abrupt, as opposed to infinite systems where singularities are characteristics of phase transitions.

For completeness, in Fig. 2.13 we compare the global minimum of the semi-classical potential and the ground state obtained by diagonalising the Hamiltonian, both as a functions of c. In this case the change in the global minimum at the point of crossing the separatrix at about $c = 0.2$ is not as noticeable as previous cases. The numerical ground state does not present a discontinuity in the vicinity of the point of crossing the

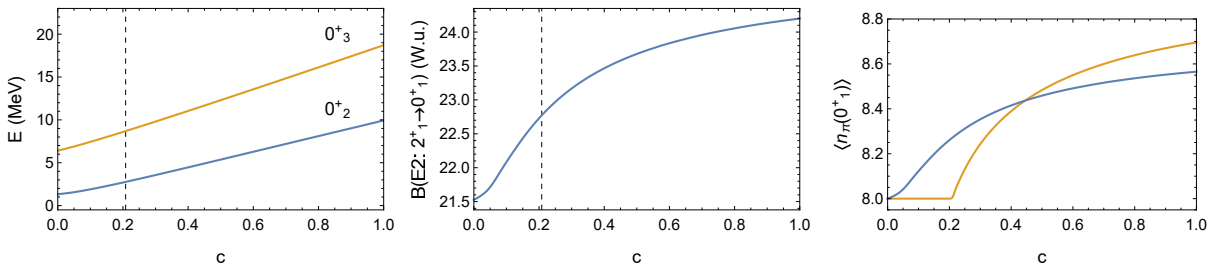

Figure 2.12: Three plots of physical quantities as functions of c for the example $^{16}\mathrm{O}+\alpha \to {}^{20}\mathrm{Ne}$. In the left plot we show the energy of the first three 0^+ states. In the center plot we show the transitions probability $B(E2)$ of the state 2^+_1 to the ground state 0^+_1. In the right plot we show the expectation value of the number of π bosons in the ground state calculated using the coherent states (yellow) and by diagonalising the Hamiltonian (blue). The vertical dashed line indicates the point where the separatrix is crossed at about $c = 0.2$.

separatrix. In the bottom plot we overlap them to compare their profile, and notice that they do not match as good as in the SU(3) limit.

2.5.1.3 Example of two deformed clusters: $^{12}\mathrm{C} + {}^{12}\mathrm{C} \to {}^{24}\mathrm{Mg}$

In this section we will consider the system of two deformed clusters: $^{12}\mathrm{C} + {}^{12}\mathrm{C} \to {}^{24}\mathrm{Mg}$, and study their properties related to phase transitions in a similar fashion as with the two spherical cluster system. For this example we have the following values: $n_0 = 12$, $\hbar\omega = 12.595$, deformations $\beta_{^{12}\mathrm{C}} = -0.38$, individual clusters irreps $(\lambda_1, \mu_1) = (\lambda_2, \mu_2) = (0, 4)$, and the intermediate cluster irrep $(\lambda_C, \mu_C) = (0, 8)$. In the numerical diagonalisation of the Hamiltonian we consider up to 4 excitation quanta, i.e. $N = 4$. We will focus on the SU(3) limit of the Hamiltonian and study the three types of trajectories previously described.

Trajectory a)

In the table below we enlist the values of the interaction parameters used to produce a trajectory in parameter space (r_1, r_2) going from region I to region IV.

Parameters for trajectory a) in example $^{12}\mathrm{C} + {}^{12}\mathrm{C} \to {}^{24}\mathrm{Mg}$						
$\bar{a}$	a	$\bar{b}$	b	c	ξ	t_1
0.0	$(-3.30, -1.40)$	0.0	-0.4	0.0	0.196	0.7175

The effects are similar to the ones obtained in the example of a two spherical cluster system. The first level avoided energy level crossing of the ground state 0^+_1 with the excited state 0^+_2 occurs at the vicinity of the crossing in parameter space. In the left plots of Fig. 2.14 we show the parameter space (top) along with the trajectory depicted as a black arrow, and the energy of the first three 0^+ states (bottom) as functions of the absolute value of a. In this example, we can see that further avoided energy level crossings occur for the 0^+_3 state with higher states not shown.

Trajectory b)

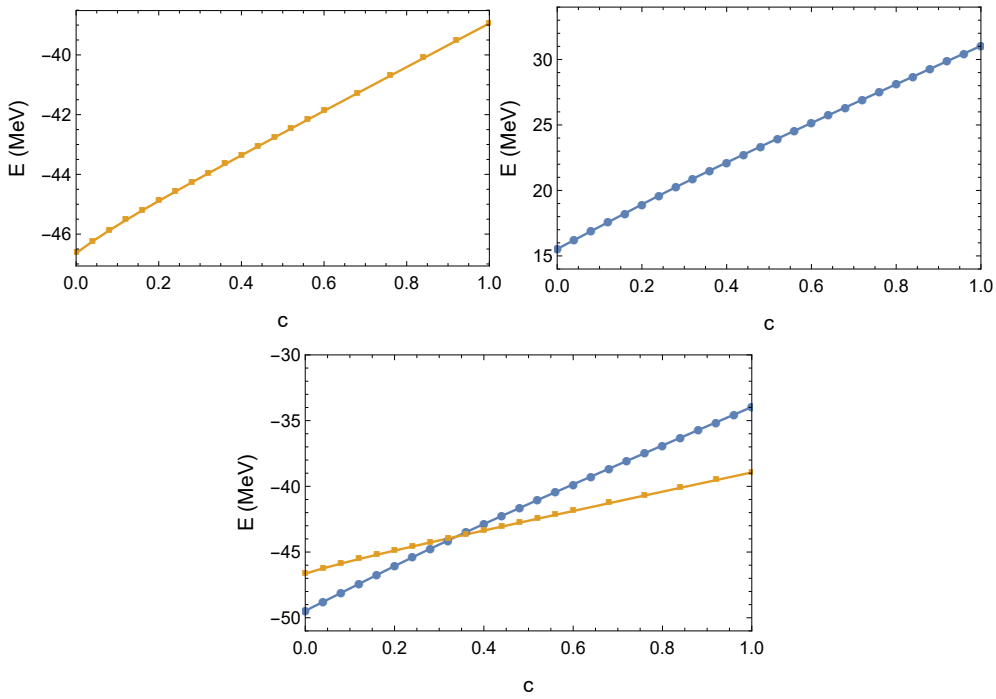

Figure 2.13: The global minimum of the semi-classical potential (right) and the numerical ground state of the diagonalisation of the Hamiltonian (left) as functions of c. In the bottom plot a comparison of their profiles is shown.

In the table below we enlist the values of the interaction parameters used to produce a trajectory in parameter space (r_1, r_2) going from region II to region III, crossing the Maxwell set.

Parameters for trajectory b) in example $^{12}\mathrm{C} + {}^{12}\mathrm{C} \to {}^{24}\mathrm{Mg}$						
$\bar{a}$	a	b	b	c	ξ	t_1
0.0	$(-2.80, -1.40)$	0.0	-0.26	0.0	0.196	0.7175

In the middle plots in Fig. 2.14 we show the parameter space (top) along with the trajectory depicted as a black arrow crossing the Maxwell set and the energy of the first three 0^+ states (bottom) as functions of the absolute value of a. Different from the example of spherical clusters, here we can see an avoided energy level crossing between the ground state 0_1^+ and the excited state 0_2^+ in the vicinity of the crossing of the Maxwell set.

Trajectory c)

In the table below we enlist the values of the interaction parameters used to produce a trajectory in parameter space (r_1, r_2) going from $r_2 > 0$ to $r_2 < 0$ passing through the origin $(r_1 = 0, r_2 = 0)$, where the potential goes as α^6 as $\alpha \to 0$.

Parameters for trajectory c) in example $^{12}\mathrm{C} + {}^{12}\mathrm{C} \to {}^{24}\mathrm{Mg}$						
$\bar{a}$	a	b	b	c	ξ	t_1
0.0	$(-2.3847, -1.7034)$	0.0	$(-0.5654, -0.2382)$	0.0	0.196	0.7175

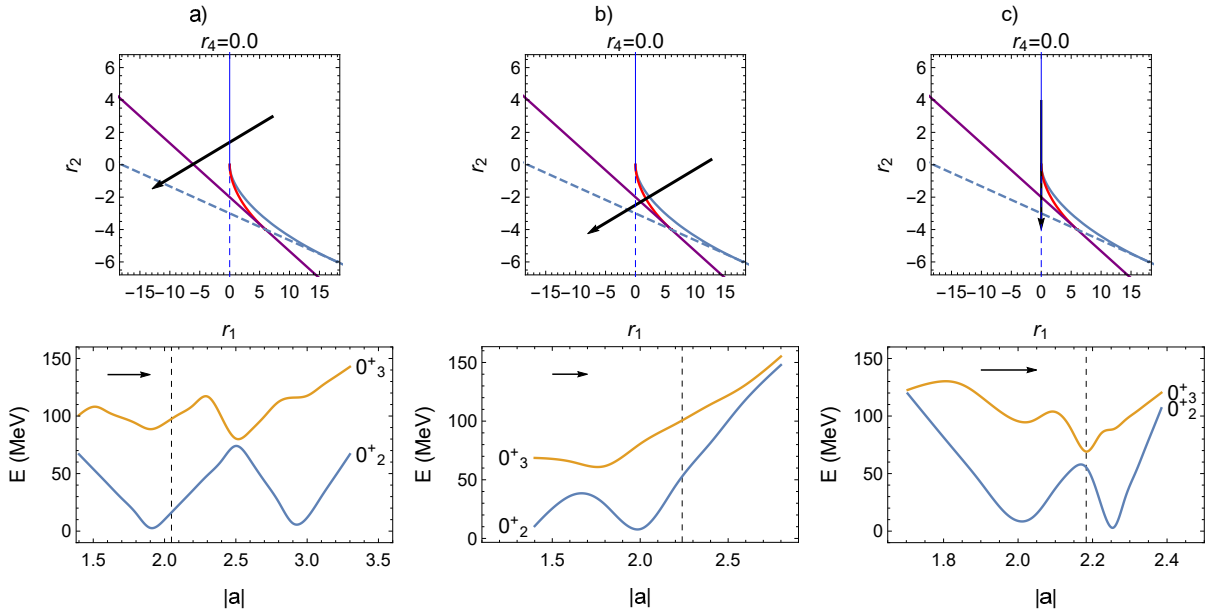

Figure 2.14: Example: $^{12}\mathrm{C} + {}^{12}\mathrm{C} \to {}^{24}\mathrm{Mg}$. In the top row are the parameter space (r_1, r_2) for the three different cases of QPT studied here, along with a black arrow depicting the path of the trajectory. In the bottom row are energies of the states 0^+_2 and 0^+_3 as functions of the absolute value of a. The energy value of the ground state 0^+_1 is equal to zero. The vertical dashed line indicates the value of $|a|$ where the respective separatrix is crossed.

In the right plots of Fig. 2.14 we show the parameter space (top) along with a black arrow depicting the trajectory crossing the origin and the energy values of the first three 0^+ states (bottom) as functions of the absolute value of a. Here we can see, similarly from the example of spherical cluster, avoided energy levels crossings in the vicinity of the point of crossing the parameter space origin.

In the following table we summarise the types of QPTs we obtained for semi-classical potential (2.87) in the SACM, along with their characteristics and signatures in the energy levels obtained by diagonalizing the Hamiltonian:

Summary of QPTs for semi-classical potential (2.87): $^{12}\mathrm{C} + {}^{12}\mathrm{C} \to {}^{24}\mathrm{Mg}$		
Transition	Order of Transition	Behaviour of the energy levels.
a) Region I to region VI	Second	Avoided crossing energy levels occur for the 0^+_1 ground state.
b) Region II to region III	First	Crossing the Maxwell set. Avoided crossing energy levels occur for the 0^+_1 ground state.
c) $r_2 > 0$ to $r_2 < 0$ at $r_1 = r_4 = 0$	Third	Avoided crossing energy levels occur for the 0^+_1 ground state.

2.5.2 Arbitrary parametrisation of coherent states

We start by remembering the semi-classical potential in (2.27):

$$V(\alpha,\theta;c_i) = V_0 + \Big(A + E\cos 2\theta\Big)\alpha^2\frac{F_{11}(\alpha^2)}{F_{00}(\alpha^2)} + \Big(B + F\cos 2\theta + C\sin^2 2\theta\Big)\,\alpha^4\frac{F_{22}(\alpha^2)}{F_{00}(\alpha^2)} - (b+\bar{b})\alpha^6\frac{F_{33}(\alpha^2)}{F_{00}(\alpha^2)} + D\cos 2\theta\alpha^2\frac{F_{20}(\alpha^2)}{F_{00}(\alpha^2)}, \tag{2.99}$$

and we can notice that the potential is independent of ϕ. The constant term V_0 is given by

$$V_0 = (a+n_0b)\langle \boldsymbol{C}_2(\lambda_C,\mu_C)\rangle + \xi\langle \boldsymbol{L}_C^2\rangle + \frac{c}{4}(N+n_0)(N+n_0-1). \tag{2.100}$$

The control parameters $c_i = \{A, B, C, D, E, F\}$ of the potential are linear combination of the Hamiltonian parameters, and are given by

$$A = \hbar\omega - b\langle \boldsymbol{C}_2(\lambda_C,\mu_C)\rangle + 4\Big((a+\bar{a}) + (b+\bar{b})(n_0-1)\Big) - \frac{c}{2}(N+n_0-1) - \frac{1}{4}\Big(a+b(n_0-1)\Big)(\Gamma_1+\Gamma_2) + 2\xi \tag{2.101}$$

$$B = a+\bar{a} + (b+\bar{b})(n_0-6) + \frac{c}{2} + \frac{b}{4}(\Gamma_1+\Gamma_2) \tag{2.102}$$

$$C = \xi - \frac{c}{4} \tag{2.103}$$

$$D = \frac{c}{2} \tag{2.104}$$

$$E = -\frac{3}{4}\Big(a+b(n_0-1)\Big)(\Gamma_1+\Gamma_2) \tag{2.105}$$

$$F = \frac{3}{4}b(\Gamma_1+\Gamma_2). \tag{2.106}$$

In this case the semi-classical potential depends on two variables, one α related to the distance between the clusters and the other θ related to their relative orientation. The main point of the catastrophe theory is to find for what combination of parameters both variables are critical. The critical points (α_c, θ_c) are the set of real values that satisfy

$$\nabla V(\alpha,\theta;c_i)|_{(\alpha_c,\theta_c)} = 0 \tag{2.107}$$

for a set value of parameters c_i. This condition can be explicitly stated as the following set of equations:

$$\frac{\partial V}{\partial\theta} = \frac{2\sin 2\theta}{F_{00}(\alpha)}\Big(E\alpha^2F_{11}(\alpha) + F\alpha^4F_{22}(\alpha) - 2C\cos 2\theta\alpha^4F_{22}(\alpha) + D\alpha^2F_{20}(\alpha)\Big) = 0 \tag{2.108}$$

$$\frac{\partial V}{\partial\alpha} = \frac{1}{F_{00}^2(\alpha)}\Big((A+E\cos 2\theta)W(F_{00}(\alpha),\alpha^2F_{11}(\alpha)) + (B+C\sin^2 2\theta)W(F_{00}(\alpha),\alpha^4F_{22}(\alpha)) + D\cos 2\theta W(F_{00}(\alpha),\alpha^2F_{20}(\alpha)) - (b+\bar{b})W(F_{00}(\alpha),\alpha^6F_{33}(\alpha))\Big) = 0, \tag{2.109}$$

with $W(f,g) = f(\alpha)g'(\alpha) - f'(\alpha)g(\alpha)$ the Wronskian determinant, with prime indicating differentiation with respect to α. Given that the $F_{pq}(\alpha)$ functions have no linear term in α, from (2.109) we find that $\alpha = 0$ is a critical point independent of the values of the parameters c_i, and we identify it as the fundamental root. We shall focus on the equation (2.108) for the variable θ. For a particular set of values of the parameters c_i there exists a fixed number of critical points (α_c, θ_c) located on the (α, θ)-plane. These critical points are joined by a continuous line signifying the line of steepest descent in the energy surface $V(\alpha, \theta; c_i) : \mathbb{R} \times \mathbb{R} \to \mathbb{R}$, for a particular set of values of the parameters c_i. In this line one of the two equations (2.108) or (2.109) is satisfied, while there is points along the line where both are satisfied. In fact we can solve (2.108) so that θ is obtained as a function of α resulting in the line of steepest descent. We are able to convert the present problem to the study of a one-dimensional potential depending solely on α and on the parameters c_i. In Appendix B we show how this approach is valid for a particular type of two real variable functions, which the present potential (2.99) falls into. Solving (2.108) for θ_c we obtain

$$\cos 2\theta_c = \frac{D}{2C}\frac{F_{20}(\alpha)}{\alpha^2 F_{22}(\alpha)} + \frac{E}{2C}\frac{F_{11}(\alpha)}{\alpha^2 F_{22}(\alpha)} + \frac{F}{2C}, \tag{2.110}$$

in the same equation we can see that it is also automatically satisfied for the constant values

$$\theta_1 = 0 \tag{2.111}$$

$$\theta_2 = \frac{\pi}{2} \tag{2.112}$$

the value $\theta = \pi$ is also a solution but it gives the same result as $\theta = 0$.

It is worthwhile to study both cases separately and compare the end results between themselves and with the other parametrisation of the coherent states.

2.5.2.1 Constant critical points $\theta_\pm$

For this case we introduce the notation $\theta_\pm$ to refer to the critical points (2.111) and (2.112), where $\theta_+ = \theta_1$ and $\theta_- = \theta_2$.

Substituting (2.111) and (2.112) in (2.99) allow us to write the one-dimensional potential

$$V(\alpha, \theta_\pm; \sigma_i) = V_0 + \frac{1}{F_{00}(\alpha)}\left[\sigma_1\alpha^2 F_{11}(\alpha) + \sigma_2\alpha^4 F_{22}(\alpha) + \sigma_3\alpha^6 F_{33}(\alpha) + \sigma_4\alpha^2 F_{20}(\alpha)\right], \tag{2.113}$$

with the σ_i parameters defined as

$$\begin{aligned}
\sigma_1 &= A \pm E = \hbar\omega - b\langle \boldsymbol{C}_2(\lambda_C, \mu_C)\rangle + 4\Big((a+\bar{a}) + (b+\bar{b})(n_0-1)\Big) \\
&\quad - \frac{1\pm 3}{4}\Big(a + b(n_0-1)\Big)(\Gamma_1+\Gamma_2) + 2\xi - \frac{c}{2}(N+n_0-1) \\
\sigma_2 &= B \pm F = a + \bar{a} + (b+\bar{b})(n_0-6) + \frac{c}{2} + \frac{1\pm 3}{4}b(\Gamma_1+\Gamma_2) \\
\sigma_3 &= -(b+\bar{b}) \\
\sigma_4 &= \pm D = \pm\frac{c}{2},
\end{aligned} \tag{2.114}$$

and with our notation the upper sign correspond to the critical point $\theta_1 = 0$, and the lower sign to the critical point $\theta_2 = \pi/2$. We notice the similitude between this and the r_i parameters from the previous parametrisation. Similarly, in accordance to the methods of catastrophe theory we now expand the potential (2.113) in a Taylor series expansion about the fundamental root $\alpha = 0$ and obtain

$$V(\alpha, \theta_\pm; \sigma_i) = V_0 + T_0 + T_1\alpha^2 + T_2\alpha^4 + T_3\alpha^6 + \dots, \tag{2.115}$$

where the first three coefficients are explicitly given by

$$\begin{aligned}
T_0 &= n_0\sigma_1 + n_0(n_0-1)\sigma_2 + n_0(n_0-1)(n_0-2)\sigma_3 \\
T_1 &= N(n_0+1)\left[\sigma_1 + 2n_0\sigma_2 + 3n_0(n_0-1)\sigma_3 + \frac{1}{2}(N-1)(n_0+2)\sigma_4\right] \\
T_2 &= -\frac{1}{3}N(n_0+1)\left[(n_0(N+1)+2)\sigma_1 + (2n_0^2(N+1) - n_0(N-5) - 2(N-1))\sigma_2\right. \\
&\quad \left. +3n_0(N(n_0(n_0-2)-2) + n_0(n_0+2))\sigma_3 + \frac{2}{3}(N-1)(n_0+2)(n_0(N+1)+3)\sigma_4\right].
\end{aligned} \tag{2.116}$$

In the limit $\alpha \to 0$ the potential tends to the constant value $V_0 + T_0$. The coefficient T_1 of α^2 vanishes with the following relations of the parameters:

$$N(n_0+1)\left[\sigma_1 + 2n_0\sigma_2 + 3n_0(n_0-1)\sigma_3 + \frac{1}{2}(N-1)(n_0+2)\sigma_4\right] = 0. \tag{2.117}$$

If (2.117) is satisfied, then the term T_2 vanishes with the following relation of the parameters, where σ_1 has been eliminated:

$$\frac{1}{2}N(N-1)(n_0+1)(n_0+2)\left[\sigma_2 + 3n_0\sigma_3 - \frac{1}{6}(n_0(N+1)+6)\sigma_4\right] = 0. \tag{2.118}$$

If (2.117) and (2.118) are satisfied, the term T_3 vanishes with following relation of the parameters, where now the parameter σ_2 has been eliminated:

$$\frac{1}{6}N(N-1)(N-2)(n_0+1)(n_0+2)(n_0+3)\left[\sigma_3 + \frac{1}{24}n_0(N+1)\sigma_4\right] = 0. \tag{2.119}$$

Now, if (2.117), (2.118) and (2.119) are satisfied the next term T_4 may no longer be eliminated by an arbitrary choice of parameters without the potential ending up being a constant value. This defines the germ of the potential at α^8, and in the SU(3) limit, when $c = 0$ (or $\sigma_4 = 0$), it becomes α^6. Equations (2.117), (2.118) and (2.119) also help us define the essential parameters R_i of the potential:

$$\begin{aligned}
R_1 &= \sigma_1 + 2n_0\sigma_2 + 3n_0(n_0-1)\sigma_3 + \frac{1}{2}(N-1)(n_0+2)\sigma_4 \\
R_2 &= \sigma_2 + 3n_0\sigma_3 - \frac{1}{6}(n_0(N+1)+6)\sigma_4 \\
R_3 &= \sigma_3 \\
R_4 &= \frac{1}{6}n_0(N+1)\sigma_4
\end{aligned} \tag{2.120}$$

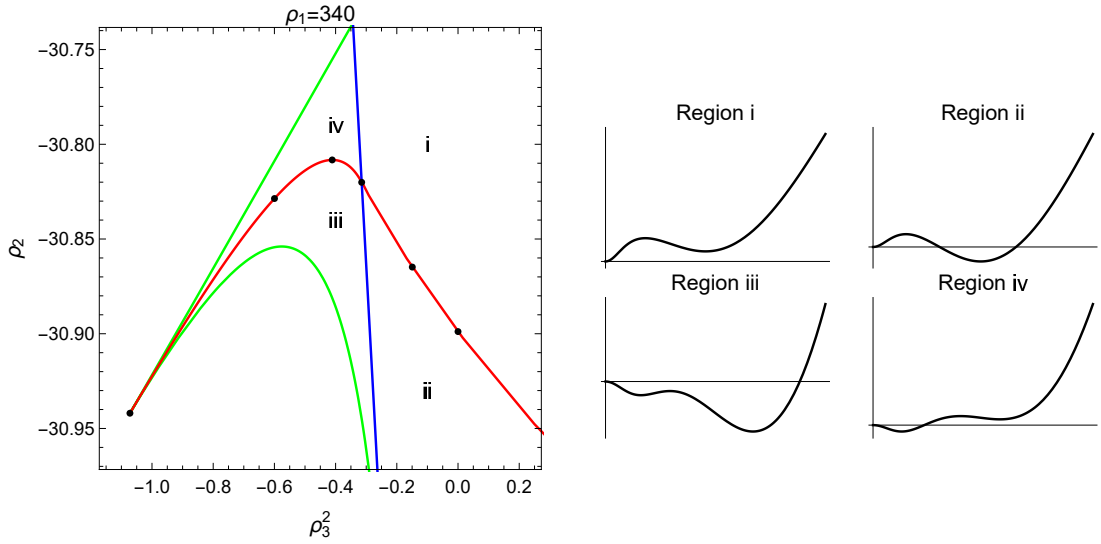

Figure 2.15: Parameter space $(\rho_3^2 = D^2/C, \rho_1)$ for $\rho_2 = 340$. The bifurcation set is shown as a green curve, and the Maxwell set is shown as a red curve. The blue line is the separatrix defined by the vanishing of the T_1 coefficient of the Taylor series expansion, and it intersects the Maxwell set at $D^2/C = -0.3147$, where a change in curvature of the red curve occurs. The points in the left plot represent the values of (ρ_3^2, ρ_1) used in the contour plots in Fig. 2.16. In the right plots we show a representative potential for each region.

where R_4 is the parameter of the SO(4) dynamical symmetry and is proportional to the interaction parameter c. This choice is made so that one of the essential parameters is directly related to this dynamical symmetry.

Subtracting the constant term T_0 of the Taylor series expansion and V_0 to the semi-classical potential (2.113) we can rewrite the potential in terms of the essential parameters and the previously defined $Q_i(\alpha)$ polynomials in (2.86):

$$\begin{aligned}\bar{V}(\alpha, \theta_\pm; R_i) &= V(\alpha, \theta_c; \sigma_i) - (n_0\sigma_1 + n_0(n_0-1)\sigma_2 + n_0(n_0-1)(n_0-2)\sigma_3) \\ &= V_0 + \frac{1}{Q_0(\alpha)}\left[R_1 Q_1(\alpha) + R_2 Q_2(\alpha) + R_3 Q_3(\alpha) + R_4 Q_4(\alpha)\right]. \end{aligned} \tag{2.121}$$

What follows is exactly analogous to the previous case and we can obtain the bifurcation and Maxwell set following the formulae of Appendix C. The other separatrices are also obtained following the steps described in the previous sections. What changes is the definition of the new essential parameters R_i in (2.120) in terms of the interaction parameters.

2.5.2.2 Critical point θ_c as a function of α

By direct substitution of (2.110) in (2.99) we arrive at the one-dimensional potential

$$V(\alpha,\theta_c;\rho_i) = V_0 + \frac{1}{F_{00}(\alpha)}\left(\rho_1\alpha^2F_{11}(\alpha) + \rho_2\alpha^4F_{22}(\alpha) + \frac{1}{4F_{22}(\alpha)}\left(\rho_3F_{20}(\alpha) + \rho_4F_{11}(\alpha)\right)^2 + \frac{\rho_5}{2}\alpha^2F_{20}(\alpha) - (b+\bar{b})F_{33}(\alpha)\right), \tag{2.122}$$

where the ρ_i parameters are given by

$$\begin{aligned}\rho_1 &= A + \frac{EF}{2C}\\ \rho_2 &= B + C + \frac{F^2}{4C}\\ \rho_3 &= \frac{D}{\sqrt{C}}\\ \rho_4 &= \frac{E}{\sqrt{C}}\\ \rho_5 &= \frac{DF}{C}.\end{aligned} \tag{2.123}$$

Here we can notice the increase of complexity in the semi-classical potential in both the definition of the parameters as function of the interaction parameters and in the structure of the functions of α that define the potential. Before starting this exercise we may consider simplifying the potential (2.122) by focusing on the case of a system of spherical clusters, which automatically sets $\rho_4 = \rho_5 = 0$, and the potential depends on three parameters. The results of this analysis can be found in [47]. In this particular case the potential is

$$\bar{V}(\alpha,\theta_c;\rho_i) = \frac{1}{F_{00}(\alpha)}\left(\rho_1\alpha^2F_{11}(\alpha) + \rho_2\alpha^4F_{22}(\alpha) + \frac{\rho_3^2}{4}\frac{F_{20}(\alpha)^2}{F_{22}(\alpha) - n_0(n_0-1)} - (b+\bar{b})\alpha^6F_{33}(\alpha)\right) - n_0\rho_1 - n_0(n_0-1)\rho_2 - n_0(n_0-1)(n_0-2), \tag{2.124}$$

where we have redefined the potential so that it vanishes at the origin $\alpha = 0$. In this case, the θ_c critical point can be written as:

$$\cos 2\theta_3 = \frac{D}{2C}\frac{F_{20}(\alpha)}{\alpha^2F_{22}(\alpha)}. \tag{2.125}$$

The bifurcation and Maxwell sets are then obtained by application of the formulae in Appendix C.

A slice of the three-dimensional space (ρ_1,ρ_2,ρ_3) for a fixed value of ρ_1 can be seen in Fig. 2.15. We identify four regions where two minima coexist: In region i the spherical minimum is dominant; in region ii the deformed minimum is dominant; in region iii the deformed minimum remains dominant but the spherical minimum becomes a deformed

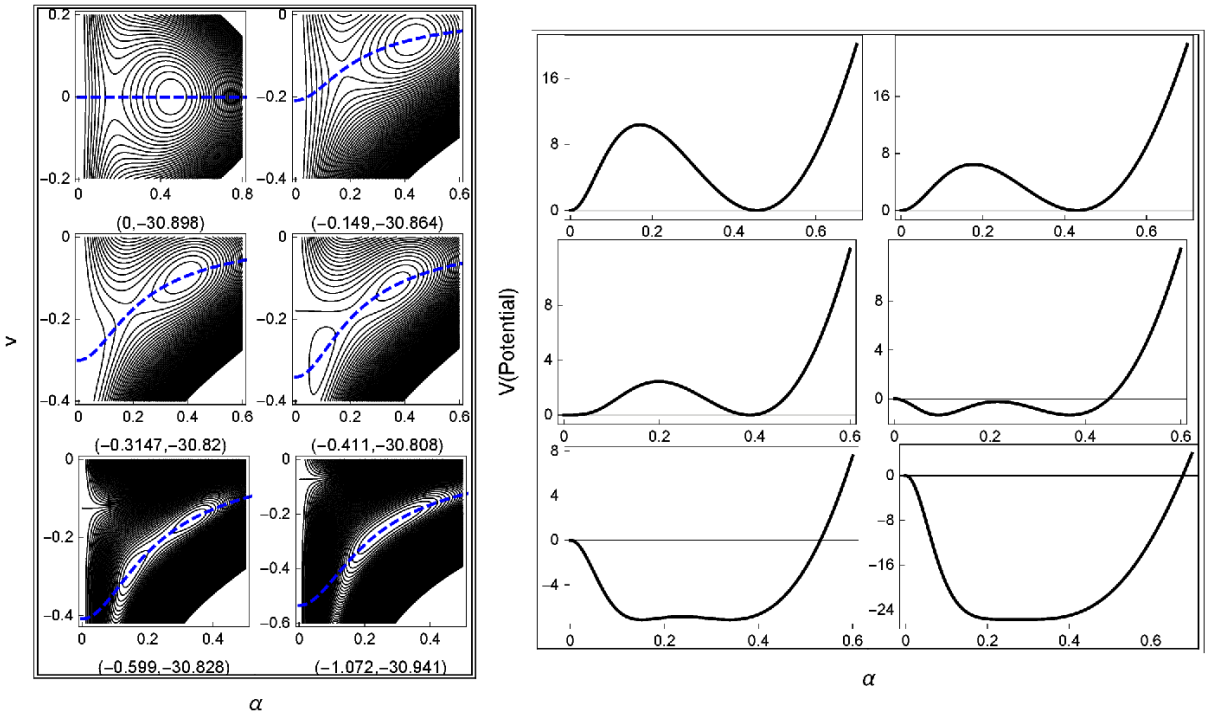

Figure 2.16: Contour plots (α, v) of the energy surface (2.99) for different values of (ρ_3^2, ρ_1) labelled under each plot (shown as points in Fig. 2.15), where $v = \cos 2\theta$. The critical values as a function of α, denoting the steepest descend path described by (2.125), are shown as the dashed (blue) lines. In the right side we plotted the potentials (2.124) as functions of α for the same parameters used in the contour plots.

minimum; and in region iv the spherical minimum becomes a deformed minimum and it is dominant. Contour plots of the semi-classical potential for different values of the ρ_i parameters are shown in Fig. 2.16 along with the critical values of θ_c as a function of α; in the right the corresponding one-dimensional semi-classical potential are plotted. In this example we travel along the Maxwell set where the two equal minima coalesce in a single minimum at the end of the Maxwell set.

To determine which of the three critical points for the variable θ is of physical significance, we have to use the parameters $\{\bar{a}, a, \bar{b}, b, c, \xi, t_1\}$ which result from the fitting of the Hamiltonian to experimental data. Then, these values of the parameters are substituted in the semi-classical potential in (2.99) and we can plot the potential surface in the variables (α, θ). The dominant minimum of this potential surface will be associated with one of the three critical points in θ, while the other critical points will correspond to either a higher minimum or to a saddle point. The analysis of the separatrices in the parameter space must be done with the critical point associated with the dominant minimum. Here we have presented an analysis of all three critical points of the variable θ for systems of spherical clusters, so that its application to particular examples can be direct.

The more general case of the analysis of a system with deformed cluster is still pending. In this case the parameter space is five-dimensional, lending itself to more opportunities

for phase transitions, but we believe that with the methods described here the different separatrices in parameter space can be constructed. It remains of interest the application of this case to systems of heavy nuclei, where a more general Hamiltonian must be used.

Chapter 3

Quantum phase transition in an effective model of QCD

In this chapter we will apply the methods based on catastrophe theory used in the SACM in previous sections to an effective model of QCD to show the usefulness of the techniques employed.

Effective models of QCD are useful for being comparatively easier to apply and study than real QCD, while also being non-perturbative. Important information about real physical properties and their consequences can be extracted by a detailed analysis of these effective models [97–100], such as the structure of the physical vacuum containing quarks, antiquarks and gluons [101]. Using these effective models the modelling of pentaquark and heptaquark states was done in [102]. A short comprehensive review of the effective model of QCD considered can be found in Ref. [103].

3.1 Description of the model and Hamiltonian operator

The model considered here was first described in [98], but we will use a different trial state for the expectation value of the Hamiltonian, and in its essence is a Lipkin model [28] where the quarks have two energy levels, one at $-\omega_q$ and the other at ω_q. Additionally a gluon state is considered at the energy ω_β. The fermiomic state energy is at $\omega_q = 0.33$ GeV, which corresponds to approximately a third of the mass of the nucleon at 1 GeV. The gluon state is at $\omega_\beta = 1.6$ GeV, corresponding to the energy of a gluon pair, with the energy of a single gluon being 0.8 GeV. In Fig. 3.1 an schematic picture of the energy scale of the model is shown. The degeneracy of the fermionic state depends on the number of degrees of freedom for the quarks $2\Omega = n_f n_c n_s = 3\times3\times2 = 18$, where n_f is the number of flavor (up, down and strange), n_c is the number of color and n_s is the number of spin orientations, and no orbital degree of freedom is considered. Using the Dirac picture in the perturbative vacuum the lowest fermion level is completely filled and to excite one quark from the lower level to the upper one requires an energy of $2\omega_q$, thus creating a particle-hole state, which corresponds to a quark-antiquark pair, with the antiquark described by the hole. Up to 2Ω quark-antiquark pairs can be created.

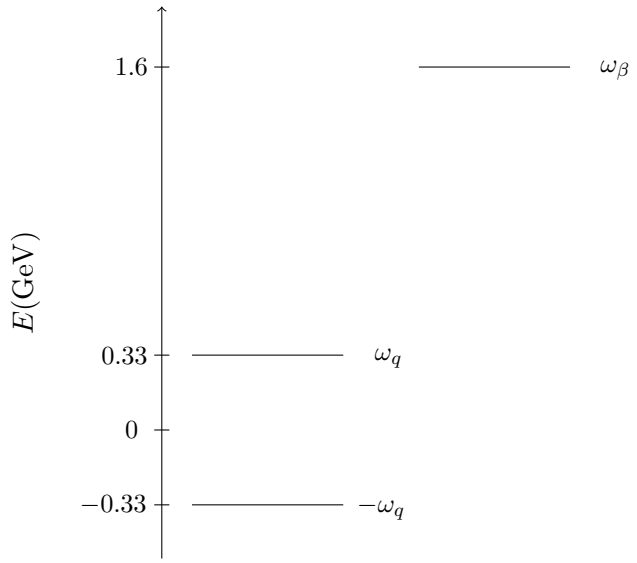

Figure 3.1: Schematic description of the energy levels of the quark and gluon states. The quarks have two possible states at $\pm\omega_q$, with $\omega_q = 0.33\,\text{GeV}$, i.e. approximately one third of the mass of a nucleon. The gluon state is at 1.6 GeV, which is the energy of a gluon pair, and the one-gluon energy is 0.8 GeV.

In this model pairs of quark-antiquarks and pairs of gluons are approximated by bosons, and their interaction is described the product of the respective creation and annihilation operators. For the quark-antiquark pair $\boldsymbol{b}_f^\dagger$ and $\boldsymbol{b}_f$ are the creation and annihilation operators, where f runs from 1 to 2Ω, and we assume that a quark from the state f in the lower level is excited to the same component in the upper level. For the gluon pairs $\boldsymbol{\beta}^\dagger$ and $\boldsymbol{\beta}$ are the creation and annihilation operators.

The Hamiltonian of the model is given by

$$\begin{aligned}\boldsymbol{H} &= 2\omega_q \boldsymbol{n}_q + \omega_\beta \boldsymbol{n}_\beta + C\left\{\left[(\boldsymbol{b}^\dagger)^2 s^2 + 2(\boldsymbol{b}^\dagger\cdot\boldsymbol{b}) + (s^\dagger)^2\boldsymbol{b}^2\right]\left(1-\frac{\boldsymbol{n}_q}{2\Omega}\right)\beta^\dagger\right. \\ &\left. +\beta\left(1-\frac{\boldsymbol{n}_q}{2\Omega}\right)\left[(\boldsymbol{b}^\dagger)^2 s^2 + 2(\boldsymbol{b}^\dagger\cdot\boldsymbol{b}) + (s^\dagger)^2\boldsymbol{b}^2\right]\right\} \quad , \end{aligned} \tag{3.1}$$

where $\boldsymbol{n}_q$ is the number of quark-antiquark pairs, $\boldsymbol{n}_\beta$ is the number of gluon pairs, and s is an auxiliary boson (analogous to $\boldsymbol{\sigma}$ in the SACM) such that it ensures that the number of all bosons remains constant: $2\Omega = n_s + n_b$, with n_s the number of s bosons and n_b the number of b bosons, corresponding to the quark-antiquark pair boson approximation.

The Hamiltonian depends only on the parameter C, which gives the intensity of the interaction. When $C = 0$ the ground state is given by the quark-antiquark pairs in the lower level and no gluon pair is present. The $\left(1-\frac{\boldsymbol{n}_q}{2\Omega}\right)$ term ensures that when the number of fermion pairs tends to the maximum value, i.e. all the quarks in the upper level, the interaction shuts off. This simulates the PEP as the total number of quarks allowed in the upper level is 2Ω, each with different quantum numbers. In Fig. 3.2 the interaction appearing in the Hamiltonian are depicted, where the double straight line corresponds to quark-antiquark pairs and the double wavy line to gluon pairs.

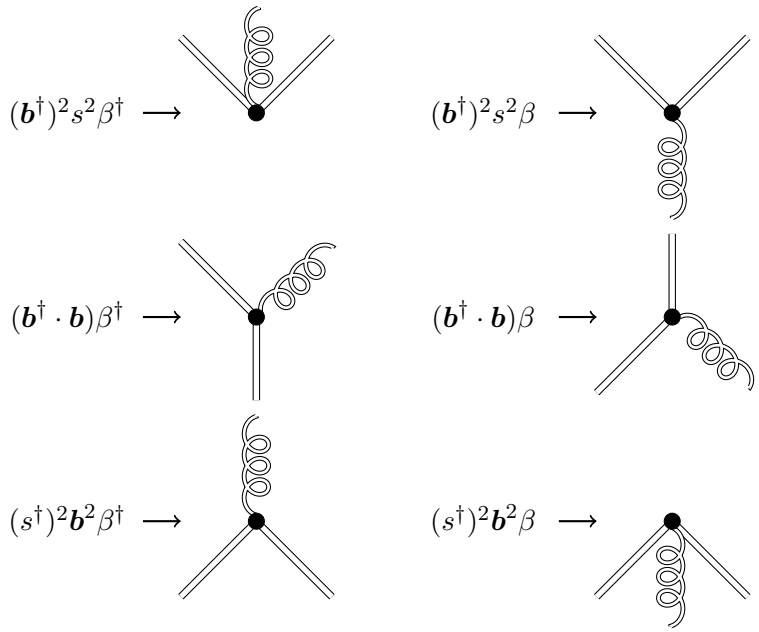

Figure 3.2: Graphical diagrams of the interactions in the Hamiltonian of the quark-antiquark and gluon pairs. They are motivated by the real QCD interaction. A double straight represents a quark-antiquark pair and a double-wavy line represents a gluon pair. The time line goes from bottom to top.

3.2 Semi-classical potential

Similarly, the semi-classical potential is obtained as the expectation value of the Hamiltonian in a coherent state basis. In analogy to the IBM [9] the coherent states are defined by

$$|\psi\rangle = \mathcal{N}_q \mathcal{N}_\beta e^{\gamma\beta^\dagger} \left[s^\dagger + (\boldsymbol{\alpha}\cdot\boldsymbol{b}^\dagger)\right]^{2\Omega} |0\rangle, \tag{3.2}$$

with the normalization factors $\mathcal{N}_q$ and $\mathcal{N}_\beta$ given by

$$\mathcal{N}_q = \frac{1}{\left[(2\Omega)!\,(1+(\boldsymbol{\alpha}^*\cdot\boldsymbol{\alpha}))^{2\Omega}\right]^{\frac{1}{2}}} \tag{3.3}$$

$$\mathcal{N}_\beta = e^{-\frac{\gamma^*\gamma}{2}}, \tag{3.4}$$

and with the vacuum state $|0\rangle = |0\rangle_q |0\rangle_\beta$ being the direct product of the quark and gluon vacuums.

The semi-classical potential is given by

$$V = 2\omega_q(2\Omega)\frac{(\boldsymbol{\alpha}^*\cdot\boldsymbol{\alpha})}{[1+(\boldsymbol{\alpha}^*\cdot\boldsymbol{\alpha})]^2} + \omega_\beta\gamma^*\gamma + 2\Omega(2\Omega-1)C(\gamma+\gamma^*)\left[\frac{(\boldsymbol{\alpha}\cdot\boldsymbol{\alpha})+(\boldsymbol{\alpha}^*\cdot\boldsymbol{\alpha}^*)}{[1+(\boldsymbol{\alpha}^*\cdot\boldsymbol{\alpha})]^2}\right.$$
$$\left.+\frac{2}{2\Omega-1}\frac{(\boldsymbol{\alpha}^*\cdot\boldsymbol{\alpha})}{[1+(\boldsymbol{\alpha}^*\cdot\boldsymbol{\alpha})]^2}\right]\left(1-\frac{(\boldsymbol{\alpha}^*\cdot\boldsymbol{\alpha})}{1+(\boldsymbol{\alpha}^*\cdot\boldsymbol{\alpha})}\right), \tag{3.5}$$

and using the following parametrization of the coherent states parameters

$$\begin{aligned}(\boldsymbol{\alpha}\cdot\boldsymbol{\alpha}) &= \alpha_{(0,0)}^2 e^{2i\phi_{(0,0)}} + \alpha_{(1,1)}^2 e^{2i\phi_{(1,1)}} \\ (\boldsymbol{\alpha}^*\cdot\boldsymbol{\alpha}) &= \alpha_{(0,0)}^2 + \alpha_{(1,1)}^2 \\ (\boldsymbol{\alpha}^*\cdot\boldsymbol{\alpha}^*) &= (\alpha_{(0,0)}^*)^2 e^{-2i\phi_{(0,0)}} + (\alpha_{(1,1)}^*)^2 e^{-2i\phi_{(1,1)}} \\ \gamma &= \gamma e^{i\phi_\gamma}\end{aligned} \tag{3.6}$$

we can write the semi-classical potential as

$$\begin{aligned}V &= 2\omega_q(2\Omega)\frac{\alpha_{(0,0)}^2+\alpha_{(1,1)}^2}{\left[1+\alpha_{(0,0)}^2+\alpha_{(1,1)}^2\right]^2} + \omega_\beta\gamma^2 \\ &\quad +2\Omega(2\Omega-1)C\gamma(e^{i\phi_\gamma}+e^{-i\phi_\gamma})\left[\frac{\alpha_{(0,0)}^2(e^{2i\phi_{(0,0)}}+e^{-2i\phi_{(0,0)}})+\alpha_{(1,1)}^2(e^{2i\phi_{(1,1)}}+e^{-2i\phi_{(1,1)}})}{\left[1+\alpha_{(0,0)}^2+\alpha_{(1,1)}^2\right]^2}\right. \\ &\quad \left.+\frac{2}{2\Omega-1}\frac{(\alpha_{(0,0)}^2+\alpha_{(1,1)}^2)}{1+\alpha_{(0,0)}^2+\alpha_{(1,1)}^2}\right]\left(1-\frac{\alpha_{(0,0)}^2+\alpha_{(1,1)}^2}{1+\alpha_{(0,0)}^2+\alpha_{(1,1)}^2}\right) \\ V &= 2\omega_q(2\Omega)\frac{\alpha^2}{(1+\alpha^2)^2}+\omega_\beta\gamma^2 \\ &\quad +2\Omega(2\Omega-1)C2\gamma\cos\phi_\gamma\left[\frac{2\alpha_{(0,0)}^2\cos 2\phi_{(0,0)}+2\alpha_{(1,1)}^2\cos 2\phi_{(1,1)}}{(1+\alpha^2)^2}\right. \\ &\quad \left.+\frac{2}{2\Omega-1}\frac{\alpha^2}{1+\alpha^2}\right]\left(1-\frac{\alpha^2}{1+\alpha^2}\right).\end{aligned} \tag{3.7}$$

In the last line we defined the new variable $\alpha^2 = \alpha_{(0,0)}^2 + \alpha_{(1,1)}^2$. The (λ,λ) notation refers to the flavor irrep of the quarks, where $(0,0)$ is flavor zero and $(1,1)$ is the flavor octet.

The semi-classical potential depends on five variables: α, γ, $\phi_{(0,0)}$, $\phi_{(1,1)}$ and ϕ_γ. However, after minimization of the potential we will be left with two variables: α and γ. The critical points of the potential are those which satisfy $\nabla V|_{\vec{\alpha}_c} = 0$, where $\vec{\alpha}_c$ represents the five critical points values of the variables. The set of equations for the angular variables are explicitly given by

$$\begin{aligned}\frac{\partial V}{\partial\phi_\gamma} &= -4\Omega(2\Omega-1)C\gamma\sin\phi_\gamma\left[\frac{2\alpha_{(0,0)}^2\cos 2\phi_{(0,0)}+2\alpha_{(1,1)}^2\cos 2\phi_{(1,1)}}{(1+\alpha^2)^2}+\frac{2}{2\Omega-1}\frac{\alpha^2}{1+\alpha^2}\right] \\ &\quad \times\left(1-\frac{\alpha^2}{1+\alpha^2}\right)=0 \\ \frac{\partial V}{\partial\phi_{(0,0)}} &= -4\Omega(2\Omega-1)C\gamma\cos\phi_\gamma\frac{4\alpha_{(0,0)}^2}{(1+\alpha^2)^2}\sin 2\phi_{(0,0)}=0 \\ \frac{\partial V}{\partial\phi_{(1,1)}} &= -4\Omega(2\Omega-1)C\gamma\cos\phi_\gamma\frac{4\alpha_{(1,1)}^2}{(1+\alpha^2)^2}\sin 2\phi_{(1,1)}=0,\end{aligned} \tag{3.8}$$

which can be solved by setting $\phi_\gamma = \phi_{(0,0)} = \phi_{(1,1)} = 0$, and we identify them as critical points. Direct substitution of them in (3.7) yields the following two variable semi-classical

potential

$$V(\alpha,\gamma;C)=4\Omega\omega_q\frac{\alpha^2}{(1+\alpha^2)^2}+\omega_\beta\gamma^2+8\Omega(2\Omega-1)C\gamma\frac{\alpha^2}{(1+\alpha^2)^2}\left[\frac{1}{1+\alpha^2}+\frac{2}{2\Omega-1}\right]. \quad (3.9)$$

The critical points of the new semi-classical potential (3.9) satisfy $\nabla V|_{(\alpha_c,\gamma_c)}=0$ and its component for the γ variable is the partial derivative

$$\left.\frac{\partial V}{\partial\gamma}\right|_{\gamma_c}=2\omega_\beta\gamma_c+8\Omega(2\Omega-1)C\frac{\alpha^2}{(1+\alpha^2)^2}\left[\frac{1}{1+\alpha^2}+\frac{2}{2\Omega-1}\right]=0, \quad (3.10)$$

which can be solved for γ and we get

$$\gamma_c=-4\Omega(2\Omega-1)\frac{C}{\omega_\beta}\frac{\alpha^2}{(1+\alpha^2)^2}\left[\frac{1}{1+\alpha^2}+\frac{2}{2\Omega-1}\right]. \quad (3.11)$$

Direct substitution of (3.11) back in (3.9) gives the new one-dimensional potential

$$V(\alpha,\gamma_c;C)=4\Omega\omega_q\left\{\frac{\alpha^2}{(1+\alpha^2)^2}-\kappa\frac{\alpha^4}{(1+\alpha^2)^4}\left[\frac{1}{1+\alpha^2}+\frac{2}{2\Omega-1}\right]^2\right\}, \quad (3.12)$$

where we defined the dimensionless parameter κ as

$$\kappa=4\Omega(2\Omega-1)^2\frac{C^2}{\omega_q\omega_\beta}. \quad (3.13)$$

The previous simplification of the initial two-dimensional potential to a one-dimensional one is justified by the calculations described in Appendix B.

3.2.1 Bifurcation and Maxwell sets

Similarly to the SACM examples discussed previously the bifurcation and Maxwell sets in the one-dimensional parameter space can be obtained by following the formulae in Appendix C.

A feature which define the critical point at the origin of the potential ($\alpha=0,\gamma=0$) can be found by calculating the Hessian determinant at that point resulting in

$$\left|\begin{array}{cc}\frac{\partial^2V(\alpha,\gamma;C)}{\partial\alpha^2} & \frac{\partial^2V(\alpha,\gamma;C)}{\partial\alpha\partial\gamma}\\ \frac{\partial^2V(\alpha,\gamma;C)}{\partial\gamma\partial\alpha} & \frac{\partial^2V(\alpha,\gamma;C)}{\partial\gamma^2}\end{array}\right|_{(\alpha=0,\gamma=0)}=16\Omega\omega_q\omega_\beta, \quad (3.14)$$

which is a positive constant independent on the parameter, meaning that the critical point ($\alpha=0,\gamma=0$) always remains a minimum.

The critical manifold of the potential (3.12) is the surface of critical points, which satisfy the equation

$$\frac{\partial V(\alpha,\gamma_c;C)}{\partial\alpha}=0, \quad (3.15)$$

spanned by the variation of the parameter κ. From (3.15) we can solve for κ and obtain

$$\kappa=-\frac{(1-\alpha^2)(1+\alpha^2)^4(2\Omega-1)^2}{2\alpha^2(\alpha^2+2\Omega)(\alpha^4+2\alpha^2(2\Omega-1)-2\Omega)}. \quad (3.16)$$

In this one-dimensional example the singular mapping of the critical manifold to the parameter space occurs when that derivative of (3.16) with respect to α is zero, which leads to a 10th degree polynomial:

$$f_B(\alpha, 2\Omega) = -4\Omega^2 + 4\Omega\alpha^2(7\Omega - 3) - 2\alpha^4(20\Omega^2 - 18\Omega + 3) + 2\alpha^6(12\Omega^2 - 18\Omega + 5) + \alpha^8(12\Omega - 7) + \alpha^{10}, \tag{3.17}$$

and after solving it for α we substitute the result back (3.16) and obtain the bifurcation set. For the set values $2\Omega = 18$, $\omega_q = 0.33\,\text{GeV}$, and $\omega_\beta = 1.6\,\text{GeV}$, we get

$$\kappa_B = 5.8997. \tag{3.18}$$

The bifurcation set in the parameter space C is obtained by substituting (3.18) in (3.13):

$$C_B = 0.017303\,\text{GeV}. \tag{3.19}$$

The Maxwell set is the subspace in parameter space where the mapping of the roots manifold is singular. The roots manifold is the surface of all the real roots satisfying

$$V(\alpha, \gamma_c; C) + V_0 = 0, \tag{3.20}$$

as the parameter κ is spanned, with V_0 a real number. We can solve (3.20) for κ, setting $V_0 = 0$ as no two minima coincide at $V_0 \neq 0$, and we get

$$\kappa = \frac{(1+\alpha^2)^4(2\Omega - 1)^2}{\alpha^2(\alpha^2 + 2\Omega)^2}. \tag{3.21}$$

Again, in this one-dimensional example the singular mapping occurs when the derivative of (3.21) with respect to α is zero. This condition leads to a 4th degree polynomial

$$f_M(\alpha, 2\Omega) = -2\Omega + 3\alpha^2(2\Omega - 1) + \alpha^4, \tag{3.22}$$

whose appropriate real roots are given by

$$\alpha = \pm\sqrt{\frac{1}{2}\left(-3(2\Omega - 1) + \sqrt{36\Omega^2 - 28\Omega + 9}\right)}. \tag{3.23}$$

Substituting (3.23) back to (3.21) we obtain the Maxwell set as a function of 2Ω:

$$\kappa_M(2\Omega) = \frac{(2\Omega - 1)^2\left(5 - 6\Omega + \sqrt{9 + 4\Omega(9\Omega - 7)}\right)^4}{2\left(3 - 6\Omega + \sqrt{9 + 4\Omega(9\Omega - 7)}\right)\left(3 - 2\Omega + \sqrt{9 + 4\Omega(9\Omega - 7)}\right)^2}. \tag{3.24}$$

For the set values $2\Omega = 18$, $\omega_q = 0.33\,\text{GeV}$, and $\omega_\beta = 1.6\,\text{GeV}$, we get

$$\kappa_M = 8.14502, \tag{3.25}$$

and using the definition (3.13) the Maxwell set in the interaction parameter space C is:

$$C_M = 0.020331\,\text{GeV}. \tag{3.26}$$

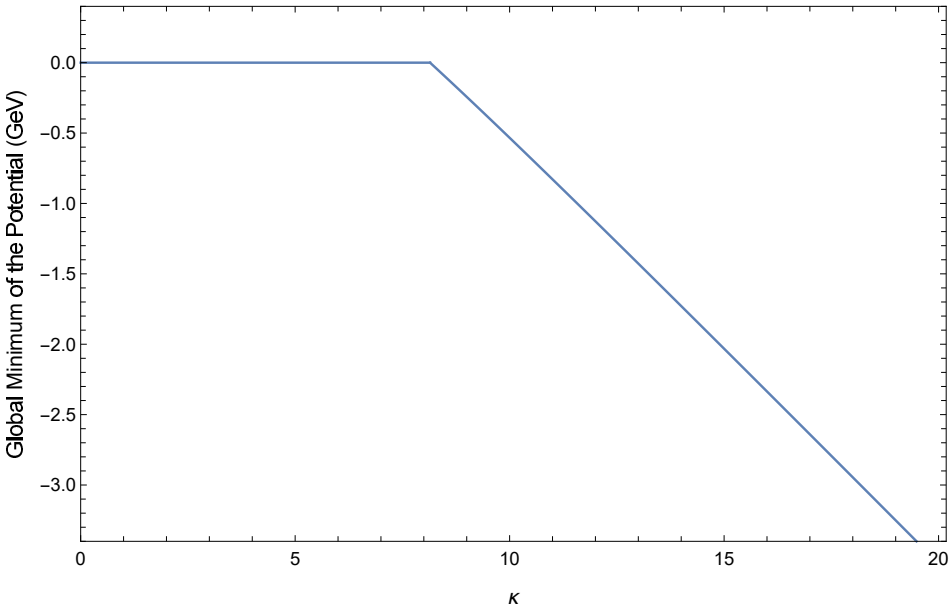

Figure 3.3: Global minimum of the semi-classical potential as a function of κ. A first order phase transitions is found at $\kappa = 8.14502$ ($C = 0.020331\,\text{GeV}$), characterised by a discontinuity in the first derivative with respect to κ. The values used in this plot are $\omega_q = 0.33\,\text{GeV}$, $\omega_\beta = 1.6\,\text{GeV}$ and $2\Omega = 18$.

3.3 Quantum phase transitions

When the interaction parameter C increases in intensity until it crosses the value C_M a *first order QPT* occurs, when a former local minimum at $\alpha > 0$ becomes the new global minimum of the potential at $V(\alpha > 0) < 0$, while the minima at the origin $V(\alpha = 0) = 0$ stays the same. In Fig. 3.3 the global minimum of the potential is plotted as a function of κ, where a discontinuity of its first derivative with respect to κ is part at the point κ_M of the Maxwell set.

In Fig. 3.4 contour plots (left) of the semi-classical potential $V(\alpha, \gamma; C)$ in (3.9), along with the critical value of γ as a function of α in (3.11), and the corresponding one-dimensional potentials (right) for different values of C are shown. For the value C_B we can see that a new local minimum is beginning to emerge, and for the value C_M two minimum are at the same height.

3.3.1 Physical observables

In this subsection we study how some physical observables related to the number of particles change as the interaction parameter C increases and the phase transition is reached. The expectation number of the quark-antiquark pairs and the gluon pairs are

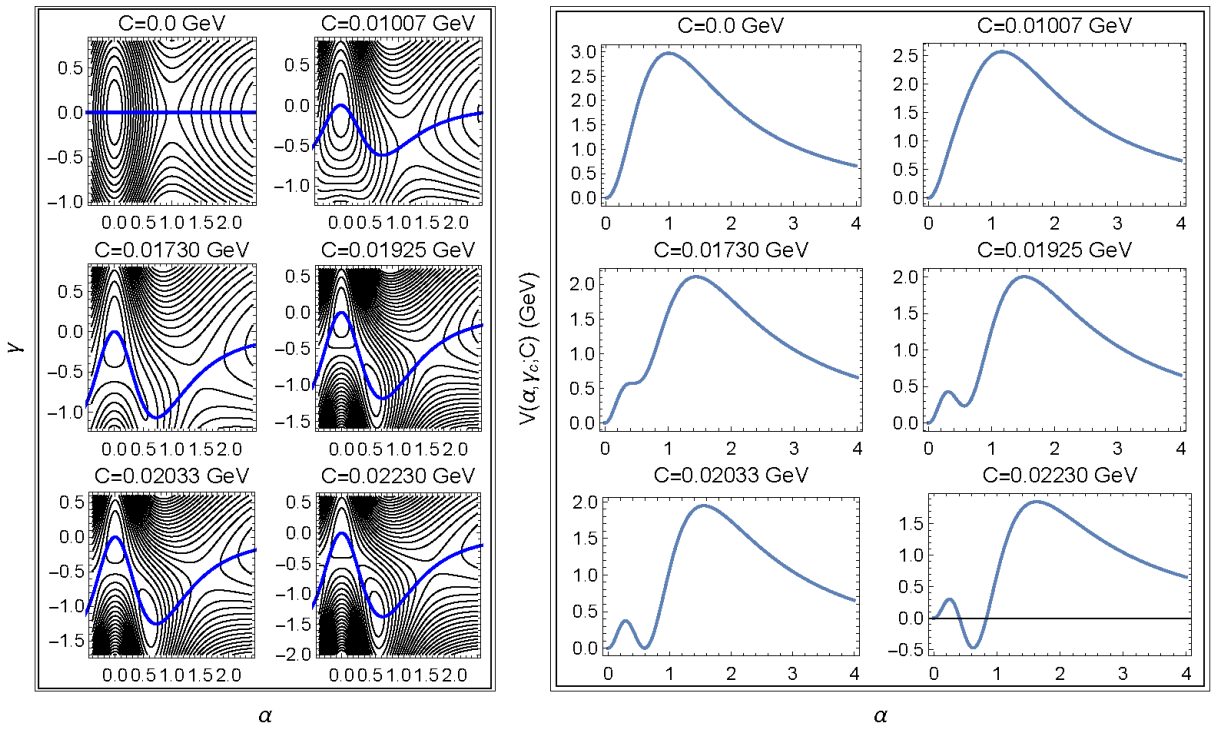

Figure 3.4: In the left side we show contour plots (α, γ) of the semi-classical potential (3.9) for different values of C. In the right side their respective one dimensional semi-classical potential (3.12) are plotted. The critical values of γ_c as a function of α given in (3.11) are depicted as blue lines in the contour plots. The values used for these plots are $\omega_q = 0.33\,\text{GeV}$, $\omega_\beta = 1.6\,\text{GeV}$ and $2\Omega = 18$.

given, respectively by

$$\langle \boldsymbol{n}_q \rangle = 2\Omega \frac{\alpha^2}{1+\alpha^2} \tag{3.27}$$

$$\langle \boldsymbol{n}_\beta \rangle = \gamma^2. \tag{3.28}$$

In Fig. 3.5 the expectation number of the quark-antiquark pairs and gluon pairs as a function of C are plotted. The plots are obtained by evaluating (3.27) and (3.28) at the critical points (α_c, γ_c) of the global minimum of the semi-classical potential. For values of the parameter C below the Maxwell set C_M the number of quark-antiquark pairs and gluon pairs is zero, as the global minimum is located at the origin. As the interaction is increased a sudden jump at C_M occurs and the number of particle pairs is non-zero. This discontinuity is a consequence of the phase transition. The number of gluon pairs surpasses the number of quark-antiquark pairs at about $C = 0.039\,\text{GeV}$, and as the interaction increases the number of quark-antiquark pairs become saturated tending to a constant value, while the number of gluon pairs continue to increase.

The results obtained from (3.27) and (3.28), shown in Fig. 3.5 can be related to physical quantities. The quark-antiquark and gluon condensate [101] in terms of the

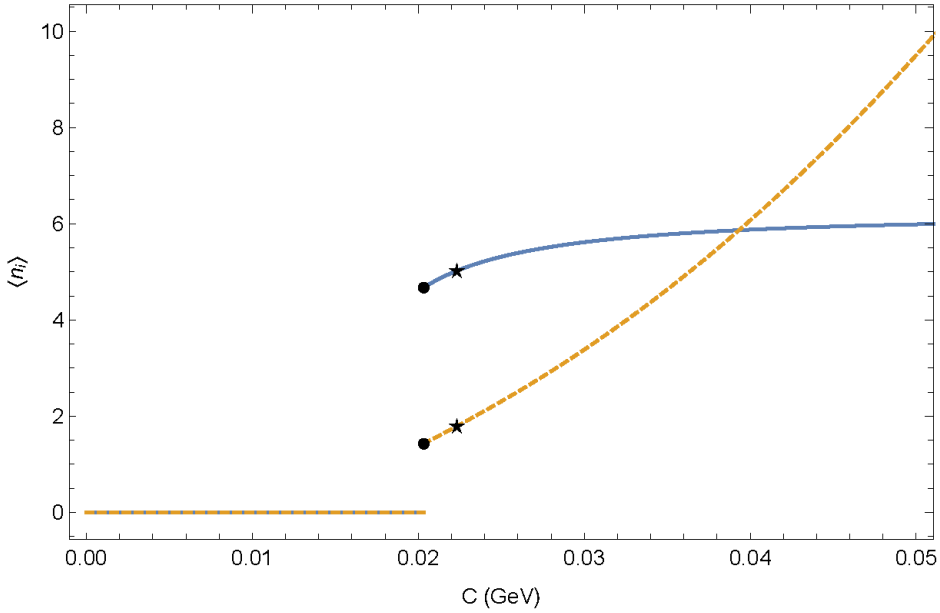

Figure 3.5: Expectation values of quark-antiquark pairs $\langle \boldsymbol{n}_q \rangle$ (blue, solid) and gluon pairs $\langle \boldsymbol{n}_\beta \rangle$ (yellow, dashed) as a function of C. The black dot and the black star depict quark-antiquark and gluon pairs at $C = 0.020331\,\text{GeV}$ (Maxwell set) and at $C = 0.022301\,\text{GeV}$, respectively. For large values of C the gluon pairs grow indefinitely, while the quark-antiquark pairs saturate at about $\langle \boldsymbol{n}_q \rangle = 6.169$. The values used for this plot are $\omega_q = 0.33\,\text{GeV}$, $\omega_\beta = 1.6\,\text{GeV}$ and $2\Omega = 18$.

number of quarks and gluons was given in [104]:

$$\begin{aligned} \langle \text{vac}|\bar{\Psi}_f \Psi_f|\text{vac}\rangle &= \frac{1}{V}\left(\frac{2n_q}{3} - 6\right) \\ \langle \text{vac}|\frac{\alpha_s}{\pi} F^a_{\mu\nu} F^{\mu\nu}_a|\text{vac}\rangle &= \left(\frac{\alpha_s 16\pi}{\omega_\beta^2 V^2}\right)(4n_\beta + 9)\,, \end{aligned} \tag{3.29}$$

where $\bar{\Psi}_f$ is the fermion function, $V = 4\pi r_0^3/3$ is the volume of a hadron with radius $r_0 = 0.875\,\text{fm} = 4.375\,\text{GeV}^{-1}$ [104], and α_s is the strong coupling constant. In [101] the respective values of the quark-antiquark and gluon condensates obtained were

$$\begin{aligned} \langle \text{vac}|\bar{\Psi}_f \Psi_f|\text{vac}\rangle &= -(0.223\,\text{GeV})^3 \\ \langle \text{vac}|\frac{\alpha_s}{\pi} F^a_{\mu\nu} F^{\mu\nu}_a|\text{vac}\rangle &= (0.360\,\text{GeV})^4. \end{aligned} \tag{3.30}$$

Using (3.30) and (3.29) we can deduce that the number of quarks for these values is approximately $n_q \approx 4$, which corresponds to the value of $\langle \boldsymbol{n}_q \rangle$ immediately after the phase transition. As an example we consider two values of C to calculate the number of quark-antiquark pairs and gluon pairs to use in (3.29) and compare the results with (3.30). The two values considered are $C_1 = C_M = 0.020331\,\text{GeV}$ and a point a little after the phase transition $C_2 = 0.022301\,\text{GeV}$. In Fig. 3.5 the number of quark-antiquark pairs

and gluon pairs for those two values are represented by a circle for C_1 and by a star for C_2. In the table below we show a summary of the results:

Values of physical quantities for two values of C				
C(GeV)	$\langle \boldsymbol{n}_q \rangle$	$\langle \boldsymbol{n}_\beta \rangle$	$\langle \text{vac}\|\bar{\Psi}_f \Psi_f\|\text{vac}\rangle$	α_s
$C_1 = 0.020331$	4.67192	1.42697	$-(0.202\,\text{GeV})^3$	7.156
$C_2 = 0.022301$	5.01946	1.79012	$-(0.1963\,\text{GeV})^3$	6.513

The value of the quark condensate obtained at the point of the transition is comparable with the value presented in [101], and the values of the strong coupling constant are also within the range of value predicted in [101]. From these results we can conclude that the model is consistent and that the physical vacuum of QCD is probably a state near a phase transition. From this study we also find that the methods of catastrophe theory are very useful in the description of phase transitions in different models in various areas of physics.

Chapter 4

Conclusions

In this thesis we studied the quantum phase transitions in an algebraic cluster model which observes the Pauli exclusion principle, namely in the SACM. Even though this property of the model adds some complexity in the semi-classical analysis, comparative to other models, we believe it is worthwhile to solve these problems as they offer a more accurate description of the physical interactions. As test examples we considered two types of cluster systems: The system of two spherical clusters $^{16}\mathrm{O} + \alpha \rightarrow {}^{20}\mathrm{Ne}$, and the system of two deformed clusters $^{12}\mathrm{C} + {}^{12}\mathrm{C} \rightarrow {}^{24}\mathrm{Mg}$.

In order to study the QPTs we used the catastrophe theory program. This allowed us to construct the separatrices in parameter space of the semi-classical potential of the SACM for two different types of parametrisations of the coherent states: One where they transform as tensors, in the same way as the creation and annihilation operators of the π bosons, and the other where they arbitrary complex variables. Going from one region to another implies a change in the stability structure of the potential, i.e. in their critical points, which are interpreted as phase transitions. A different method to obtain the Maxwell set separatrix based on the essence of catastrophe theory was developed. This new method is useful when dealing with complicated and involved potentials. Three types of phase transitions were identified:

i) Region I $\rightarrow$ Region IV: The spherical global minimum $V(\alpha = 0) = 0$ continuously and becomes a deformed global minimum $V(\alpha > 0) < 0$ resulting in a *second order phase transition*.

ii) Region II $\rightarrow$ Region III (crossing the Maxwell set): The global minimum of the potential suddenly jumps from a spherical global minimum $V(\alpha = 0) = 0$ to a deformed global minimum $V(\alpha > 0) < 0$ resulting in a *first order phase transition*.

iii) $r_2 > 0$ to $r_2 < 0$ at $r_1 = 0$: The spherical global minimum $V(\alpha = 0) = 0$ continuously changes and becomes a deformed global minimum $V(\alpha > 0) < 0$, where the potential goes as α^6 in the limit $\alpha \rightarrow 0$, resulting in a *third order phase transition*.

We explored two different ways of obtaining trajectories in parameter space for the purpose of going from one region to another:

a) In the SU(3) limit we fix the interaction parameters $\{\bar{b}, b, c, \xi, t_1\}$ and vary the parameter $a(\bar{a})$ of the quadrupole interaction (second order Casimir operator of SU(3)).

b) When mixing with the SO(4) symmetry is allowed we fix the interaction parameters $\{\bar{a}, a, \bar{b}, b, \xi, t_1\}$ and vary the parameter c of the second order Casimir operator of SO(4), which results in a second order QPT, where a spherical minimum becomes a deformed minimum.

We were able to map the results obtained of phase transitions semi-classically to effects in the energy levels and other physical observables obtained with the diagonalisation of the Hamiltonian in the space of the SACM. In the SU(3) limit it was possible to find signatures of a QPT in the energy levels of the 0^+ states as avoided energy levels with the ground state 0_1^+ in the vicinity of the value of $a(\bar{a})$ where it crosses the relevant separatrix. In the case with SO(4) symmetry mixing smooth changes where found in the $B(E2)$ probability transition of the state 2_1^+ to 0_1^+ and in the expectation number of π bosons in the ground state as functions of c near the crossing of the separatrix, when going from region I to region IV. These smooth changes were more sharp and drastic in the semi-classical analysis with coherent states.

In this thesis we also applied the catastrophe theory methodology to a different physical problem: An effective model of QCD. This shows the effectiveness and usefulness of the methods developed in this work. The Hamiltonian of the model depends only on one interacting parameter and the parameter space is one-dimensional. When the intensity of the interaction is strong enough and surpasses the value of the Maxwell set a first order phase transition occurs. We were able to extract physical information when studying the expectation value of the number of quark-antiquark pairs and gluon pairs, and relating them to the quark and gluon condensates. A value for the strong coupling constant just after the point of the phase transition was obtained and was found to be consistent and within the limits established by [101] for low energy. This way we can interpreted the physical vacuum as a state just after a phase transition. In both of these examples the phase transitions are obtained by increasing one of the interacting parameters until it reaches a critical value. This results in the trajectory described in parameter space crossing of one of the separatrices and the structure of the potential is changed.

The present work developed in this thesis can be expanded and improved, and a number of different applications to other areas of physics are possible. Of immediate interest is the application to the SACM for heavy nuclei, which has been recently developed in [105] based on the pseudo-SU(3) model [106, 107], and study QPTs in heavy cluster systems. The comparison of experimental data which can be identified as the phenomena of QPTs is of significant importance and remains to be study in detail in the future. The use of the cranking method to study QPTs of excited rotational states for systems of deformed clusters still remains to be fully analysed, and we hope that the results presented in this thesis may be useful for this and many other purposes.

Appendix A

Expectation values in the coherent state basis

The geometrical mapping of the SACM was given in [70]. The coherent states were defined as

$$\begin{aligned} |\alpha\rangle &= \mathcal{N}_{N,n_0}(\boldsymbol{\alpha}^* \cdot \boldsymbol{\pi}^\dagger)^{n_0}[\boldsymbol{\sigma}^\dagger + (\boldsymbol{\alpha}^* \cdot \boldsymbol{\pi}^\dagger)]^N|0\rangle \\ &= \frac{N!}{(N+n_0)!}\mathcal{N}_{N,n_0}\frac{d^{n_0}}{d\gamma^{n_0}}[\boldsymbol{\sigma}^\dagger + \gamma(\boldsymbol{\alpha}^* \cdot \boldsymbol{\pi}^\dagger)]^{N+n_0}|0\rangle\Big|_{\gamma=1} \end{aligned} \tag{A.1}$$

with the normalisation constant given by

$$\mathcal{N}^{-2}_{N,n_0} = \frac{(N!)^2}{(N+n_0)!}\frac{d^{n_0}}{d\gamma_1^{n_0}}\frac{d^{n_0}}{d\gamma_2^{n_0}}[1+\gamma_1\gamma_2(\boldsymbol{\alpha}^* \cdot \boldsymbol{\alpha})]^{N+n_0}\Big|_{\gamma_1=\gamma_2=1}. \tag{A.2}$$

The coherent states depend on the minimal number of π bosons n_0, on the total number of bosons $N + n_0$ and on the α_m. As mentioned in the text in Section 2.2 there are two main cases for the nature of the coherent states parameters:

i) The α_m behave as tensors and transform in the same way as the $\boldsymbol{\pi}^\dagger_m$ and $\boldsymbol{\pi}^m$ operators, i.e.
$$\alpha^*_m = (-1)^{1-m}\alpha_{-m} \tag{A.3}$$

ii) The α_m are completely arbitrary complex variables.

In the following all expressions will be written with the case ii) knowing that the case i) is easily obtainable using (A.3).

The direct product appearing in (A.1) are explicitly given by

$$(\boldsymbol{\alpha} \cdot \boldsymbol{\pi}^\dagger) = \sum_{m=-1}^{1} \alpha_m \pi^\dagger_m. \tag{A.4}$$

The expectation value of an arbitrary operator $\boldsymbol{O}$ is explicitly given by

$$\langle\alpha|\boldsymbol{O}|\alpha\rangle = \mathcal{N}^2_{N,n_0}\left[\frac{N!}{(N+n_0)!}\right]^2 \frac{\mathrm{d}^{n_0}}{\mathrm{d}\gamma_1^{n_0}}\frac{\mathrm{d}^{n_0}}{\mathrm{d}\gamma_2^{n_0}}\langle 0|[\boldsymbol{\sigma} + \gamma_1(\boldsymbol{\alpha} \cdot \boldsymbol{\pi})]^{N+n_0}\boldsymbol{O}[\boldsymbol{\sigma}^\dagger + \gamma_2(\boldsymbol{\alpha} \cdot \boldsymbol{\pi}^\dagger)]^{N+n_0}|0\rangle \tag{A.5}$$

The operators that appear in the Hamiltonian are couplings of the creation and annihilation operators of the U(4) group to spin $S = 0, 1, 2$. In the following we enlist the expectation values of these type of operators [62, 70]:

$$\begin{aligned}
\langle\alpha|[\boldsymbol{\pi}^\dagger \otimes \boldsymbol{\pi}]^{[S]}_m|\alpha\rangle &= [\boldsymbol{\alpha}^* \times \tilde{\boldsymbol{\alpha}}]^{[S]}_m \frac{F_{11}(\alpha)}{F_{00}(\alpha)} \\
\langle\alpha|[[\boldsymbol{\pi}^\dagger \otimes \boldsymbol{\pi}^\dagger]^{[S_1]} \otimes [\boldsymbol{\pi} \otimes \boldsymbol{\pi}]^{[S_2]}]^{[S]}_m|\alpha\rangle &= [[\boldsymbol{\alpha}^* \times \boldsymbol{\alpha}^*]^{[S_1]} \times [\tilde{\boldsymbol{\alpha}} \times \tilde{\boldsymbol{\alpha}}]^{[S_2]}]^{[S]}_m \frac{F_{22}(\alpha)}{F_{00}(\alpha)} \\
\langle\alpha|[\boldsymbol{\pi}^\dagger \otimes \boldsymbol{\pi}^\dagger]^{[S]}_m \boldsymbol{\sigma}^2|\alpha\rangle &= [\boldsymbol{\alpha}^* \times \boldsymbol{\alpha}^*]^{[S]}_m \frac{F_{20}(\alpha)}{F_{00}(\alpha)} \\
\langle\alpha|(\boldsymbol{\sigma}^\dagger)^2[\boldsymbol{\pi} \otimes \boldsymbol{\pi}]^{[S]}_m|\alpha\rangle &= [\tilde{\boldsymbol{\alpha}} \times \tilde{\boldsymbol{\alpha}}]^{[S]}_m \frac{F_{20}(\alpha)}{F_{00}(\alpha)} \\
\langle\alpha|(\boldsymbol{\sigma}^\dagger)^2\boldsymbol{\sigma}^2|\alpha\rangle &= (N + n_0)(N + n_0 - 1) \\
&\quad - 2(N + n_0 - 1)(\boldsymbol{\alpha}^* \cdot \boldsymbol{\alpha})\frac{F_{11}(\alpha)}{F_{00}(\alpha)} + (\boldsymbol{\alpha}^* \times \boldsymbol{\alpha})^2 \frac{F_{22}(\alpha)}{F_{00}(\alpha)}
\end{aligned} \tag{A.6}$$

where we introduced the notation $\tilde{\alpha}_m = (-1)^{1-m}\alpha_{-m}$, and the $F_{pq}(\alpha)$ functions are defined as [62]:

$$\begin{aligned}
F_{pq}(\alpha^2) = &\frac{(N!)^2}{(N + n_0 - \max(p, q))!} \\
&\times \sum_{k=\max(n_0-p, n_0-q)}^{N+n_0-\max(p,q)} \binom{N + n_0 - \max(p, q)}{k} \frac{(k + p)!}{(k + p - n_0)!} \frac{(k + q)!}{(k + q - n_0)!} \alpha^{2k}.
\end{aligned} \tag{A.7}$$

Using the results in (A.6) we can obtain the expectation value of the Casimir operator $\boldsymbol{C}_2(\lambda, \mu)$:

$$\begin{aligned}
\langle\alpha|\boldsymbol{C}_2(\lambda, \mu)|\alpha\rangle = &\langle \boldsymbol{C}_2(\lambda_C, \mu_C)\rangle + 2\sqrt{3}\langle \boldsymbol{Q}_{C,0}\rangle [\boldsymbol{\alpha}^* \times \tilde{\boldsymbol{\alpha}}]^{[2]}_0 \frac{F_{11}(\alpha)}{F_{00}(\alpha)} + (\boldsymbol{\alpha}^* \cdot \boldsymbol{\alpha})\frac{F_{11}(\alpha)}{F_{00}(\alpha)} \\
&+ (\boldsymbol{\alpha}^* \cdot \boldsymbol{\alpha})^2 \frac{F_{22}(\alpha)}{F_{00}(\alpha)}.
\end{aligned} \tag{A.8}$$

Finally, we define the square of the relative angular momentum as

$$\boldsymbol{L}^2 = \boldsymbol{L}_R \cdot \boldsymbol{L}_R = -2\sqrt{3}[[\boldsymbol{\pi}^\dagger \otimes \boldsymbol{\pi}]^1 \otimes [\boldsymbol{\pi}^\dagger \otimes \boldsymbol{\pi}]^1]^0_0, \tag{A.9}$$

the minus sign is to maintain the Cartesian $\boldsymbol{L}^2 = \boldsymbol{L}_x^2 + \boldsymbol{L}_y^2 + \boldsymbol{L}_z^2$. This is because the spherical components of $\boldsymbol{L}$, i.e. the components on the spherical basis, are defined as

$$\boldsymbol{L}_{+1} = \sqrt{2}[\boldsymbol{\pi}^\dagger \otimes \boldsymbol{\pi}]^1_{+1} \tag{A.10}$$

$$\boldsymbol{L}_{-1} = \sqrt{2}[\boldsymbol{\pi}^\dagger \otimes \boldsymbol{\pi}]^1_{-1} \tag{A.11}$$

$$\boldsymbol{L}_0 = \sqrt{2}[\boldsymbol{\pi}^\dagger \otimes \boldsymbol{\pi}]^1_0, \tag{A.12}$$

so that

$$\boldsymbol{L}^2 = -\boldsymbol{L}_{-1}\boldsymbol{L}_{+1} + \boldsymbol{L}_0\boldsymbol{L}_0 - \boldsymbol{L}_{+1}\boldsymbol{L}_{-1} = \boldsymbol{L}_x^2 + \boldsymbol{L}_y^2 + \boldsymbol{L}_z^2, \tag{A.13}$$

which is effectively recreated in (A.13). The expectation value of (A.13) is

$$\begin{aligned}
\langle\alpha|\boldsymbol{L}^2|\alpha\rangle &= -2\sqrt{3}\langle\alpha|[[\boldsymbol{\pi}^\dagger\otimes\boldsymbol{\pi}]^1\otimes[\boldsymbol{\pi}^\dagger\otimes\boldsymbol{\pi}]^1]^0_0|\alpha\rangle \\
&= -2\sqrt{3}\sum_{m_a m_b}\frac{(-1)^{1-m_a}}{\sqrt{3}}\delta_{m_a-m_b} \\
&\quad\times\sum_{m_1m_2}\sum_{m_3m_4}(1m_11m_2|1m_a)(1m_31m_4|1m_b)\langle\alpha|\boldsymbol{\pi}^\dagger_{m_1}\boldsymbol{\pi}_{m_2}\boldsymbol{\pi}^\dagger_{m_3}\boldsymbol{\pi}_{m_4}|\alpha\rangle \\
&= -2\sum_m(-1)^{1-m}\sum_{m_1m_2}\sum_{m_3m_4}(1m_11m_2|1m)(1m_31m_4|1-m)\langle\alpha|\boldsymbol{\pi}^\dagger_{m_1}\boldsymbol{\pi}_{m_2}\boldsymbol{\pi}^\dagger_{m_3}\boldsymbol{\pi}_{m_4}|\alpha\rangle
\end{aligned}$$

and with

$$\boldsymbol{\pi}_{m_2}\boldsymbol{\pi}^\dagger_{m_3} = (-1)^{1-m_2}\boldsymbol{\pi}^{-m_2}\boldsymbol{\pi}^\dagger_{m_3} = (-1)^{1-m_2}\delta^{-m_2}_{m_3} + \boldsymbol{\pi}^\dagger_{m_3}\boldsymbol{\pi}_{m_2} \tag{A.14}$$

we get

$$\begin{aligned}
\langle\alpha|\boldsymbol{L}^2|\alpha\rangle &= -2\sum_m(-1)^{1-m}\sum_{m_1m_2m_4}(-1)^{1-m_2}(1m_11m_2|1m)(1-m_21m_4|1-m)\langle\alpha|\boldsymbol{\pi}^\dagger_{m_1}\boldsymbol{\pi}_{m_4}|\alpha\rangle \\
&\quad-2\sum_m(-1)^{1-m}\sum_{m_1m_2}\sum_{m_3m_4}(1m_11m_2|1m)(1m_31m_4|1-m)\langle\alpha|\boldsymbol{\pi}^\dagger_{m_1}\boldsymbol{\pi}^\dagger_{m_3}\boldsymbol{\pi}_{m_2}\boldsymbol{\pi}_{m_4}|\alpha\rangle \\
&= -2\sum_m(-1)^{1-m}\sum_{m_1m_2m_4}(-1)^{1-m_2}(1m_11m_2|1m)(1-m_21m_4|1-m)\alpha^*_{m_1}\tilde{\alpha}_{m_4}\frac{F_{11}(\alpha^2)}{F_{00}(\alpha^2)} \\
&\quad-2\sum_m(-1)^{1-m}\sum_{m_1m_2}\sum_{m_3m_4}(1m_11m_2|1m)(1m_31m_4|1-m)\alpha^*_{m_1}\alpha^*_{m_3}\tilde{\alpha}_{m_2}\tilde{\alpha}_{m_4}\frac{F_{22}(\alpha^2)}{F_{00}(\alpha^2)} \\
&= 2\sum_{m_1m_4}(-1)^{1-m_1}\delta_{m_1-m_4}\alpha^*_{m_1}\tilde{\alpha}_{m_4}\frac{F_{11}(\alpha^2)}{F_{00}(\alpha^2)} \\
&\quad-2\sum_m(-1)^{1-m}\sum_{m_1m_2}\sum_{m_3m_4}(1m_11m_2|1m)(1m_31m_4|1-m)\alpha^*_{m_1}\tilde{\alpha}_{m_2}\alpha^*_{m_3}\tilde{\alpha}_{m_4}\frac{F_{22}(\alpha^2)}{F_{00}(\alpha^2)} \\
&= \sum_m\alpha^*_m\alpha_m\frac{F_{11}(\alpha^2)}{F_{00}(\alpha^2)} - 2\sqrt{3}[[\boldsymbol{\alpha}^*\times\tilde{\boldsymbol{\alpha}}]^1\times[\boldsymbol{\alpha}^*\times\tilde{\boldsymbol{\alpha}}]^1]^0_0\frac{F_{22}(\alpha^2)}{F_{00}(\alpha^2)}
\end{aligned} \tag{A.15}$$

where we used the following identity

$$-\sum_m(-1)^{1-m}\sum_{m_1m_2m_4}(-1)^{1-m_2}(1m_11m_2|1m)(1-m_21m_4|1-m) = \sum_{m_1m_4}(-1)^{1-m_1}\delta_{m_1-m_4}. \tag{A.16}$$

Appendix B

Critical points of a function of two variables

Two particular examples of functions depending on two variables and four parameters are studied. In the first example the function has a linear and a quadratic term in the variable y. In the second example the function has a quadratic and a quartic term in the variable y. In both examples the dependence on the variable x is given by non-singular rational functions.

In this work we encounter two potential functions, which depend on two variables. Both of these potential functions, one in the SACM and one in the QCD example, fall into the first example discussed here. The second example of functions are simply added to illustrate a particular type of potential functions for which the methods discussed are still applicable.

B.1 First example

Let us consider the two variables function f of the form:

$$f(x, y; a_1, a_2, a_3, a_4) = g_5(x) + a_4 g_4(x) + a_3 y^2 g_3(x) + a_2 y g_2(x) + a_1 g_1(x), \tag{B.1}$$

where $x, y, a_1, a_2, a_3, a_4 \in \mathbb{R}$, and $g_i(x)$ are real non-singular rational functions.

The critical points (x_c, y_c) are the pair of values that satisfy the condition

$$\nabla f(x, y)|_{(x_c, y_c)} = 0. \tag{B.2}$$

This condition may be written as the following set of equations:

$$\frac{\partial f}{\partial x} = \frac{\partial g_5}{\partial x} + a_4 \frac{\partial g_4}{\partial x} + a_3 y^2 \frac{\partial g_3}{\partial x} + a_2 y \frac{\partial g_2}{\partial x} + a_1 \frac{\partial g_1}{\partial x} = 0 \tag{B.3}$$

$$\frac{\partial f}{\partial y} = 2 a_3 y g_3(x) + a_2 g_2(x) = 0. \tag{B.4}$$

Then, the critical points (x_c, y_c) are those that satisfy (B.3) and (B.4) simultaneously.

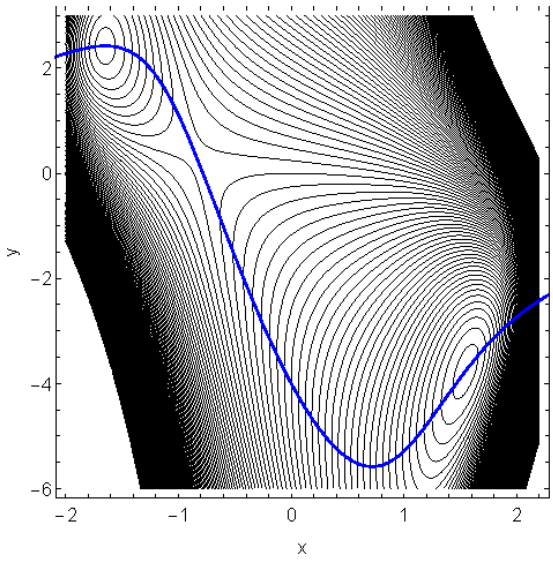

Figure B.1: Contour plot of the example in (B.10), with $a_4 = 20$, $a_3 = 10$, $a_2 = 80$, $a_1 = 20$. The blue curve represents the critical points of y as a function of x given in (B.11).

We can solve for y in (B.4) and obtain

$$y_c(x) = -\frac{a_2}{2a_3}\frac{g_2(x)}{g_3(x)}, \tag{B.5}$$

and by direct substitution in (B.3) obtain an equation solely for the x variable

$$\frac{\partial f}{\partial x} = \frac{\partial g_5}{\partial x} + a_4\frac{\partial g_4}{\partial x} + \frac{a_2^2}{4a_3}\left(\frac{g_2^2(x)}{g_3^2(x)}\frac{\partial g_3}{\partial x} - 2\frac{g_2(x)}{g_3(x)}\frac{\partial g_2}{\partial x}\right) + a_1\frac{\partial g_1}{\partial x} = 0, \tag{B.6}$$

so that the solution of (B.6) provides us with the critical values of x which in turn, by direct substitution in (B.5), also provides us with the critical values of y.

We will now show that by direct substitution of (B.5) in the initial function (B.1) we obtain a one dimensional function in the variable x, whose critical points condition is equal to (B.6), thus allowing us to treat the problem as a one dimensional system where the y variable is always critical.

Substituting (B.5) in (B.1) we get

$$f(x, y_c(x); a_1, a_2, a_3, a_4) = g_5(x) + a_4 g_4(x) - \frac{a_2^2}{4a_3}\frac{g_2^2(x)}{g_3(x)} + a_1 g_1(x), \tag{B.7}$$

and differentiating with respect to x we get

$$\frac{\partial f}{\partial x} = \frac{\partial g_5}{\partial x} + a_4\frac{\partial g_4}{\partial x} + \frac{a_2^2}{4a_3}\left(\frac{g_2^2(x)}{g_3^2(x)}\frac{\partial g_3}{\partial x} - 2\frac{g_2(x)}{g_3(x)}\frac{\partial g_2}{\partial x}\right) + a_1\frac{\partial g_1}{\partial x}, \tag{B.8}$$

which is identically to equation (B.6).

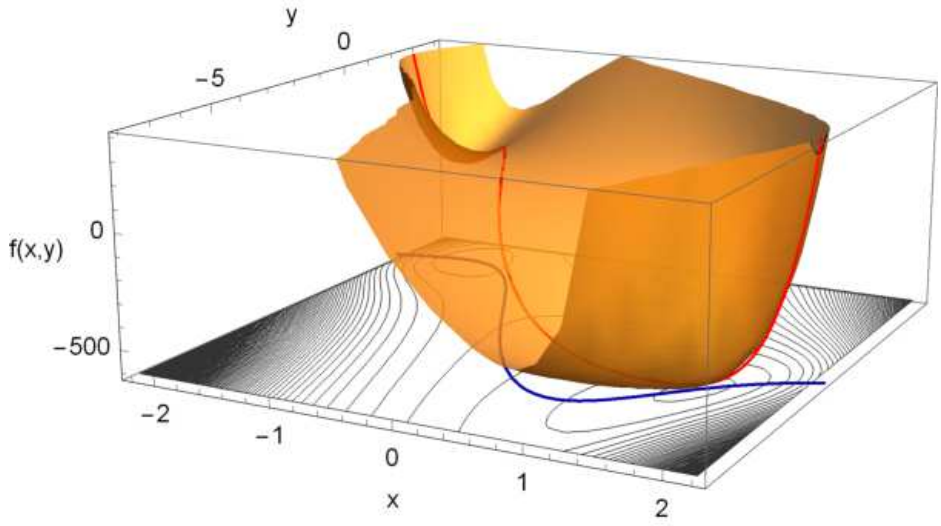

Figure B.2: Plot of function $f(x, y)$ in (B.10), with $a_4 = 20$, $a_3 = 10$, $a_2 = 80$, $a_1 = 20$. The red curve along the 2-dimensional surface is the one-dimensional function $f(x, y_c(x), a_1, a_2, a_3)$ and its projection in the (x, y)-plane is shown as the blue line in the contour plot.

As a particular example to illustrate this result we consider the following functions for $g_i(x)$ in (B.1):

$$\begin{aligned} g_5(x) &= 0 \\ g_4(x) &= \frac{x^8}{8} + \frac{x^6}{6} + \frac{x^4}{4} + \frac{x^2}{2} + 1 \\ g_3(x) &= \frac{x^6}{6} + \frac{x^4}{4} + \frac{x^2}{2} + 1 \\ g_2(x) &= \frac{x^5}{5} + \frac{x^3}{3} + x + 1 \\ g_1(x) &= \frac{x^2}{2} + 1 \end{aligned} \tag{B.9}$$

and obtain the two variable function

$$\begin{aligned} f(x, y; a_1, a_2, a_3, a_4) = a_4 \left(\frac{x^8}{8} + \frac{x^6}{6} + \frac{x^4}{4} + \frac{x^2}{2} + 1 \right) + a_3 y^2 \left(\frac{x^6}{6} + \frac{x^4}{4} + \frac{x^2}{2} + 1 \right) \\ + a_2 y \left(\frac{x^5}{5} + \frac{x^3}{3} + x + 1 \right) + a_1 \left(\frac{x^2}{2} + 1 \right). \end{aligned} \tag{B.10}$$

In Fig. B.1 we show the contour plot of (B.9) for a particular set of values of the parameters. The blue curve represents the critical points of y as a function of x, which from (B.5) and (B.9), are

$$y_c(x) = -4 \frac{\frac{x^5}{5} + \frac{x^3}{3} + x + 1}{\frac{x^6}{6} + \frac{x^4}{4} + \frac{x^2}{2} + 1}. \tag{B.11}$$

In Fig. B.2 we show the three-dimensional plot of (B.10). As a red curve along the 2-dimensional surface is the one-dimensional function $f(x, y_c, a_1, a_2, a_3)$ and its projection in the (x, y)-plane is shown as the blue line in the contour plot.

B.2 Second example

Let us consider the two variables function f of the form:

$$f(x, y; a_1, a_2, a_3, a_4) = g_5(x) + a_4 g_4(x) + a_3 y^4 g_3(x) + a_2 y^2 g_2(x) + a_1 g_1(x), \tag{B.12}$$

where $x, y, a_1, a_2, a_3, a_4 \in \mathbb{R}$, and $g_i(x)$ are arbitrary real functions and $g_3(x)$ has no real roots.

The critical points (x_c, y_c) are those that satisfy the condition

$$\nabla f(x, y)|_{(x_c, y_c)} = 0, \tag{B.13}$$

this condition may be written as the following set of equations:

$$\frac{\partial f}{\partial x} = \frac{\partial g_5}{\partial x} + a_4 \frac{\partial g_4}{\partial x} + a_3 y^4 \frac{\partial g_3}{\partial x} + a_2 y^2 \frac{\partial g_2}{\partial x} + a_1 \frac{\partial g_1}{\partial x} = 0 \tag{B.14}$$

$$\frac{\partial f}{\partial y} = 4 a_3 y^3 g_3(x) + 2 a_2 y g_2(x) = 0. \tag{B.15}$$

Then, the critical points (x_c, y_c) are those that satisfy (B.14) and (B.15) simultaneously.

We can solve y in (B.15) and obtain

$$y_0(x) = 0 \tag{B.16}$$

$$y_\pm(x) = \pm \sqrt{-\frac{a_2}{2a_3} \frac{g_2(x)}{g_3(x)}}, \tag{B.17}$$

which are now three different solutions for y. Direct substitution of (B.17) in (B.14) obtain an equation solely for the x variable

$$\frac{\partial f}{\partial x} = \frac{\partial g_5}{\partial x} + a_4 \frac{\partial g_4}{\partial x} + \frac{a_2^2}{4a_3} \left(\frac{g_2^2(x)}{g_3^2(x)} \frac{\partial g_3}{\partial x} - 2 \frac{g_2(x)}{g_3(x)} \frac{\partial g_2}{\partial x} \right) + a_1 \frac{\partial g_1}{\partial x} = 0, \tag{B.18}$$

so that the solution of (B.18) provides us with the critical values of x which in turn, by direct substitution in (B.17), also provides us with the critical values of y.

We will now show that by direct substitution of (B.17) in the initial function (B.12) we obtain a one dimensional function in the variable x, whose critical points condition is equal to (B.18), thus allowing us to treat the problem as a one dimensional system where the y variable is always critical.

Substituting (B.17) in (B.12) we get

$$f(x, y_\pm(x); a_1, a_2, a_3, a_4) = g_5(x) + a_4 g_4(x) - \frac{a_2^2}{4a_3} \frac{g_2^2(x)}{g_3(x)} + a_1 g_1(x), \tag{B.19}$$

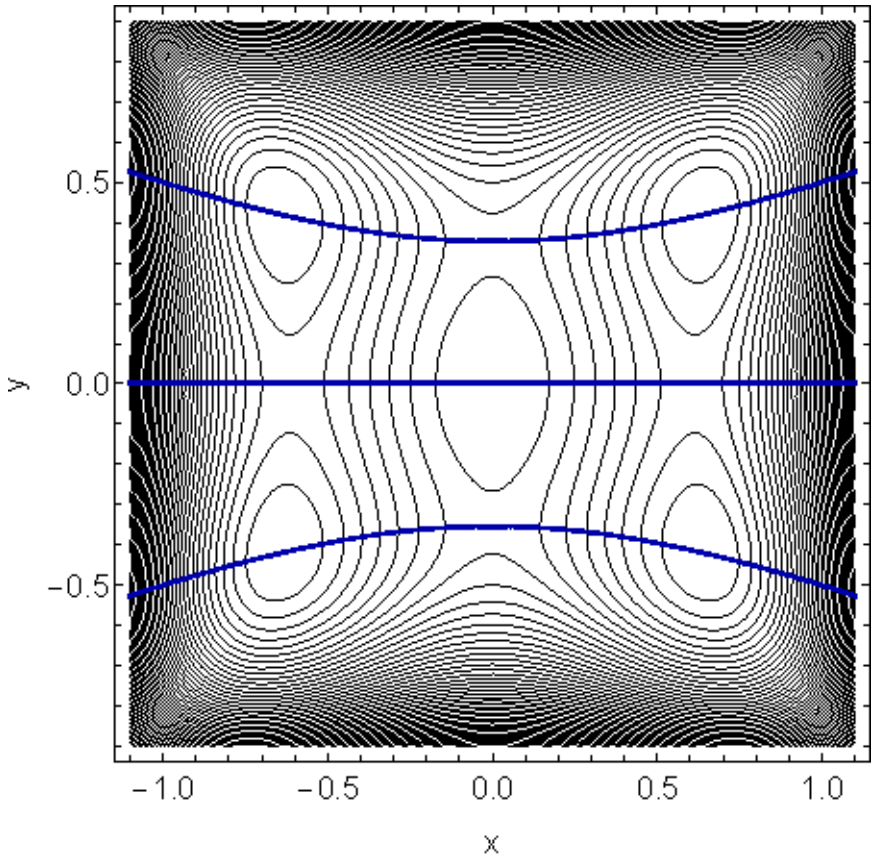

Figure B.3: Contour plot of the example in (B.22), with $a_4 = 2.4$, $a_3 = 4$, $a_2 = -1$, $a_1 = -1.8$. The blue curves are the critical points of y as a function of x given in (B.23) and (B.24).

and differentiation with respect to x we get

$$\frac{\partial f}{\partial x} = \frac{\partial g_5}{\partial x} + a_4 \frac{\partial g_4}{\partial x} + \frac{a_2^2}{4a_3}\left(\frac{g_2^2(x)}{g_3^2(x)}\frac{\partial g_3}{\partial x} - 2\frac{g_2(x)}{g_3(x)}\frac{\partial g_2}{\partial x}\right) + a_1 \frac{\partial g_1}{\partial x}, \tag{B.20}$$

which is identically to equation (B.18).

As a particular example we consider the following functions for $g_i(x)$ in (B.12):

$$\begin{aligned} g_5(x) &= 0 \\ g_4(x) &= x^4 \\ g_3(x) &= 1 \\ g_2(x) &= 1 + x^2 \\ g_1(x) &= x^2 \end{aligned} \tag{B.21}$$

and obtain the two variable function

$$f(x, y; a_1, a_2, a_3, a_4) = a_4 x^4 + a_3 y^4 + a_2 y^2 (1 + x^2) + a_1 x^2. \tag{B.22}$$

In order to illustrate the critical points, etc., we choose the parameters: $a_4 = 2.4$, $a_3 = 4$, $a_2 = -1$, $a_1 = -1.8$. In Fig. B.3 we show the countour plot of (B.22) for the chosen values of the parameters. The blue curves represent the critical points of y as a function of x, which from (B.16), (B.17) and (B.21), are

$$y_0(x) = 0 \tag{B.23}$$

$$y_\pm(x) = \pm\sqrt{\frac{1}{8}(1+x^2)}. \tag{B.24}$$

In Fig. B.4 we show the three-dimensional plot of the function example in (B.22). As light blue curves along the two-dimensional surface are the one-dimensional functions $f(x, y_0(x), a_1, a_2, a_3, a_4)$ and $f(x, y_\pm(x), a_1, a_2, a_3, a_4)$, and their projections are shown as the blue lines in the contour plot.

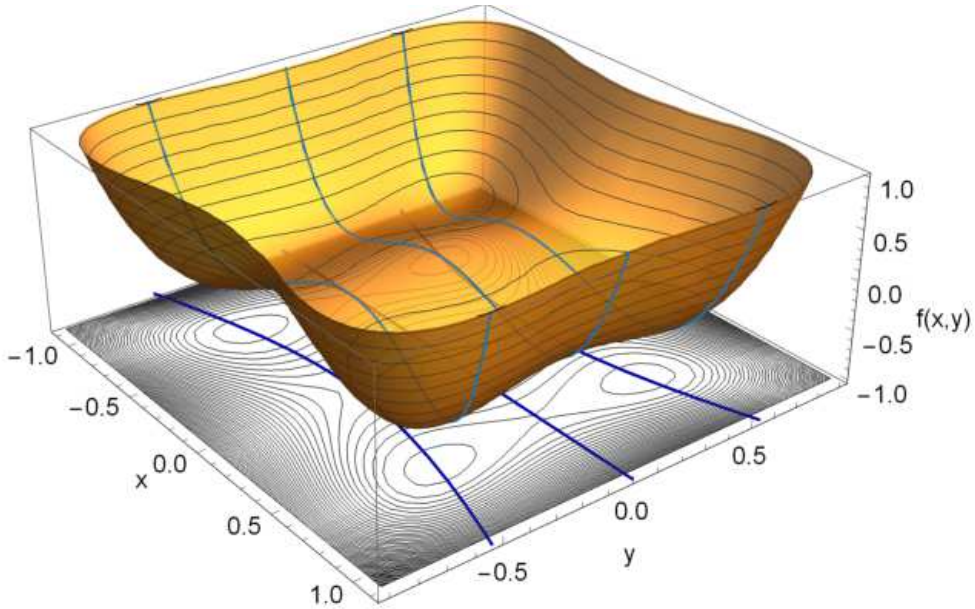

Figure B.4: Plot of function $f(x, y)$ (B.22), with $a_4 = 2.4$, $a_3 = 4$, $a_2 = -1$, $a_1 = -1.8$. The light blue curves along the two-dimensional surface are the one-dimensional functions $f(x, y_0(x), a_1, a_2, a_3, a_4)$ and $f(x, y_\pm(x), a_1, a_2, a_3, a_4)$, and their projections are shown as the blue lines in the contour plot

Appendix C

Bifurcation and Maxwell sets for an arbitrary potential

Let us consider potential $V(x; r_1, r_2, r_3)$ that is a real function of the form

$$V(x; r_1, r_2, r_3) = r_1 g_1(x) + r_2 g_2(x) + r_3 g_3(x) + g_4(x), \tag{C.1}$$

where $g_j(x)$ are arbitrary one-dimensional rational functions with no singularities in the domain of x, and r_i three real parameters. The parameter space of the function (C.1) is three-dimensional and is expressed as (r_1, r_2, r_3).

By gradually changing the parameters the qualitative structure of the potential, i.e. its minima, maxima, and saddle points, also change. Therefore the critical points x_c of the potential are functions of the parameters. Catastrophe theory provides us with a framework of dividing the parameters space with separatrices in regions where the qualitative behaviour of the potential remains the same, so that when given a particular set of values of the parameters, i.e. a point in parameter space, we are able to know the structure of the potential, in particular, how many minima does the potential have. Two of the most important separatrices are the so-called bifurcation set and Maxwell set [41].

As we will see, according to catastrophe theory the bifurcation set and the Maxwell set of a parameter dependent function are subspaces in parameter space defined by the points where the mapping of a certain manifold to the parameter space is singular. In this Appendix we will use this approach to write compact parametric expressions for both the bifurcation set and the Maxwell set of a general one-dimensional potential function.

C.1 Bifurcation set

This separatrix divides the parameter space in two regions: In one region the function has no extrema, at the separatrix it has a saddle point, and in the other region it has a maximum and a minimum. In Fig. C.1 a schematic depiction of a function in the vicinity of the bifurcation set is shown. The bifurcation set is then the subspace in parameter space where critical points emerge.

We begin by taking the derivative of the potential (C.1) with respect to x and equating

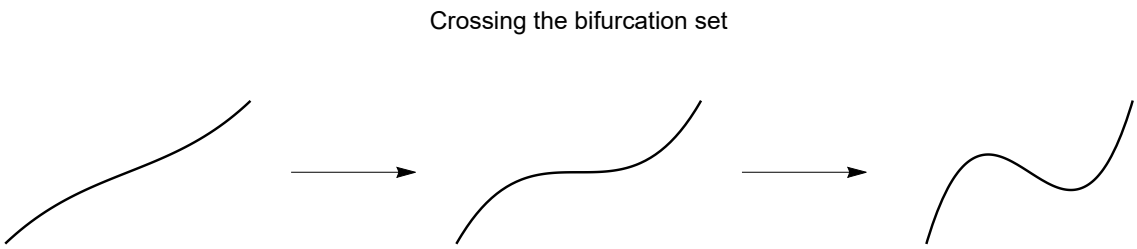

Figure C.1: In the left, before crossing the bifurcation set separatrix, the function has no extrema. In the middle, at the bifurcation set, the function has a saddle point. In the right, after crossing the bifurcation set separatrix, the function has a maximum and a minimum.

it to zero:

$$\left.\frac{\mathrm{d}V}{\mathrm{d}x}\right|_{x=x_c} = r_1 g_1'(x_c) + r_2 g_2'(x_c) + r_3 g_3'(x_c) + g_4'(x_c) = 0. \tag{C.2}$$

This define the critical points x_c of the potential (C.1) for any particular selection of the parameters.

The critical manifold is the hypersurface of all critical points spanned by the variation of the parameters:

$$\mathcal{M}_B = \left\{ (x_c, r_1, r_2, r_3) \in \mathbb{R}^4 \mid \left.\frac{\mathrm{d}V}{\mathrm{d}x}\right|_{x=x_c} = 0 \right\}. \tag{C.3}$$

The bifurcation set is the subspace in parameter space (r_1, r_2, r_3), where the mapping $(x_c, r_1, r_2, r_3) \mapsto (r_1, r_2, r_3)$ of the critical manifold to the parameter space is singular, or in other words when the Jacobian determinant of this transformation is zero [41].

From (C.2) we solve for r_1 and get

$$r_1 = -\frac{1}{g_1'(x_c)} \left(r_2 g_2'(x_c) + r_3 g_3'(x_c) + g_4'(x_c) \right). \tag{C.4}$$

This results in r_1 being expressed as a function of the critical points x_c and the parameters r_2 and r_3. The mapping of the critical manifold to the parameter space then becomes $(x_c, r_2, r_3) \mapsto (r_1, r_2, r_3)$. The Jacobian determinant of the mapping is given by

$$\begin{vmatrix} \frac{\partial r_1}{\partial x_c} & \frac{\partial r_1}{\partial r_2} & \frac{\partial r_1}{\partial r_3} \\ \frac{\partial r_2}{\partial x_c} & \frac{\partial r_2}{\partial r_2} & \frac{\partial r_2}{\partial r_3} \\ \frac{\partial r_3}{\partial x_c} & \frac{\partial r_3}{\partial r_2} & \frac{\partial r_3}{\partial r_3} \end{vmatrix} = \begin{vmatrix} \frac{\partial r_1}{\partial x_c} & \frac{\partial r_1}{\partial r_2} & \frac{\partial r_1}{\partial r_3} \\ 0 & 1 & 0 \\ 0 & 0 & 1 \end{vmatrix} = \frac{\partial r_1}{\partial x_c}, \tag{C.5}$$

and it is singular when it is equal to zero. Using (C.4) we obtain

$$\frac{\partial r_1}{\partial x_c} = \frac{1}{\left(g_1'(x_c)\right)^2} \Big(r_2 W(g_2', g_1') + r_3 W(g_3', g_1') + W(g_4', g_1') \Big) = 0, \tag{C.6}$$

where $W(f, g) = f(x)g'(x) - f'(x)g(x)$ is the Wronskian determinant. From (C.6) we can solve for r_2 and get

$$r_2 = -\frac{1}{W(g_1', g_2')} \Big(r_3 W(g_1', g_3') + W(g_1', g_4') \Big), \tag{C.7}$$

as a function x_c and r_3. Finally, direct substitution of (C.7) in (C.4) gives us r_1 as a function of x_c and r_3 as

$$r_1 = \frac{1}{W(g_1', g_2')}\Big(r_3 W(g_2', g_3') + W(g_2', g_4')\Big). \tag{C.8}$$

Then, the bifurcation set of the potential function (C.1) is the parametric surface in three-dimensional space defined by (C.7) and (C.8):

$$\mathcal{C}_B = \Big\{\Big(r_1(x_c, r_3), r_2(x_c, r_3), r_3\Big) \mid x_c, r_3 \in \mathbb{R}\Big\}. \tag{C.9}$$

C.2 Maxwell set

This separatrix divides the parameter space in two regions: In one region the function has two or more extrema at different values, e.g. two minima with one being lower than the other; in the Maxwell set two or more extrema have the same value, e.g. both minima have equal depth; and in the other the extrema have again different values, e.g. the minima the had a higher value is now the lower one. In Fig. C.2 a schematic depiction of a function in the vicinity of the Maxwell set of two minima is shown.

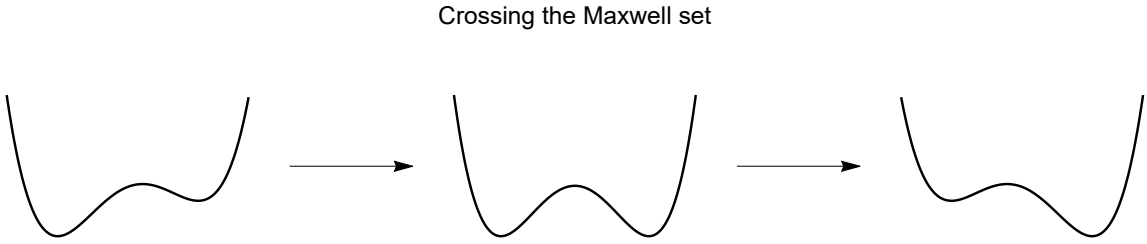

Figure C.2: Transition of a function with two minima across the Maxwell set. In the left, before crossing the Maxwell set separatrix, the minimum on the left is lower than the minimum on the right. In the middle, at the Maxwell set, the two minima have same value. In the right, after crossing the Maxwell set separatrix, the minimum on the left is higher than the minimum on the right.

The Maxwell set is the subspace in parameter space where for at least two critical points x_1 and x_2 the following condition holds

$$V(x_1; r_1, r_2, r_3) = V(x_2; r_1, r_2, r_3) = -V_c, \tag{C.10}$$

where $V_c \in \mathbb{R}$ and $-V_c$ is the value of the extrema. This condition can be written as the following expression:

$$V(x_r; r_1, r_2, r_3) + V_c = 0, \tag{C.11}$$

where we consider all the values x_r such that the potential function equals $-V_c$ for a particular choice of the parameters r_i. We are only interested in the cases when x_r are also critical points.

Analogous to the bifurcation set case we consider a roots manifold defined as:

$$\mathcal{M}_M = \left\{(x_r, r_1, r_2, r_3) \in \mathbb{R}^4 \mid V(x_r; r_1, r_2, r_3) + V_c = 0\right\}, \tag{C.12}$$

i.e. the hypersurface of all real roots of (C.11) spanned by the variation of parameters. The reasoning is as follows: As the parameters are arbitrarily varied a critical point arises when two real roots (or a conjugate complex pair) of (C.11) coalesce; in this case we will have a critical point x_r such that the value of the function is $-V_c$ for the respective values of the parameters. This occurs at the intersection of the critical manifold (C.3) and the roots manifold (C.12), which happens when the mapping of the roots manifold to the parameter space is singular. Then, we can define the Maxwell set as the subspace of parameter space where the mapping $(x_r, r_1, r_2, r_3) \mapsto (r_1, r_2, r_3)$ of the roots manifold to the parameter space is singular for two different critical points (roots) x_1 and x_2 for the same value of the parameters.

From (C.11) we solve for r_1 and get:

$$r_1 = -\frac{1}{g_1(x_r)}\Big(r_2 g_2(x_r) + r_3 g_3(x_r) + g_4(x_r) + V_c\Big). \tag{C.13}$$

Similarly to (C.5) the Jacobian determinant of the transformation is

$$\frac{\partial r_1}{\partial x_r} = \frac{1}{g_1^2(x_r)}\Big(r_2 W(g_2, g_1) + r_3 W(g_3, g_1) + W(g_4, g_1) + g_1'(x_r) V_c\Big), \tag{C.14}$$

and the mapping is singular when (C.14) is equal to zero.

From (C.14) we can solve for r_2 and get

$$r_2 = -\frac{1}{W(g_1, g_2)}\Big(r_3 W(g_1, g_3) + W(g_1, g_4) - g_1'(x_r) V_c\Big), \tag{C.15}$$

which is given in terms of the critical points x_r and the parameter r_3 and V_c. By direct substitution of (C.15) in (C.13) we can obtain r_1 as:

$$r_1 = \frac{1}{W(g_1, g_2)}\Big(r_3 W(g_2, g_3) + W(g_2, g_4) - g_2'(x_r) V_c\Big), \tag{C.16}$$

also given in terms of x_r, r_3 and V_c. The parametric surface defined by (C.15) and (C.16) corresponds to the values of (r_1, r_2, r_3) for which there exists a critical point x_r such that the value of the extremum is $-V_c$. We can show that the x_r which satisfy both (C.15) and (C.16) are critical points by direct substitution in (C.2), with $x_c = x_r$, and seeing that the expression is automatically satisfied.

For the particular case where the potential function (C.1) always has an extremum at $V_c = 0$ the Maxwell set is the parametric surface in three-dimensional space defined by (C.15) and (C.16) setting $V_c = 0$:

$$\mathcal{C}_M^0 = \{(r_1(x_r, r_3), r_2(x_r, r_3), r_3) \mid x_r, r_3 \in \mathbb{R}\}. \tag{C.17}$$

We continue by supposing that there exist two different values x_1 and x_2 such that the following set of algebraic equations are simultaneously satisfied:

$$r_2(x_1; r_3, V_c) = r_2(x_2; r_3, V_c) \tag{C.18}$$

$$r_1(x_1; r_3, V_c) = r_1(x_2; r_3, V_c), \tag{C.19}$$

with r_2 and r_1 given by (C.15) and (C.16), respectively. We can rewrite (C.18) and (C.19) as the following set of equations:

$$r_2 \;:\; r_3 W_{13}(x_1,x_2) + W_{14}(x_1,x_2) - V_c G_1(x_1,x_2) = 0 \tag{C.20}$$
$$r_1 \;:\; r_3 W_{23}(x_1,x_2) + W_{24}(x_1,x_2) - V_c G_2(x_1,x_2) = 0 \tag{C.21}$$

where we defined the following functions:

$$W_{ij}(x_1,x_2) = W(g_i,g_j)|_{x_1} W(g_1,g_2)|_{x_2} - W(g_i,g_j)|_{x_2} W(g_1,g_2)|_{x_1} \tag{C.22}$$
$$G_i(x_1,x_2) = g_i'(x_1)\, W(g_1,g_2)|_{x_2} - g_i'(x_2)\, W(g_1,g_2)|_{x_1}\,. \tag{C.23}$$

Eliminating V_c from (C.20) and (C.21) we obtain r_3 as a function of x_1 and x_2:

$$\begin{aligned} &r_3\Big(G_2(x_1,x_2)W_{13}(x_1,x_2) - G_1(x_1,x_2)W_{23}(x_1,x_2)\Big) \\ &+G_2(x_1,x_2)W_{14}(x_1,x_2) - G_1(x_1,x_2)W_{24}(x_1,x_2) = 0, \end{aligned} \tag{C.24}$$

and eliminating r_3 from (C.20) and (C.21) we obtain V_c as a function of x_1 and x_2:

$$\begin{aligned} &V_c\Big(G_1(x_1,x_2)W_{23}(x_1,x_2) - G_2(x_1,x_2)W_{13}(x_1,x_2)\Big) \\ &+W_{13}(x_1,x_2)W_{24}(x_1,x_2) - W_{23}(x_1,x_2)W_{14}(x_1,x_2) = 0. \end{aligned} \tag{C.25}$$

Then, for every value value of r_3 one can solve (C.24) and determine the values of x_1 and x_2, which in turn can be substituted in (C.25) to obtain the corresponding value of V_c. We finally substitute everything back in (C.15) and (C.16), so that now r_1 and r_2 are given in terms of x_1, x_2 and r_3, and we obtain the Maxwell set as the parametric surface in three-dimensional space defined as:

$$\mathcal{C}_M = \{(r_1(x_1,x_2,r_3), r_2(x_1,x_2,r_3), r_3) \mid x_1,x_2,r_3 \in \mathbb{R}\}\,, \tag{C.26}$$

where x_1 and x_2 satisfy (C.18) and (C.19).

To reduce computation times we find that the combinations of functions appearing in (C.24) and (C.25) can be written as:

$$\begin{aligned} &G_2(x_1,x_2)W_{1i}(x_1,x_2) - G_1(x_1,x_2)W_{2i}(x_1,x_2) \\ &= W(g_1,g_2)|_{x_1} W(g_1,g_2)|_{x_2} \Big(g_1'(x_1)\, W(g_2,g_i)|_{x_2} + g_1'(x_2)\, W(g_2,g_i)|_{x_1} \\ &\quad - g_2'(x_1)\, W(g_1,g_i)|_{x_2} - g_2'(x_2)\, W(g_1,g_i)|_{x_1} \\ &\quad + g_i'(x_1)\, W(g_1,g_2)|_{x_2} + g_i'(x_2)\, W(g_1,g_2)|_{x_1} \Big), \end{aligned} \tag{C.27}$$

and

$$\begin{aligned} &W_{23}(x_1,x_2)W_{14}(x_1,x_2) - W_{13}(x_1,x_2)W_{24}(x_1,x_2) \\ &= -\,W(g_1,g_2)|_{x_1} W(g_1,g_2)|_{x_2} \Big(W(g_1,g_2)|_{x_1} W(g_3,g_4)|_{x_2} + W(g_1,g_2)|_{x_2} W(g_3,g_4)|_{x_1} \\ &\quad - W(g_1,g_3)|_{x_1} W(g_2,g_4)|_{x_2} - W(g_1,g_3)|_{x_2} W(g_2,g_4)|_{x_1} \\ &\quad + W(g_1,g_4)|_{x_1} W(g_2,g_3)|_{x_2} + W(g_1,g_4)|_{x_2} W(g_2,g_3)|_{x_1} \Big), \end{aligned} \tag{C.28}$$

where in both expressions the common term $W(g_1,g_2)|_{x_1} W(g_1,g_2)|_{x_2}$ can be factored out of the equations.

Appendix D

Definition of the $Q_i(\alpha)$ polynomials

The definition of the $F_{pq}(\alpha)$ functions, which appear when calculating the expectation values of the operators in the Hamiltonian, is given by the following expression [62]:

$$F_{pq}(\alpha^2) = \frac{(N!)^2}{(N+n_0-\max(p,q))!} \times \sum_{k=\max(n_0-p,n_0-q)}^{N+n_0-\max(p,q)} \binom{N+n_0-\max(p,q)}{k} \frac{(k+p)!}{(k+p-n_0)!}\frac{(k+q)!}{(k+q-n_0)!}\alpha^{2k}. \tag{D.1}$$

In order to express the semi-classical potential in terms of the essential parameters it is necessary to rewrite (D.1) in a suitable way. For this purpose we begin by expanding (D.1) explicitly for the values of p and q which appear in the semi-classical potential:

$$\alpha^{2p}F_{pp}(\alpha) = N!n_0!\alpha^{2n_0}\left[\frac{n_0!}{(n_0-p)!} + \ldots + \frac{N!}{(N-k)!}\frac{(n_0+k)!}{n_0!}\frac{(n_0+k)!}{(n_0+k-p)!}\frac{\alpha^{2k}}{(k!)^2} + \ldots + \frac{[(N+n_0)!]^2}{N!n_0!(N+n_0-p)!}\alpha^{2N}\right] \tag{D.2}$$

$$\alpha^2 F_{20}(\alpha) = N!n_0!\alpha^{2n_0}\left[N(N-1)(n_0+2)(n_0+1)\frac{\alpha^2}{2!} + \frac{N!}{(N-3)!}\frac{(n_0+3)!}{n_0!}\frac{\alpha^4}{3!} + \ldots + \frac{N!}{(N-k-1)!}\frac{(n_0+k+1)!}{n_0!}\frac{\alpha^{2k}}{(k+1)!(k-1)!} + \ldots + \frac{(N+n_0)!}{n_0!(N-2)!}\alpha^{2N-2}\right],$$

with $p = q = 1, 2, 3$.

When subtracting the constant term T_0 (2.77) of the Taylor series expansion about $\alpha = 0$ of the semi-classical potential to (2.69) we obtain linear combinations of the $F_{pq}(\alpha)$ functions. In what follows we deal with those expressions and manipulate them to rewrite them as linear combinations of some new polynomials which will be multiplied by the essential parameters r_i (2.83).

Expression for $f_{11}(\alpha) \equiv \alpha^2 F_{11}(\alpha) - n_0 F_{00}(\alpha)$:

$$f_{11}(\alpha) = N!n_0!\alpha^{2n_0}\sum_{k=1}^{N}\frac{N!}{(N-k)!}\frac{(n_0+k)!}{n_0!}\frac{\alpha^{2k}}{k!(k-1)!} \tag{D.3}$$

Expression for $f_{22}(\alpha) \equiv \alpha^4 F_{22}(\alpha) - n_0(n_0-1)F_{00}(\alpha)$:

$$f_{22}(\alpha) = N! n_0! \alpha^{2n_0} \left[2n_0 \sum_{k=1}^{N} \frac{N!}{(N-k)!} \frac{(n_0+k)!}{n_0!} \frac{\alpha^{2k}}{k!(k-1)!} + \sum_{k=2}^{N} \frac{N!}{(N-k)!} \frac{(n_0+k)!}{n_0!} \frac{\alpha^{2k}}{k!(k-2)!} \right], \tag{D.4}$$

where we used

$$(n_0+k)(n_0+k-1) - n_0(n_0-1) = 2n_0 k + k(k-1). \tag{D.5}$$

Expression for $f_{33}(\alpha) \equiv \alpha^6 F_{33}(\alpha) - n_0(n_0-1)(n_0-2)F_{00}(\alpha)$:

$$\begin{aligned} f_{33}(\alpha) = N! n_0! \alpha^{2n_0} \Bigg[& 3n_0(n_0-1) \sum_{k=1}^{N} \frac{N!}{(N-k)!} \frac{(n_0+k)!}{n_0!} \frac{\alpha^{2k}}{k!(k-1)!} \\ & + 3n_0 \sum_{k=2}^{N} \frac{N!}{(N-k)!} \frac{(n_0+k)!}{n_0!} \frac{\alpha^{2k}}{k!(k-2)!} \\ & + \sum_{k=3}^{N} \frac{N!}{(N-k)!} \frac{(n_0+k)!}{n_0!} \frac{\alpha^{2k}}{k!(k-3)!} \Bigg] \end{aligned} \tag{D.6}$$

where we used

$$(n_0+k)(n_0+k-1)(n_0+k-2) - n_0(n_0-1)(n_0-2) = 3n_0(n_0-1)k + 3n_0 k(k-1) + k(k-1)(k-2). \tag{D.7}$$

Expression for $\alpha^2 F_{20}(\alpha)$:

$$\begin{aligned} \alpha^2 F_{20}(\alpha) = N! n_0! \alpha^{2n_0} \Bigg[& \frac{1}{2}(N-1)(n_0+2) \sum_{k=1}^{N} \frac{N!}{(N-k)!} \frac{(n_0+k)!}{n_0!} \frac{\alpha^{2k}}{k!(k-1)!} \\ & - \frac{1}{6}(n_0(N+1)+6) \sum_{k=2}^{N} \frac{N!}{(N-k)!} \frac{(n_0+k)!}{n_0!} \frac{\alpha^{2k}}{k!(k-2)!} \\ & + \frac{1}{6} n_0 (N+1) \sum_{k=3}^{N} \frac{N!}{(N-k)!} \frac{(n_0+k)!}{n_0!} \frac{\alpha^{2k}}{(k+1)!(k-3)!} \Bigg] \end{aligned} \tag{D.8}$$

where we used

$$\begin{aligned} & -\frac{1}{k!(k-1)!}\frac{1}{2}(N-1)(n_0+2) + \frac{1}{k!(k-2)!}\frac{1}{6}(n_0(N+1)+6) + \frac{(N-k)(n_0+k+1)}{(k+1)!(k-1)!} \\ & = \frac{1}{(k+1)!(k-3)!}\frac{1}{6} n_0 (N+1). \end{aligned} \tag{D.9}$$

Defining the polynomials appearing in (D.3), (D.4), (D.6) and (D.8) as

$$\begin{aligned} Q_i(\alpha) &= \sum_{k=i}^{N} \frac{N!}{(N-k)!} \frac{(n_0+k)!}{n_0!} \frac{\alpha^{2k}}{k!(k-i)!}, \qquad i = 1, 2, 3. \\ Q_4(\alpha) &= \sum_{k=3}^{N} \frac{N!}{(N-k)!} \frac{(n_0+k)!}{n_0!} \frac{\alpha^{2k}}{(k+1)!(k-3)!}, \end{aligned} \tag{D.10}$$

we are able to write the previous expressions as linear combinations of (D.10):

$$\begin{aligned}
f_{00}(\alpha) &= N!n_0!\alpha^{2n_0}Q_0(\alpha) \\
f_{11}(\alpha) &= N!n_0!\alpha^{2n_0}Q_1(\alpha) \\
f_{22}(\alpha) &= N!n_0!\alpha^{2n_0}\left[2n_0Q_1(\alpha)+Q_2(\alpha)\right] \\
f_{33}(\alpha) &= N!n_0!\alpha^{2n_0}\left[3n_0(n_0-1)Q_1(\alpha)+3n_0Q_2(\alpha)+Q_3(\alpha)\right] \\
\alpha^2F_{20}(\alpha) &= N!n_0!\alpha^{2n_0}\left[\frac{1}{2}(N-1)(n_0+2)Q_1(\alpha)-\frac{1}{6}(n_0(N+1)+6)Q_2(\alpha)\right. \\
&\quad \left.+\frac{1}{6}n_0(N+1)Q_4(\alpha)\right].
\end{aligned} \tag{D.11}$$

When dealing with large values of N, such that $N-n_0-p-1>0$ and $p\geq q$ are satisfied, it is possible to factorize the function $\alpha^{2q}F_{pq}(\alpha^2)$ in the following way:

$$\alpha^{2q}F_{pq}(\alpha^2) = N!n_0!\alpha^{2n_0}(1+\alpha^2)^{N-n_0-p}G_{pq}(\alpha), \tag{D.12}$$

where the function $G_{pq}(\alpha)$ is a polynomial of order $2n_0+2q$ defined as

$$G_{pq}(\alpha) = \sum_{k=0}^{n_0+q} c_{pq}(k)\alpha^{2k}, \tag{D.13}$$

with the coefficients $c_{pq}(k)$ given by

$$c_{pq}(k) = \sum_{j=0}^{k}(-1)^j p! \binom{N}{p-q+k}\binom{n_0+k}{k}\binom{n_0+p-q+k}{p}\binom{N-n_0-p+j-1}{j}. \tag{D.14}$$

Then, it is possible to cancel out the term $\alpha^{2n_0}(1+\alpha^2)^{N-n_0}$ in the semi-classical potential.

References

[1] S. Sachdev, *Quantum Phase Transitions*. Cambridge University Press, 2011.

[2] R. F. Casten and E. A. McCutchan, "Quantum phase transitions and structural evolution in nuclei," *Journal of Physics G: Nuclear and Particle Physics*, vol. 34, pp. R285–R320, may 2007.

[3] R. F. Casten, "Quantum phase transitions and structural evolution in nuclei," *Progress in Particle and Nuclear Physics*, vol. 62, no. 1, pp. 183–209, 2009.

[4] E. López-Moreno and O. Castaños, "Shapes and stability within the interacting boson model: Dynamical symmetries," *Phys. Rev. C*, vol. 54, pp. 2374–2384, Nov 1996.

[5] E. López-Moreno and O. Castaños, "Shapes and stability within the interacting boson model: effective Hamiltonians," *Rev. Mex. Fis. S.*, vol. 44, pp. 48–54, oct 1998.

[6] P. Cejnar, J. Jolie, and R. F. Casten, "Quantum phase transitions in the shapes of atomic nuclei," *Rev. Mod. Phys.*, vol. 82, pp. 2155–2212, Aug 2010.

[7] A. Arima and F. Iachello, "Collective Nuclear States as Representations of a SU(6) Group," *Phys. Rev. Lett.*, vol. 35, pp. 1069–1072, Oct 1975.

[8] J. P. Elliott, "The interacting boson model of nuclear structure," *Reports on Progress in Physics*, vol. 48, pp. 171–222, feb 1985.

[9] F. Iachello and A. Arima, *The Interacting Boson Model*. Cambridge University Press, 1987.

[10] A. E. L. Dieperink, O. Scholten, and F. Iachello, "Classical Limit of the Interacting-Boson Model," *Phys. Rev. Lett.*, vol. 44, pp. 1747–1750, Jun 1980.

[11] D. H. Feng, R. Gilmore, and S. R. Deans, "Phase transitions and the geometric properties of the interacting boson model," *Phys. Rev. C*, vol. 23, pp. 1254–1258, Mar 1981.

[12] P. Cejnar, "Shape phase transitions in rotating nuclei via cranking the interacting boson model," *Phys. Rev. C*, vol. 65, p. 044312, Mar 2002.

[13] F. Iachello and N. V. Zamfir, "Quantum Phase Transitions in Mesoscopic Systems," *Phys. Rev. Lett.*, vol. 92, p. 212501, May 2004.

[14] J. M. Arias, J. E. García-Ramos, and J. Dukelsky, "Phase Diagram of the Proton-Neutron Interacting Boson Model," *Phys. Rev. Lett.*, vol. 93, p. 212501, Nov 2004.

[15] M. A. Caprio and F. Iachello, "Phase Structure of the Two-Fluid Proton-Neutron System," *Phys. Rev. Lett.*, vol. 93, p. 242502, Dec 2004.

[16] S. Heinze, P. Cejnar, J. Jolie, and M. Macek, "Evolution of spectral properties along the O(6)-U(5) transition in the interacting boson model. I. Level dynamics," *Phys. Rev. C*, vol. 73, p. 014306, Jan 2006.

[17] M. Macek, P. Cejnar, J. Jolie, and S. Heinze, "Evolution of spectral properties along the O(6)-U(5) transition in the interacting boson model. II. Classical trajectories," *Phys. Rev. C*, vol. 73, p. 014307, Jan 2006.

[18] P. Cejnar, "Quantum phase transitions in finite algebraic systems," *Journal of Physics: Conference Series*, vol. 322, p. 012012, oct 2011.

[19] J. E. García-Ramos, J. M. Arias, and J. Dukelsky, "Disentangling phase transitions and critical points in the proton–neutron interacting boson model by catastrophe theory," *Physics Letters B*, vol. 736, pp. 333–338, 2014.

[20] R. F. Casten and J. A. Cizewski, "The O(6) $\rightarrow$ rotor transition in the PtOs nuclei," *Nuclear Physics A*, vol. 309, no. 3, pp. 477–505, 1978.

[21] P. Cejnar and J. Jolie, "Dynamical-symmetry content of transitional IBM-1 hamiltonians," *Physics Letters B*, vol. 420, no. 3, pp. 241–247, 1998.

[22] P. V. Isacker, "Dynamical symmetries in the structure of nuclei," *Reports on Progress in Physics*, vol. 62, pp. 1661–1717, dec 1999.

[23] J. Jolie and P. Cejnar, "Should the Casten triangle be a pentagon?," *Journal of Physics G: Nuclear and Particle Physics*, vol. 25, pp. 843–845, jan 1999.

[24] F. Iachello, "Dynamic symmetries in nuclei," *Journal of Physics G: Nuclear and Particle Physics*, vol. 25, pp. 655–660, jan 1999.

[25] A. Leviatan, "Partial dynamical symmetries," *Progress in Particle and Nuclear Physics*, vol. 66, no. 1, pp. 93–143, 2011.

[26] Leviatan, A., "SU(3) partial dynamical symmetry and nuclear shapes," *Eur. Phys. J. Special Topics*, vol. 229, pp. 2405–2427, 2020.

[27] P. Cejnar and J. Jolie, "Quantum phase transitions in the interacting boson model," *Progress in Particle and Nuclear Physics*, vol. 62, no. 1, pp. 210–256, 2009.

[28] H. J. Lipkin, N. Meshkov, and A. J. Glick, "Validity of many-body approximation methods for a solvable model: (I). Exact solutions and perturbation theory," *Nuclear Physics*, vol. 62, no. 2, pp. 188–198, 1965.

[29] R. H. Dicke, "Coherence in Spontaneous Radiation Processes," *Phys. Rev.*, vol. 93, pp. 99–110, Jan 1954.

[30] K. Hepp and E. H. Lieb, "On the superradiant phase transition for molecules in a quantized radiation field: the dicke maser model," *Annals of Physics*, vol. 76, no. 2, pp. 360–404, 1973.

[31] O. Castaños, R. López-Peña, J. G. Hirsch, and E. López-Moreno, "Phase transitions and accidental degeneracy in nonlinear spin systems," *Phys. Rev. B*, vol. 72, p. 012406, Jul 2005.

[32] O. Castaños, R. López-Peña, J. G. Hirsch, and E. López-Moreno, "Classical and quantum phase transitions in the Lipkin-Meshkov-Glick model," *Phys. Rev. B*, vol. 74, p. 104118, Sep 2006.

[33] F. Leyvraz and W. D. Heiss, "Large-N Scaling Behavior of the Lipkin-Meshkov-Glick Model," *Phys. Rev. Lett.*, vol. 95, p. 050402, Jul 2005.

[34] E. López-Moreno and M. Grether, "Coherent qubits stability and quantum phase transitions in the Lipkin–Meshkov–Glick model," *Quantum Studies: Mathematics and Foundations*, vol. 1, pp. 203–211, nov 2014.

[35] L. F. Quezada, A. Martín-Ruiz, and A. Frank, "Quantum phase transition of two-level atoms interacting with a finite radiation field," *Journal of Mathematical Physics*, vol. 61, no. 6, p. 062104, 2020.

[36] D. Gutiérrez-Ruiz, D. Gonzalez, J. Chávez-Carlos, J. G. Hirsch, and J. D. Vergara, "Quantum geometric tensor and quantum phase transitions in the Lipkin-Meshkov-Glick model," *Phys. Rev. B*, vol. 103, p. 174104, May 2021.

[37] M. Calixto, A. Mayorgas, and J. Guerrero, "Role of mixed permutation symmetry sectors in the thermodynamic limit of critical three-level Lipkin-Meshkov-Glick atom models," *Phys. Rev. E*, vol. 103, p. 012116, Jan 2021.

[38] J. G. Hirsch, O. Castaños, E. Nahmad-Achar, and R. López-Peña, "Quantum phase crossovers with finite atom number in the Dicke model," *Physica Scripta*, vol. T153, p. 014033, mar 2013.

[39] M. Kloc, P. Stránský, and P. Cejnar, "Quantum phases and entanglement properties of an extended Dicke model," *Annals of Physics*, vol. 382, pp. 85–111, 2017.

[40] Guerra, Camilo A. Estrada, Mahecha-Gómez, Jorge, and Hirsch, Jorge G., "Quantum phase transition and Berry phase in an extended Dicke model," *Eur. Phys. J. D*, vol. 74, no. 10, p. 200, 2020.

[41] R. Gilmore, *Catastrophe Theory for Scientists and Engineers*. New York: Wiley, 1981.

[42] V. I. Arnol'd, *Catastrophe Theory*. Berlin: Springer-Verlag, 1986.

[43] T. Poston and I. Stewart, *Catastrophe theory and its applications*. New York: Dover, 1996.

[44] E. López-Moreno, M. Grether, and V. Velázquez, "Energy level structure and quantum phase transitions of spin systems with nonaxially symmetric Hamiltonians," *Journal of Physics A: Mathematical and Theoretical*, vol. 44, p. 475301, nov 2011.

[45] J. E. García-Ramos, P. Pérez-Fernández, J. M. Arias, and E. Freire, "Phase diagram of the two-fluid Lipkin model: A "butterfly" catastrophe," *Phys. Rev. C*, vol. 93, p. 034336, Mar 2016.

[46] A. Leviatan and N. Gavrielov, "Quantum catastrophes from an algebraic perspective," *Journal of Physics: Conference Series*, vol. 1612, p. 012020, aug 2020.

[47] D. S. Lohr-Robles, E. López-Moreno, and P. O. Hess, "Quantum Phase Transitions within the Semimicroscopic Algebraic Cluster Model," *Nuclear Physics A*, vol. 992, p. 121629, 2019.

[48] D. S. Lohr-Robles, E. López-Moreno, and P. O. Hess, "Quantum phase transitions within a nuclear cluster model and an effective model of QCD," *Nuclear Physics A*, vol. 1016, p. 122335, 2021.

[49] M. Freer, H. Horiuchi, Y. Kanada-En'yo, D. Lee, and U.-G. Meißner, "Microscopic clustering in light nuclei," *Rev. Mod. Phys.*, vol. 90, p. 035004, Aug 2018.

[50] B. Zhou, Y. Funaki, H. Horiuchi, and A. Tohsaki, "Nonlocalized clustering and evolution of cluster structure in nuclei," *Frontiers of Physics*, vol. 15, p. 14401, 08 2020.

[51] R. Bijker and F. Iachello, "Cluster structure of light nuclei," *Progress in Particle and Nuclear Physics*, vol. 110, p. 103735, 2020.

[52] J. Cseh, "Semimicroscopic algebraic description of nuclear cluster states. Vibron model coupled to the SU(3) shell model," *Physics Letters B*, vol. 281, no. 3, pp. 173–177, 1992.

[53] J. Cseh and G. Lévai, "Semimicroscopic Algebraic Cluster Model of Light Nuclei. I. Two-Cluster-Systems with Spin-Isospin-Free Interactions," *Annals of Physics*, vol. 230, no. 2, pp. 165–200, 1994.

[54] P. O. Hess, "12C within the Semimicroscopic Algebraic Cluster Model," *Eur. Phys. J. A*, vol. 54, no. 3, p. 32, 2018.

[55] P. O. Hess, J. R. M. Berriel-Aguayo, and L. J. Chávez-Nuñez, "16O within the Semimicroscopic Algebraic Cluster Model and the importance of the Pauli Exclusion Principle," *Eur. Phys. J. A*, vol. 55, no. 5, p. 71, 2019.

[56] J. R. M. Berriel-Aguayo and P. O. Hess, "The Role of the Pauli Exclusion Principle in Nuclear Physics Models," *Symmetry*, vol. 12, no. 5, 2020.

[57] J. P. Elliott, "Collective motion in the nuclear shell model. I. Classification schemes for states of mixed configurations," *Proceedings of the Royal Society of London. Series A. Mathematical and Physical Sciences*, vol. 245, no. 1240, pp. 128–145, 1958.

[58] J. P. Elliott, "Collective motion in the nuclear shell model II. The introduction of intrinsic wave-functions," *Proceedings of the Royal Society of London. Series A. Mathematical and Physical Sciences*, vol. 245, no. 1243, pp. 562–581, 1958.

[59] M. Harvey, "The Nuclear SU3 Model," *Advances in Nuclear Physics*, vol. 1, pp. 67–182, 1968.

[60] F. Iachello, "Algebraic approach to nuclear quasimolecular spectra," *Phys. Rev. C*, vol. 23, pp. 2778–2780, Jun 1981.

[61] F. Iachello, "Algebraic methods for molecular rotation-vibration spectra," *Chemical Physics Letters*, vol. 78, no. 3, pp. 581–585, 1981.

[62] H. Yépez-Martínez, P. R. Fraser, P. O. Hess, and G. Lévai, "Phenomenological and microscopic cluster models. I. The geometric mapping," *Phys. Rev. C*, vol. 85, p. 014316, Jan 2012.

[63] J. P. Elliott and B. H. Flowers, "The structure of the nuclei of mass 18 and 19," *Proceedings of the Royal Society of London. Series A. Mathematical and Physical Sciences*, vol. 229, no. 1179, pp. 536–563, 1955.

[64] J. P. Elliott and T. H. R. Skyrme, "Centre-of-mass effects in the nuclear shell-model," *Proceedings of the Royal Society of London. Series A. Mathematical and Physical Sciences*, vol. 232, no. 1191, pp. 561–566, 1955.

[65] J. P. Elliott and M. Harvey, "Collective motion in the nuclear shell model III. The calculation of spectra," *Proceedings of the Royal Society of London. Series A. Mathematical and Physical Sciences*, vol. 272, no. 1351, pp. 557–577, 1963.

[66] K. Wildermuth and Y. C. Tang, *A Unified Theory of the Nucleus*. Braunschweig: Friedr. Vieweg & Sohn Verlagsgesselschaft mbH, 1977.

[67] J. Blomqvist and A. Molinari, "Collective 0- vibrations in even spherical nuclei with tensor forces," *Nuclear Physics A*, vol. 106, no. 3, pp. 545–569, 1968.

[68] W. Greiner and J. A. Maruhn, *Nuclear models*. Berlin: Springer, 1996.

[69] K. T. Hecht, *The vector coherent state method and its application to problems of higher symmetries*. Heidelberg: Springer, 1987.

[70] P. O. Hess, G. Lévai, and J. Cseh, "Geometrical interpretation of the semimicroscopic algebraic cluster model," *Phys. Rev. C*, vol. 54, pp. 2345–2355, Nov 1996.

[71] G. E. Morales-Hernández, H. Yépez-Martínez, and P. O. Hess, "Phase transitions for excited states in $^{16}O+\alpha \rightarrow {}^{20}Ne$ within the SACM," *Journal of Physics: Conference Series*, vol. 387, p. 012019, sep 2012.

[72] E. López-Moreno, G. E. Morales-Hernández, P. O. Hess, and H. Yépez-Martínez, "Phase transitions for rotational states within an algebraic cluster model," *Journal of Physics: Conference Series*, vol. 730, p. 012017, jul 2016.

[73] H. Yépez-Martínez and P. O. Hess, "Cranking the semimicroscopic algebraic cluster model," *Rev. Mex. Fis. S.*, vol. 54, pp. 69–73, dic 2008.

[74] P. R. Fraser, H. Yépez-Martínez, P. O. Hess, and G. Lévai, "Phenomenological and microscopic cluster models. II. Phase transitions," *Phys. Rev. C*, vol. 85, p. 014317, Jan 2012.

[75] J. Gravesen, "Catastrophe Theory and Caustics," *SIAM Review*, vol. 25, no. 2, pp. 239–247, 1983.

[76] M. G. Brown and F. D. Tappert, "Catastrophe theory, caustics and traveltime diagrams in seismology," *Geophysical Journal International*, vol. 88, pp. 217–229, 01 1987.

[77] I. Stewart, "Catastrophe theory in physics," *Rep. Prog. Phys.*, vol. 45, pp. 185–221, feb 1982.

[78] V. D. Sedykh, "On the topology of singularities of Maxwell sets," *Mosc. Math. J.*, vol. 3, pp. 1097–1112, 2003.

[79] F. V. Kusmartsev, "Application of catastrophe theory to molecules and solitons," *Physics Reports*, vol. 183, no. 1, pp. 1–35, 1989.

[80] M. Siino and T. Koike, "Topological classification of black holes: Generic Maxwell set and crease set of a horizon," *International Journal of Modern Physics D*, vol. 20, no. 06, pp. 1095–1122, 2011.

[81] P. O. Hess and E. López-Moreno, "Kerr Black Holes within a Modified Theory of Gravity," *Universe*, vol. 5, no. 9, p. 191, 2019.

[82] M. V. Berry, "Waves and Thom's theorem," *Advances in Physics*, vol. 25, no. 1, pp. 1–26, 1976.

[83] S. V. Pavlov, "Classification of Phenomenological Models of Phase Transitions with Three-Component Order Parameters by Methods of Catastrophe Theory: $L = T_d(\bar{4}3m)$," *Moscow University Physics Bulletin*, vol. 74, pp. 186–190, mar 2019.

[84] W. D. Heiss and A. L. Sannino, "Avoided level crossing and exceptional points," *Journal of Physics A: Mathematical and General*, vol. 23, pp. 1167–1178, apr 1990.

[85] J. G. Hirsch, O. Castaños, R. López-Peña, and O. Jiménez F., "Hartree-Fock description of spin systems," *Rev. Mex. Fis. S.*, vol. 53, pp. 41–47, dic 2007.

[86] P. Cejnar and P. Stránský, "Impact of quantum phase transitions on excited-level dynamics," *Phys. Rev. E*, vol. 78, p. 031130, Sep 2008.

[87] O. Castaños, M. Calixto, F. Pérez-Bernal, and E. Romera, "Identifying the order of a quantum phase transition by means of Wehrl entropy in phase space," *Phys. Rev. E*, vol. 92, p. 052106, Nov 2015.

[88] P. Stránský and P. Cejnar, "Classification of excited-state quantum phase transitions for arbitrary number of degrees of freedom," *Physics Letters A*, vol. 380, no. 34, pp. 2637–2643, 2016.

[89] M. Šindelka, L. F. Santos, and N. Moiseyev, "Excited-state quantum phase transitions studied from a non-Hermitian perspective," *Phys. Rev. A*, vol. 95, p. 010103, Jan 2017.

[90] P. Stránský, M. Dvořák, and P. Cejnar, "Exceptional points near first- and second-order quantum phase transitions," *Phys. Rev. E*, vol. 97, p. 012112, Jan 2018.

[91] M. Znojil, "Hermitian-to-quasi-Hermitian quantum phase transitions," *Phys. Rev. A*, vol. 97, p. 042117, Apr 2018.

[92] Q. Wang and F. Pérez-Bernal, "Excited-state quantum phase transition and the quantum-speed-limit time," *Phys. Rev. A*, vol. 100, p. 022118, Aug 2019.

[93] A. Carollo, D. Valenti, and B. Spagnolo, "Geometry of quantum phase transitions," *Physics Reports*, vol. 838, pp. 1–72, 2020.

[94] L. Fortunato, "Quantum phase transitions in algebraic and collective models of nuclear structure," *Progress in Particle and Nuclear Physics*, vol. 121, p. 103891, 2021.

[95] M. A. Caprio, P. Cejnar, and F. Iachello, "Excited state quantum phase transitions in many-body systems," *Annals of Physics*, vol. 323, no. 5, pp. 1106–1135, 2008.

[96] P. Cejnar, P. Stránský, M. Macek, and M. Kloc, "Excited-state quantum phase transitions," *Journal of Physics A: Mathematical and Theoretical*, vol. 54, p. 133001, mar 2021.

[97] S. Lerma H., S. Jesgarz, P. O. Hess, O. Civitarese, and M. Reboiro, "Schematic model for QCD at finite temperature," *Phys. Rev. C*, vol. 66, p. 045207, Oct 2002.

[98] S. Lerma H., S. Jesgarz, P. O. Hess, O. Civitarese, and M. Reboiro, "Schematic model for QCD. I. Low energy meson states," *Phys. Rev. C*, vol. 67, p. 055209, May 2003.

[99] S. Jesgarz, S. Lerma H., P. O. Hess, O. Civitarese, and M. Reboiro, "Schematic model for QCD. II. Finite temperature regime," *Phys. Rev. C*, vol. 67, p. 055210, May 2003.

[100] M. V. Nuñez, S. H. Lerma, P. O. Hess, S. Jesgarz, O. Civitarese, and M. Reboiro, "Schematic model for QCD. III. Hadronic states," *Phys. Rev. C*, vol. 70, p. 035208, Sep 2004.

[101] L. Reinders, H. Rubinstein, and S. Yazaki, "Hadron properties from QCD sum rules," *Physics Reports*, vol. 127, no. 1, pp. 1–97, 1985.

[102] M. Nuñez V., S. Lerma H., P. O. Hess, S. Jesgarz, O. Civitarese, and M. Reboiro, "Modeling pentaquark and heptaquark states," *Phys. Rev. C*, vol. 70, p. 025201, Aug 2004.

[103] P. O. Hess and O. Civitarese, "A review on the advances of an effective model of QCD at low energy," *Rev. Mex. Fis. S.*, vol. 52, pp. 38–43, nov 2006.

[104] O. Civitarese and P. O. Hess, "Modelling the non-perturbative vacuum of QCD," *International Journal of Modern Physics E*, vol. 15, no. 06, pp. 1233–1242, 2006.

[105] P. O. Hess and L. J. Chávez-Nuñez, "A semimicroscopic algebraic cluster model for heavy nuclei - I: One heavy and one light cluster," *Eur. Phys. J. A*, vol. 57, no. 4, p. 146, 2021.

[106] K. T. Hecht and A. Adler, "Generalized seniority for favored $J \neq 0$ pairs in mixed configurations," *Nuclear Physics A*, vol. 137, no. 1, pp. 129–143, 1969.

[107] A. Arima, M. Harvey, and K. Shimizu, "Pseudo LS coupling and pseudo SU_3 coupling schemes," *Physics Letters B*, vol. 30, no. 8, pp. 517–522, 1969.